
Theses and Dissertations

Spring 2017

Effects of prepolymer structure on photopolymer network formation and thermomechanical properties

Jon Paul Scholte
University of Iowa

Follow this and additional works at: <https://ir.uiowa.edu/etd>

 Part of the [Chemical Engineering Commons](#)

Copyright © 2017 Jon Paul Scholte

This dissertation is available at Iowa Research Online: <https://ir.uiowa.edu/etd/5624>

Recommended Citation

Scholte, Jon Paul. "Effects of prepolymer structure on photopolymer network formation and thermomechanical properties." PhD (Doctor of Philosophy) thesis, University of Iowa, 2017.
<https://doi.org/10.17077/etd.ptj5w2kq>

Follow this and additional works at: <https://ir.uiowa.edu/etd>

 Part of the [Chemical Engineering Commons](#)

EFFECTS OF PREPOLYMER STRUCTURE ON PHOTOPOLYMER NETWORK
FORMATION AND THERMOMECHANICAL PROPERTIES

by

Jon Paul Scholte

A thesis submitted in partial fulfillment
of the requirements for the Doctor of Philosophy
degree in Chemical and Biochemical Engineering in the
Graduate College of
The University of Iowa

May 2017

Thesis Supervisor: Professor C. Allan Guymon

Graduate College
The University of Iowa
Iowa City, Iowa

CERTIFICATE OF APPROVAL

PH.D. THESIS

This is to certify that the Ph.D. thesis of

Jon Paul Scholte

has been approved by the Examining Committee for
the thesis requirement for the Doctor of Philosophy degree
in Chemical and Biochemical Engineering at the May 2017 graduation.

Thesis Committee:

C. Allan Guymon, Thesis Supervisor

Julie Jessop

David Rethwisch

Alexei Tivanski

Tai Yeon Lee

To my family and friends.

ACKNOWLEDGEMENTS

To begin, I would like to thank Dr. C. Allan Guymon for his keen eye and attention to detail. He has suffered more of my writing than anyone should yet still always made time to help me clarify my points and better develop my hypotheses.

Next I would like to thank my committee, Dr. Julie Jessop, Dr. David Rethwisch, Dr. Alexi Tivanski, and Dr. Tai Yeon Lee. Your insights to my research proved invaluable in the completion of my work. Specifically, I would like to thank Dr. Tai Yeon Lee for his willingness to help me develop a passion for science and my own voice as a scientific researcher. Your inexhaustible patience and interest in this work made it possible to continue on the work when things became difficult.

To my friends and colleagues, Brad Forney, Kristan Sorenson Worthington, Clint Cook, Celine Baguenard, Todd Thorson, Jacob McLaughlin, Brian Green, Braden Leigh, Erion Hasa, and Daniel Lippert I would like to say thank you for the support, encouragement, and insight. Many of my best ideas required your polish and suggestions to attain the high quality required for PhD research. To Kevin Smith, Jensen Karp, Matthew Robinson, and Justin, Travis, Griffin McElroy, I would like to thank you for your podcasts as they made the late nights in lab much easier.

Lastly, I'd be remiss to overlook the loving support of my family and loved ones. Mom, Dad, and Ian, your love and constant presence in my life made all of the difference in being able to achieve my goals. Your reminders to take care of myself and take time to breath and refocus helped immensely. Alli, I only wish I could have met you sooner. The last two years have been significantly improved ($p < 0.0001$, I guarantee it) and I can't wait to see where we will go next.

ABSTRACT

Photopolymerization is a growing field within the realms of polymer and material science. With diverse applications, ranging from coatings and adhesives to newer technologies such as 3D printing photopolymerization continues to increase its prevalence and influence. This research examines fundamental structure property relationships between large prepolymer structures within a formulation and the resulting impact on thermo-mechanical properties in photocurable resins. Most prepolymer molecules utilize a “one pot” synthesis with little to no control over the placement of photoreactive moieties such as epoxies and (meth) acrylates. We have utilized novel prepolymer molecules synthesized using controlled radical polymerization to allow direct control over the placement of reactive groups. The ability to control the location of reactive groups in prepolymer molecules can also lead to the formation of multiple domains within the resulting photocured thermoset. This separation is achieved by concentrating the reactive groups at specific locations in the prepolymer backbone, e.g. at the end or near the center of the prepolymer molecule. The nonreactive groups may form one domain within the thermoset network while the reactive portion of the prepolymer forms a second phase with reactive diluent molecules. Additionally, various architectures allow greater control over polymer network formation and crosslink density. Through these manipulations of macromolecular architecture, we have been able to manipulate various thermo-mechanical properties. Using various architected prepolymer, we have been able to generate materials with multiple glass transitions while also increasing the rate of reaction and total conversion as compared to randomly functionalized control formulations.

PUBLIC ABSTRACT

Photopolymerization is the process of joining multiple molecules together by exposing them to light. This process has been used to make coatings and adhesives cheaply and efficiently as well as enabling new technologies like 3D printing. In order to provide new materials with the necessary properties to answer the problems of tomorrow, this research examines how the structure of the initial molecules influence the final material properties. Special, chemically reactive large molecules, or prepolymers, were made with the placement of the reactive groups deliberately chosen to influence and create differences at the nanoscale within the network. By controlling how the nanoscale structures are formed, we show that it is possible to produce materials that are very stiff while also maintaining high elongation. By controlling how the special molecules are made we are able to further control the ways in which the molecules interact. Some methods allow for the final material to be responsive to continued light exposure. The continued light exposure allows for the networks to rearrange and assume a more relaxed conformation which produces a more homogenous network with improved stiffness and resistance to sudden deformations, two critical measures of industrial and academic interest. Overall, this work lays the foundation for further advancements in the design of specialty molecules and design of photopolymer systems.

TABLE OF CONTENTS

LIST OF TABLES	ix
LIST OF FIGURES	x
CHAPTER 1 INTRODUCTION	1
Radical Photopolymerization.....	3
Radical Photoinitiation.....	3
Propagation	4
Termination.....	5
Applications and Shortcomings	6
Cationic Photopolymerization	9
Cationic Photoinitiation	10
Propagation and Transfer	11
Termination.....	12
Uses and Shortcoming	12
Photopolymerization Formulations.....	13
Controlled Radical Polymerization.....	15
Nitroxide Mediated Polymerization.....	16
Reversible Addition Fragmentation Chain Transfer (RAFT).....	17
Applications of Controlled Radical Polymerization	20
Photopolymer Networks	21
Step Growth Networks.....	21
Dual Networks	22
Research Plan.....	24
References and Notes.....	26
CHAPTER 2 OBJECTIVES	37
CHAPTER 3 MATERIALS AND METHODS.....	41
Prepolymer Synthesis.....	41
Film Formation and Characterization	43
References and Notes.....	47
CHAPTER 4 EFFECTS OF DIRECTED ARCHITECTURE IN EPOXY FUNCTIONALIZED PREPOLYMERS FOR PHOTOCURABLE THIN FILMS	48

Introduction.....	49
Experimental.....	52
Materials.....	52
Methods.....	54
Results and Discussion.....	56
Conclusions.....	77
References and Notes.....	79
CHAPTER 5 PHOTOPOLYMERIZATION RATE AND PREPOLYMER EPOXIDE LOCATION ON NETWORK MORPHOLOGY.....	82
Introduction.....	82
Experimental.....	84
Materials.....	84
Methods.....	85
Results and Discussion.....	87
Conclusions.....	99
References and Notes.....	101
CHAPTER 6 EFFECT OF ACRYLATE GROUP PLACEMENT AND SYNTHETIC ROUTE ON PHOTOPOLYMER NETWORK FORMATION.....	104
Abstract.....	104
Introduction.....	105
Experimental.....	108
Materials.....	108
Methods.....	110
Results and Discussion.....	111
Conclusions.....	127
References and Notes.....	129
CHAPTER 7 EFFECTS OF MONOMER COMPOSITION AND ENVIRONMENTAL IMPACT ON CATIONIC PHOTOPOLYMERIZATION.....	133
Introduction.....	133
Experimental.....	135
Materials.....	135
Methods.....	136

Results and Discussion	137
Conclusion	153
Notes and Referenes	155
CHAPTER 8 CONCLUSIONS AND RECOMMENDATIONS	157

LIST OF TABLES

Table 4.1 Prepolymers used in this study.	53
Table 5.1 Prepolymers used in this study	85
Table 6.1 Prepolymers used in this study.	110
Table 7.1 Conditions for DOE screening of photopolymerization conditions for cationic photopolymerization.....	138
Table 7.2. Responses from screening experiments	139

LIST OF FIGURES

Figure 1.1. Common monomer (A-F) and photoinitiator (G-H) molecular structures for radical photopolymerization.	7
Figure 1.2. Common monomer (A-E) and photoacid generator (F-G) chemical structures used in cationic photopolymerization.	10
Figure 1.3. General structures of common RAFT agents dithiobenzoates (A), trithiocarbonates (B), and dithiocarbamates (C).	18
Figure 2.1. Molecular structures of chemicals used in this work. Shown are diaryl iodonium hexafluoroantimonate (PC-2506, A), 2,2-dimethoxyphenyl acetophenone (DMPA, B), 1,6 hexanediol diacrylate (HDDA, C), butyl acrylate (BA, D), cycloaliphatic epoxide methacrylate (METH-B, E), 3,4-Epoxy cyclohexylmethyl 3,4-epoxycyclohexanecarboxylate (EEC, F), bis[(2,2-dihydromethyl) butyl] ether (DOX, G), Neopentyl diglycidyl ether (NPGDGE, H), Limonene Monoxide (LMO, I), Limonene Dioxide (LDO, J), (1-(diethoxyphosphinyl)-2,2-dimethylpropyl 1,1-dimethylethyl nitroxide) (SG-1, K), Methyl-2-methyl-3-nitro-2-nitrosopropionate (NMMA, L), Dibenzyl trithiocarbonate (DBTTC, M).	44
Figure 4.1. Normalized heat flow as a function of time during photopolymerization of formulations using end 20k16 (—●—) and random 20k16 (—□—) 70 wt% oligomer species using NPGDGE (A) and EEC (B) as reactive diluents and photopolymerized at 65 mW/cm ² . 2 wt% PC-2506 and 1wt% ITX were used as a photoinitiators.	58
Figure 4.2. Storage modulus and Tan (δ) profiles as a function of temperature of end 20k16 (—●—) and random 20k16 (—□—) oligomer species formulated with 70 wt% EEC. All samples were photopolymerized with 2 wt% PC-2506 and 1wt% ITX at 13.5 mW/cm ² for 30 minutes.	61
Figure 4.3. Stress-strain behavior in tensile mode at 30°C of end 20k16 (—●—), end 13k8 (—□—), and random 20k16 (—○—) oligomer species formulated with 30 wt% EEC. All samples were photopolymerized with 2 wt% PC-2506 and 1wt% ITX at 13.5 mW/cm ² for 30 minutes.	63
Figure 4.4. Creep test at 30°C using constant application of 4 MPa of Stress on end 13k8 at 60 wt% (—●—), 70 wt% (—□—), and 60 wt% random 13k8 (—○—) oligomer species formulated with 40 wt% EEC. All samples were photopolymerized using 2 wt% PC-2506 and 1wt% ITX at 13.5 mW/cm ² for 30 minutes.	65
Figure 4.5. AFM Phase images of 70 wt% end 13k8 (A) and random 13k8 (b) oligomers formulated with 30 wt% EEC. All samples were photopolymerized using 2 wt% PC-2506 and 1wt% ITX at 13.5 mW/cm ² for 30 minutes 2 wt% PC-2506 and 1wt% ITX at 13.5 mW/cm ² for 30 minutes.	68
Figure 4.6. Storage modulus and Tan (δ) profiles as a function of temperature of end 20k16 with 60 wt% (—●—) 70 wt% (—□—), 80 wt% (—×—) and	

90 wt% (—□—) oligomer species formulated with the corresponding wt% EEC. All samples were photopolymerized using 2 wt% PC-2506 and 1wt% ITX at 13.5 mW/cm ² for 30 minutes.	70
Figure 4.7. Stress-strain behavior at 30°C of with 60 wt% (—●—) 70 wt% (—□—), 80 wt% (—×—) and 90 wt% (—□—) end 20k16 species formulated with the corresponding wt% EEC. All samples were photopolymerized using 2 wt% PC-2506 and 1wt% ITX at 13.5 mW/cm ² for 30 minutes.	72
Figure 4.8. Storage modulus and Tan (δ) profiles as a function of temperature of end 16k8 % (—●—) and end 20k16 (—□—) oligomer species formulated with 40 wt% EEC. All samples were photopolymerized using 2 wt% PC-2506 and 1wt% ITX at 13.5 mW/cm ² for 30 minutes.	75
Figure 4.9. Stress-strain behavior at 30°C of 60 wt% end 16k8 (—●—) and end 20k16 (—□—) species formulated with 40 wt% EEC. All samples were photopolymerized using 2 wt% PC-2506 and 1wt% ITX at 13.5 mW/cm ² for 30 minutes.	76
Figure 5.1. Photo-DSC (PDSC) profiles for center and randomly functionalized prepolymer/DOX formulations with and without LDO. Photopolymerizations were initiated with 2 wt% PC-2506 using 280-400 nm light at 25 mW/cm ²	89
Figure 5.2 Functional group conversion profiles for oxetane (A) and epoxide (B) groups in 60 wt% prepolymer formulations. Photopolymerizations were initiated with 2 wt% PC-2506 using 280-400 nm light at 25 mW/cm ²	90
Figure 5.3. Storage modulus(A) and the tan (δ) (B) profiles as a function of temperature for both center and random prepolymer formulations with and without a terpene oxide accelerant. All samples where photopolymerized using 2 wt% IHA under standard room temperature conditions at 25 mW/cm ² for 10 min. All samples were annealed at 60°C for 24 hours.	93
Figure 5.4. Stress-strain behavior in tensile mode at 30°C for both center and randomly functionalized prepolymers formulated with and without LDO as an accelerant. All samples where photopolymerized using 2 wt% IHA under standard room temperature conditions at 25 mW/cm ² for 10 min. All samples were annealed at 60°C for 24 hours.	95
Figure 5.5. AFM Phase images of 60 wt% center (A and B) and random (C and D) prepolymers formulated with 40 wt% DOX. Figure 5.5B and 5.5D incorporate 5 mol% LDO. All samples were photopolymerized using 2 wt% PC-2506 at 25 mW/cm ² for 10 minutes. All samples were annealed at 60°C for 24 hours.	97
Figure 5.6. Water contact angle measurements for lauryl methacrylate/ oxetane thin films. All samples were photopolymerized using 2 wt% PC-2506 at 25 mW/cm ² for 10 minutes. All samples were annealed at 60°C for 24 hours.	99
Figure 6.1. Acrylate functional group conversion of prepolymer/HDDA formulations as a function of time is shown. Figures 1A and 1C show fractional conversion for formulations utilizing nitroxide synthesized end	

and random structured prepolymers respectively. Figure 1B and 1D show the fractional conversion of formulations using end and randomly functionalized prepolymers synthesized via the RAFT Mechanism. Samples were photopolymerized with 0.5 wt% DMPA at 10 mW/cm ² .	114
Figure 6.2. Storage modulus as a function of temperature for prepolymer/HDDA formulations. Figures 6.2A and 6.2C show the storage modulus as a function of temperature for NMP synthesized end and random prepolymers, respectively. Figures 6.2B and 6.2D show storage modulus as a function of temperature for RAFT synthesized prepolymer formulations. All samples were photopolymerized at 10 mW/cm ² with 0.5 wt% DMPA for 10 minutes.	117
Figure 6.3 Tan (δ) profiles as a function of temperature for all prepolymer/HDDA formulations. Figures 6.3a and 6.3c show the tan (δ) as a function of temperature for NMP synthesized end and random prepolymers respectively. Figures 6.3b and 6.3d show Tan (δ) as a function of temperature for RAFT synthesized prepolymer formulations. All samples were photopolymerized at 10 mW/cm ² with 0.5 wt% DMPA for 10 minutes.	119
Figure 6.4. Stress strain behavior at 25°C for end and randomly functionalized prepolymer formulations synthesized by NMP (A) or RAFT (B). All samples were photopolymerized at 10 mW/cm ² with 0.5 wt% DMPA for 10 minutes.	122
Figure 6.5. Strain as a function of time for end and randomly functionalized prepolymer formulations synthesized by NMP (A) or RAFT (B). 1 MPa of stress was applied for 10 minutes. Strain recovery was observed for 30 minutes after the initial strain was removed. All samples were photopolymerized at 10 mW/cm ² with 0.5 wt% DMPA for 10 minutes.	124
Figure 6.6. Shrinkage Stress normalized to the N-Random sample. All samples were photopolymerized at 10 mW/cm ² with 0.5 wt% DMPA and 40 wt% HDDA for 10 minutes.	127
Figure 7.1. Normalized Rate of Polymerization for Run 1 vs Run 5 as described in Table 1. All samples were photopolymerized at 10 mW/cm ² with 2 wt% PC-2506 for 2.5 minutes.	140
Figure 7.2. Pareto charts for models predicting percent monomer conversion (A) and maximum normalized rate of polymerization (B).	141
Figure 7.3. Rate of photopolymerization for NPGDGE, EEC, and DOX monomers when homopolymerized. All samples were photopolymerized at room temperature and 10 mW/cm ² , using 2 wt% PC-2506 for 10 minutes.	144
Figure 7.4. Normalized rates of polymerization as measured via photo-DSC. All samples were photopolymerized at room temperature and 10 mW/cm ² , using 2 wt% PC-2506 as a photoacid generator initiator.	145
Figure 7.5. Conversion profiles for all formulations using common epoxide or oxetane monomers both neat and containing 5 mol% mono- and	

diepoxidized terpene accelerants. All samples were photopolymerized under at 30°C and 10 mW/cm² with 2 wt% PC-2506 for 10 minutes. 147

Figure 7.6. Storage modulus as a function of temperature of glycidyl ether (A), cycloaliphatic epoxy (B), and oxetane monomer systems (C) copolymerized with 5 mol% limonene mono- and dioxide. All samples were photopolymerized at 10 mW/cm² with 2 wt% PC-2506 for 10 minutes. 149

Figure 7.7. Tan (δ) as a function of temperature of glycidyl ether (A), cycloaliphatic (B), and oxetane monomer systems copolymerized with 5 mol% limonene mono- and dioxide. All samples were photopolymerized using 2 wt% PC-2506 under standard room temperature conditions at 10 mW/cm² for 15 minutes. 152

CHAPTER 1

INTRODUCTION

Polymer formulation is key when determining and tuning properties for designing crosslinked networks or polymer blends. Being able to tune a formulation via the constituent components is an important industrial tool commonly used to produce materials adequate for specific applications. In thermoplastic elastomeric resins, formulations often consist of block copolymers or polyurethane materials. In both cases, a combination of hard and soft domains are present at the nanoscale to enhance various properties of the network. The hard domains in block copolymers and polyurethanes typically originate from chemical and/or physical interactions, respectively. In block copolymer materials the differences in hard and soft domains are largely dictated by the monomers used in the synthesis. Usually a high glass transition temperature monomer is selected based on application, with styrene and methyl methacrylate among the most common.^{1,2} On the other hand, a low T_g monomer segment then creates a soft, flexible block. This low T_g segment can consist of several different monomers, with double bond containing elastomer rubbers, such as butadiene or isoprene, frequently selected.^{3,4}

Polyurethanes, meanwhile, are generally created via the step-growth polymerization of diisocyanates and diols to form the urethane linkages.⁵ In polyurethane materials, much of the hard segment comes from the hydrogen bonding associated with the urethane group.⁶ This physical phenomenon accounts for much of the novelty and broad applications of polyurethanes by tuning the amount of hard physically linked domains and soft flexible chains.^{7,8} Correspondingly, the soft segments in polyurethane materials consist of long flexible diol or poly-ol segments. Much of the tailorability of

polyurethane materials stems from the selection of diol or polyol monomers as over 95% of industrially relevant materials use only 2 diisocyanates, methylene diphenyl diisocyanate and toluene diisocyanate.⁹ Other isocyanate monomers have been investigated though none have come close to the performance allowed by these two monomers.

This thesis draws inspiration from both types of thermoplastic elastomers due to their ability to combine multiple, seemingly contradictory properties into a single material. Through chemical and/or physical bonds, thermoplastic elastomers show both high elasticity and a strong ability to resist deformation via the incorporation of both soft and hard domains respectively.^{10,11,12} In traditional photopolymer systems little control over the resulting network structure can be achieved.¹³ However, better access to different thermomechanical properties could be achieved by having multiple domains within photocured systems. For instance, in this work, we use controlled radical polymerization to specially synthesize prepolymer molecules with epoxy moieties. These molecules then act to modify and potentially provide a specific structure to the resulting photopolymer network. By utilizing different locations of photo-reactive groups, such as epoxide or acrylate moieties, we have elucidated the effects of the structure of the prepolymer on the resulting thermomechanical properties. The mechanisms and aspects of both radical and cationic photopolymerization are key to understanding our research. Building on this discussion, an introduction to photocurable resin formulation will illustrate the necessity for each component in a photocurable resin while showing the shortcomings of current formulation methodologies. Synthesis techniques of various prepolymer species crucial to this project and photocurable formulations will be examined followed by the interaction

of these various oligomer and prepolymer species on network formation and photo-induced phase separation.

Radical Photopolymerization

Photopolymerization utilizes light to generate materials with broad applications, including but not limited to biomaterials, floor coatings, and 3D printing. The spatiotemporal accuracy of photopolymerization enables applicability to a wide variety of industrially relevant uses, and continued academic investigation. While multiple chemistries are available for photopolymerization, such as thiol-ene, base catalyzed reactions, and cationic photopolymerization, which will be discussed later, radical photopolymerization is perhaps the best understood, making it the most widely used industrially, allowing for a diverse catalog of widely available monomers to be produced.

Radical Photoinitiation

In radical photopolymerization, a Norrish type 1 or 2 initiation system begins the reaction via dissociation into radical species upon absorption of a photon. In a Norrish type 1 photoinitiation event, a single molecule absorbs a photon of light, reaching an excited singlet state and, through intersystem crossing to the triplet state, homolysis occurs to form the initiating radicals. This homolysis event generates two radical molecules as seen in Equation 1.



Each of these radicals may initiate the polymerization by forming the radical reactive species, though this is often not significant enough to effect the photopolymerization. One example is the common radical photo initiator Irgacure 651, the two radicals do not necessarily form equally reactive radicals though this is often over

looked. After these radicals are rapidly formed upon illumination, they may react with the monomer species to begin the polymerization reaction, as seen in equation 2:



Where M represents the unreacted monomer, M_1^* represents the new radical reacted species, and k_i is the initiation rate constant. The rate of initiation of the photopolymer reaction can thus be described as dependent on the consumption of these photoinitiated radicals, as described in equation 3.

$$R_i = 2\phi I_o \quad (3)$$

Where R_i is again the rate of initiation, ϕ is the quantum efficiency, and I_o is the intensity of the absorbed light.

Propagation

The propagation step in photopolymerizable systems involves the addition of monomer molecules onto the growing polymer chain as given by equation 4:



Where M_n^* represents a growing polymer radical, M represents unreacted monomer, and M_{n+1}^* represents the growing polymer chain with one more unit. The propagation rate constant k_p is generally considered independent of the chain length of the growing polymer chains. The rate of polymerization can therefore be described as the disappearance of unreacted monomer species by the equation 5:

$$R_p = k_p [M][M^*] \quad (5)$$

Termination

As the polymerization continues to high conversion, propagation and termination slow as the majority of the monomer is consumed. There are two basic mechanisms by which termination reactions occur, as seen below in equations 7 and 8:



where the rate constants for termination by combination and disproportionation are indicated by k_{tc} and k_{td} , respectively. The difference between these mechanisms is based in how the two radical polymer chains interact during the termination event. In a combination termination reaction, the radicals form a new bond by combining the two growing polymer chains. Meanwhile, in a disproportionation reaction, one polymer chain will abstract a hydrogen from the other chain yielding two individual polymer chains. In order to derive a general rate equation, it is assumed that the initiation rate is equal to the total rate of termination, commonly known as the pseudo-steady state assumption. The pseudo-steady state assumption then allows development of the general rate of polymerization equation as follows:

$$R_p = k_p [M] \left(\frac{R_i}{2k_t} \right)^{1/2} \quad (9)$$

in which equation 3 can be substituted in for the R_i value to make a general rate of photopolymerization, shown in equation 10:

$$R_p = k_p [M] \left(\frac{\phi I_0}{k_t} \right)^{1/2} \quad (10)$$

Applications and Shortcomings

Radical photopolymerization has been used in a vast variety of applications, ranging from coatings and adhesives to biomedical devices and 3D printing.^{14,15} Several common monomers can be seen below in Figure 1.1. Photopolymerization is a growing field within the realms of polymer and material science. With diverse applications, ranging from coatings and adhesives to newer technologies such as 3D printing photopolymerization continues to increase its prevalence and influence. This research examines fundamental structure property relationships between large prepolymer structures within a formulation and the resulting impact on thermo-mechanical properties in photocurable resins. Most prepolymer molecules utilize a “one pot” synthesis with little to no control over the placement of photoreactive moieties such as epoxies and (meth) acrylates. We have utilized novel prepolymer molecules synthesized using in-situ nitroxide mediating radicals that allow direct control over the placement of reactive groups. The ability to control the location of reactive groups in prepolymer molecules can also lead to the formation of multiple domains within the resulting photocured thermoset. This separation is achieved by concentrating the reactive groups at specific locations in the prepolymer backbone, e.g. at the end or near the center of the prepolymer molecule. The nonreactive groups may form one domain within the thermoset network while the reactive portion of the prepolymer forms a second phase with reactive diluent molecules. Additionally, various architectures allow greater control over polymer network formation and crosslink density. Through these manipulations of macromolecular architecture, we have been able to manipulate various thermo-mechanical properties. Using the architected materials, we have been able to generate materials with multiple glass

transitions while also increasing the rate of reaction and total conversion as compared to randomly functionalized control formulations. Lastly, the use of architected prepolymers increases the overall strength and toughness of the formulation again without altering the monomers used in the formation of the photocured thermosets.

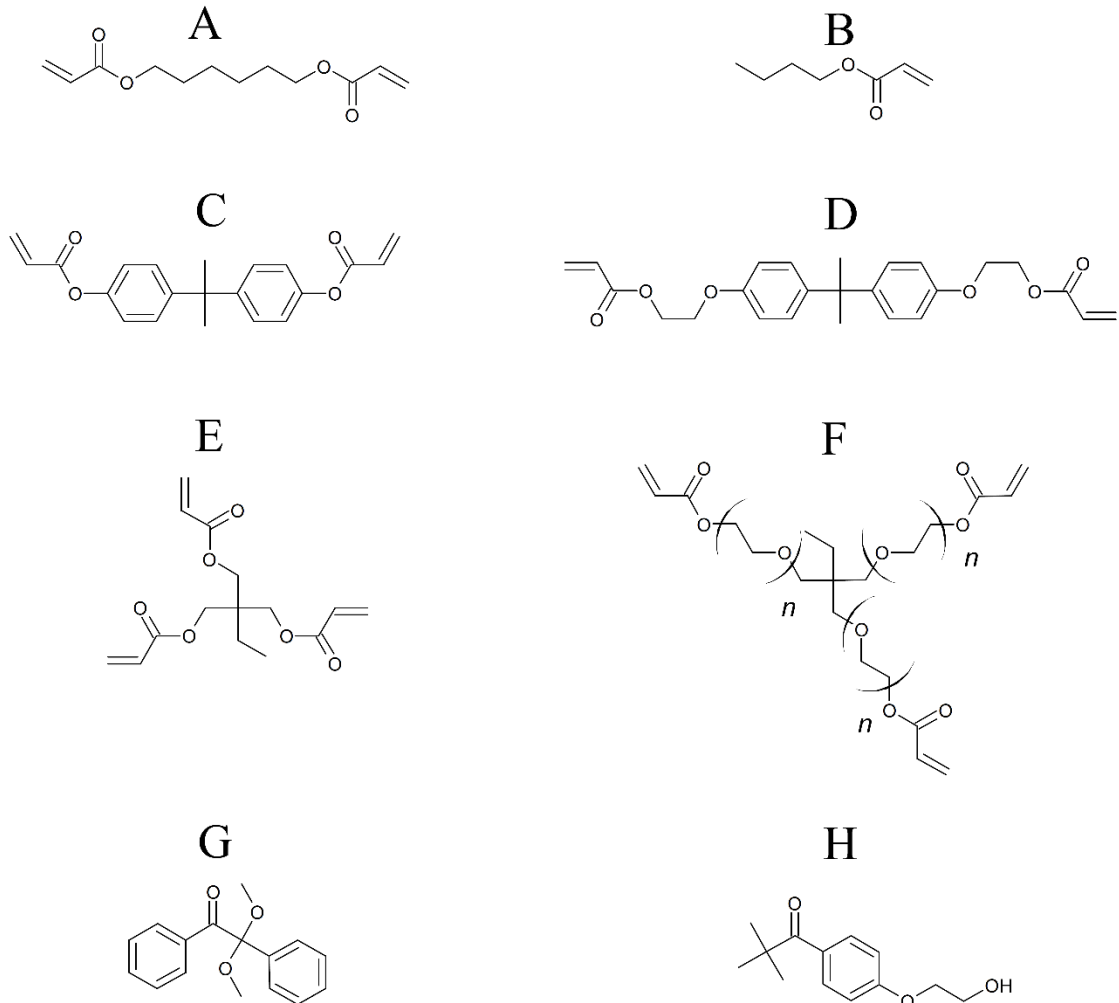


Figure 1.1. Common monomer (A-F) and photoinitiator (G-H) molecular structures for radical photopolymerization.

The wide variety of monomer chemistries and rapid cure rates associated with radical photopolymerization allow for the diversity of these applications. Small amounts of low

molecular weight/viscosity monomers of a difunctional monomer, such as hexanediol diacrylate, are often employed in the adhesive area where the polymer network must be easily flowable to promote adhesion to a substrate.¹⁶ On the other hand, 3D printing and coatings formulations favor higher concentrations of multifunctional monomers in their formulations.^{17,18} These highly functional monomers allow for high degrees of crosslinking, which in turn significantly increase the overall stiffness and abrasion resistance of these systems.

While industrial applications capitalize on the versatility of radically-based photopolymerization, several limitations involving radical photopolymerization in these applications still exist and need to be overcome. Foremost, oxygen inhibition can limit the processing of photopolymer materials requiring one or more methods to overcome the inhibition.¹⁹ Environmental oxygen exists in the triplet state and can readily quench both initiating radicals and propagating polymer chains in the formulation. This problem is exacerbated in thin film applications as the oxygen can diffuse through the entire film instead of being limited to the top several microns.¹⁹ Efforts to combat oxygen inhibition include inerting the environment with a nonreactive gas, such as nitrogen or argon, though this method is often avoided at the industrial level due to the associated significant costs associated.²⁰ Alternatively, increasing the number of initiating radicals by increasing the photoinitiator concentration is often more cost efficient, although it can lead to bleaching and yellowing issues in the final film or product.⁵

Another significant issue with radical photopolymerization is the shrinkage stress. In photocurable resins, volumetric shrinkage can reach up to 27% in (meth)acrylate systems.²¹ This shrinkage typically results from the free volume change as the individual

monomer molecules polymerize, becoming one polymer chain.²² Although many photopolymer applications benefit from hardness and abrasion resistance stemming from multifunctional monomers, the concentration of these multifunctional prepolymers and oligomers is directly related to the shrinkage and the shrinkage stress associated with the photopolymerization.¹³ The combination of shrinkage and shrinkage stress may cause samples to break prematurely if improperly formulated, but may also cause premature breakage even when the multifunctional oligomers are balanced with a reactive diluent.²³ With that said, one method to alleviate the shrinkage stress associated with small molecule polymerization is to include larger molecular weight species.²⁴ By increasing the molecular weight of the multifunctional species, the overall free volume change will decrease. Unfortunately, with increasing prepolymer content comes little control over the resulting photopolymer network. The resulting monomers produce more flexible films, which may not be favorable to formulations needing a high-modulus, stiff material.²⁵ For these reasons new methods to control network heterogeneities and modify photocurable formulation will be integral to the continued develop of photopolymerization.

Cationic Photopolymerization

Cationic ring opening polymerizations may be initiated via photo-acid generators and offer different properties than the more commonly used radical photopolymerization. The ring opening reaction experiences much less shrinkage than traditional radical photopolymerization, making these applications suited to coatings for complex and fragile electronic components and circuit boards.²⁶ Additionally, cationic photopolymerization can be used to complement radical photopolymerization in 3D

printing applications due to their relatively slower polymerization but higher overall strength. Figure 1.2 shows common monomer and photo-acid generator used in cationic photopolymerization.

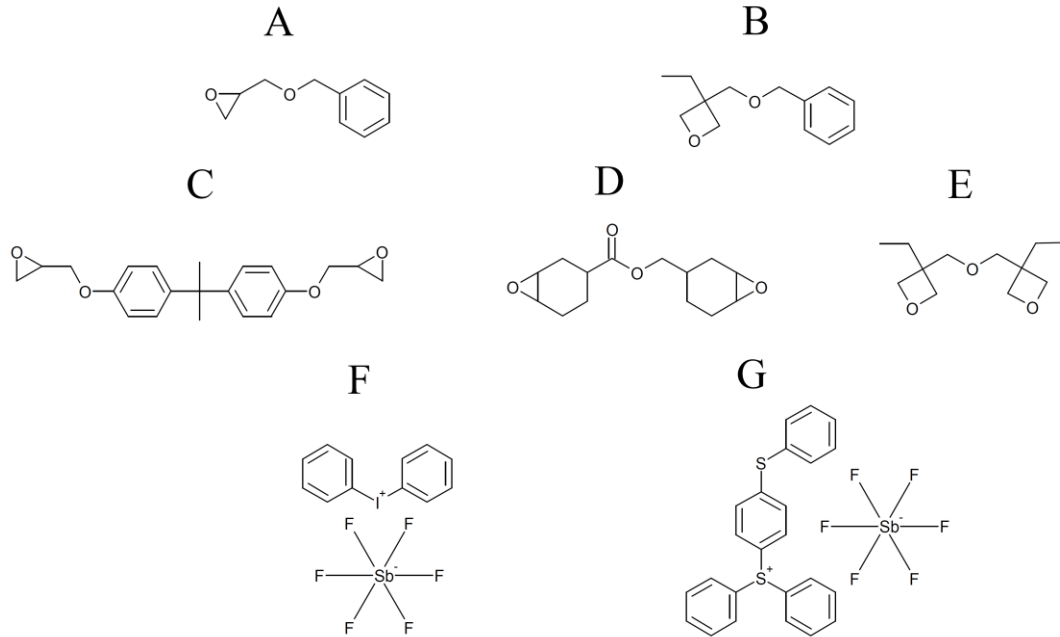


Figure 1.2. Common monomer (A-E) and photoacid generator (F-G) chemical structures used in cationic photopolymerization.

Cationic Photoinitiation

Photoacid generators absorb light, leading to the initiation of cationic photopolymerization from the formation of a super acid. The invention of iodonium and sulfonium salts in the 1970s was crucial to the industrial application of cationic photopolymerization. These salts exhibit absorbance ranges which overlap with the output of commonly used medium pressure mercury arc lamps.²⁷ Additionally, each salt displays not only differences in UV absorption but also thermal stability with iodonium salts forming super acids as low as 60°C, while sulfonium salts are thermally stable at

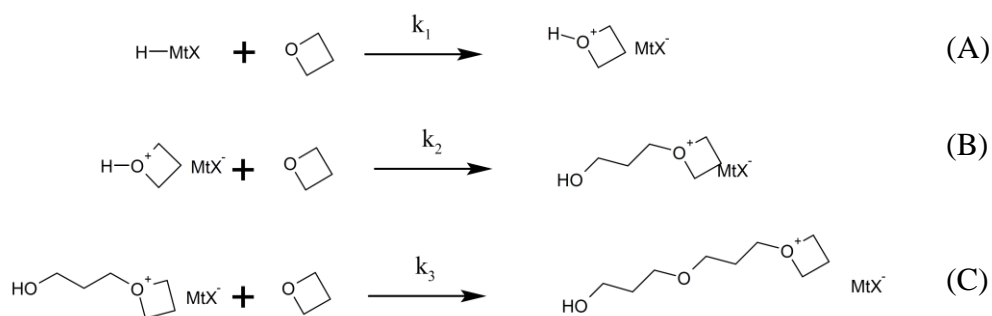
temperatures as high as 120°C. Upon illumination, these onium salts dissociate to provide a super acid as in the simplified example mechanism shown below for an iodonium salt:



After forming the super acid, this molecule proceeds to react with the cationically polymerizable monomers. This step can often be the rate limiting step as the secondary oxonium ion may be stable. When this is the case, as is observed in oxetane monomers²⁸, an inhibition time is frequently observed until the equilibrium shifts from the secondary oxonium ion to the tertiary oxonium ion. The propagating center for the cationic ring opening reaction is formed once the tertiary oxonium ions are formed.^{29,30}

Propagation and Transfer

As in radical photopolymerization, the propagation step in cationic photopolymerization involves adding monomer species to the propagating chain. Instead of the reaction occurring through a double bond, as is the case with radical polymerization, the various oxirane and oxetane monomers experience a ring opening reaction as observed below in Mechanisms A-C



In mechanism A the recently formed super acid protonates the monomer species to form a secondary oxonium ion. Mechanism B shows the formation of a tertiary oxonium ion which is the propagating center in cationic photopolymerization. Mechanism C then shows the actual propagation of cationic center.^{31,32}

Termination

Termination in cationic photopolymerization requires the recombination of the propagating cation and the anion from the photo-acid generator.³³ The recombination reaction does not occur with much frequency which is why cationic ring opening polymerizations are considered living polymerization. The frequency of this event is partially governed by the size of the anion with larger anionic species recombining far less than small anions.³³

Uses and Shortcoming

As mentioned briefly above, cationic photopolymerization can be used in many of the same systems as radical based photocurable resins.³⁴ A main limitation of cationic photopolymerization is increased cost of monomers compared to radical systems. Indeed, as cationic photocurable resins show less shrinkage than radical formulations, they are often employed in electronic applications where the shrinkage associated with radical polymerization would damage the delicate electronic materials.³⁵

Additionally, cationic photopolymerization is frequently used in the photopolymerization of composite materials.³⁶ Composite materials are a class of materials which utilize fillers, frequently in the form of micro and nanoparticles, to increase overall toughness and durability while maintaining low weight crucial to various applications such as aerospace and construction materials.³⁷ A primary reason that

cationic photopolymerization is useful for composite materials is the long living nature of the cationic propagating centers. Since termination is so rare in cationic photopolymerization, these systems can see high conversions even after the initiating light source has been extinguished (i.e. dark curing).³⁸ Another area that takes advantage of this dark curing ability is in hybrid 3D resins.³⁹ In these systems both cationic and radical monomer systems are combined. The radical system is used to establish a preliminary network. The cationic system is then allowed to continue to cure in the dark to increase the strength of the final product.

As with radical photopolymerization the impact of environmental factors are important to consider. While cationic photopolymerization is not effected by molecular oxygen, these systems experience large degrees of chain transfer in the presence of water or other hydroxyl containing systems.³² Indeed, the presence of hydroxyl groups can significantly increase the induction period for both epoxide and oxetane photocurable systems. Further, if hydroxyl groups become protonated, the resulting photopolymer network is significantly affected. As the concentration of the hydroxyl groups increases, the T_g consequently decreases as the distance between crosslinks decreases and overall polymer network becomes more uniform.

Photopolymerization Formulations

For standard photocurable resins four components are frequently incorporated including photoinitiator, reactive diluent/monomer, oligomer, and fillers. In general, the photoinitiator is a mandatory component for a photocurable formulation as it is what allows the polymerization reaction to be triggered by UV or visible light. In research and industry, 2,2-dimethoxy-2-phenylacetophenone and 1-[4-(2-hydroxyethoxy)-phenyl]-2-

hydroxy-2-methyl-1-propane-1-one are two of the most commonly used radical photoinitiators while triaryl sulfonium and diaryl iodonium salts are common in cationic photopolymerization work. In industrial formulations combinations of photoinitiators are often employed due to uneven light penetration through the system.⁴⁰ As UV light often does not penetrate thick systems well, a photoinitiator that absorbs in the visible spectra is often employed to ensure a thorough cure of the system. As cationic centers do not properly terminate, dark cure is used to increase the conversion of epoxy and oxetane monomers.⁴¹

The reactive diluent or monomer component is selected for a variety of reasons. Photocurable formulations are designed to be highly reactive, and cure rapidly all while maintaining a high conversion of functional groups. In order to achieve these goals low viscosity is important to allow the high processing speeds of photocurable resins. These monomers can be selected for a variety of reasons such as super absorbancy, antimicrobial properties, super hydrophobicity, or to add a stimuli responsive component such as heat, light, or pH.⁴²⁻⁴⁷ Furthermore, the monomer component can be used to easily tune both the ultimate T_g of a photocurable formulation altering the degree of crosslinking in the system. Reactive diluents also serve to modify the viscosity of the formulation.^{48,49}

Oligomers govern the bulk properties of the photocurable resin. These reactive large molecules are often multi-acrylate or epoxy materials which will crosslink the system. The crosslinking species must be carefully considered as crosslinking rapidly builds the viscosity of a solution until it is essentially a solid.²² As the network begins to gel the propagation reaction may become diffusionally limited, meaning propagation requires monomer to diffuse to the propagating chains that are otherwise confined in the

polymer network.^{21,50} This can create different local regions of high and low crosslinked material. This network heterogeneity with significantly different microenvironments can lead to increased shrinkage stress.^{51,52}

Fillers such as clay and silica nanoparticles may be used to improve properties.⁵³⁻⁵⁵ These materials will not only modify the rheology and network formation of the material but can often increase the modulus while decreasing shrinkage of the material. Thermal properties can also be increased as the thermal degradation decreases with increased filler content. Dental applications will often employ functionalized silica nanoparticles to decrease shrinkage, match coefficients of thermal expansion as well as to modify the refractive index of a given resin.⁵⁶ This is critical for dental applications as it allows proper placement of the resin on the tooth.

Controlled Radical Polymerization

As stated above one important aspect of a photopolymer resin is the choice of oligomer as it dictates much of the bulk mechanical properties of the photocured thin films.⁵⁷ While most films will use relatively small molecules of less than 1 kDa, a promising avenue of study is to incorporate molecules that are 1 to 2 orders of magnitude larger.²⁴ Controlled radical polymerization (CRP), including nitroxide mediated polymerization (NMP) and reversible addition and fragmentation chain transfer (RAFT), provides versatile synthetic methods for the synthesis of well-defined large prepolymers for incorporation into photocurable formulations.⁵⁸

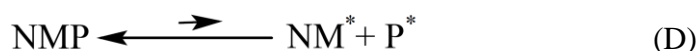
In order for a radical polymerization to be considered controlled several conditions must be met.^{5,58} One of the more important is that the polydispersity index, PDI, should be below 1.5. If the PDI of a sample is above 1.5 it means that either the

reversible termination or chain transfer was insufficient to actually produce well defined prepolymer molecules. To obtain a PDI below 1.5 requires the polymer chains to not only grow at approximately equal rates, but also for the chains to begin growing at almost the same time. Additionally, specific targeted molecular weights can be generated either through the monomer or CRP agent concentration. Many CRP techniques also allow for re-initiation of the growing polymer chains which allows for facile synthesis of block copolymers.

Nitroxide Mediated Polymerization

Nitroxide mediated polymerization is a form of controlled radical polymerization that utilizes the extremely stable nitroxide radicals to control the polymerization. NMP was first discovered in the 1980's and was initially used to create well defined polystyrene molecules without the use of anionic polymerization which is far more susceptible to contamination. NMP utilizes various nitroso and nitroxide compounds which form extremely stable radicals, which through thermally reversible termination reactions can control the polymerization.^{59,60}

Stable nitroxide radicals can control the polymerization reaction via a reversible termination reaction as seen in the mechanism below,



NMP favors the combined state (P) for the mediating radical which prevents continued propagation, which would prevent control of the reaction and the polymerization would proceed as normal.^{61,62} In the NMP mechanism, the nitroxide radical is activated via multiple sources including both heat and light which will be discussed briefly below.^{63,64}

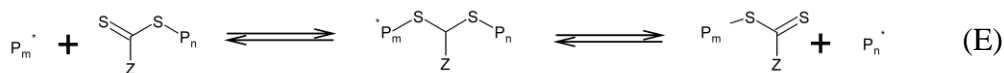
In general, several factors can affect not only the rate of nitroxide mediated polymerization but also the relative monomer efficiency including the steric hindrance of the nitroxide radical. Bulky and sterically hindered radicals are more compatible with active monomers. While somewhat counter intuitive, the additional steric bulk increases the rate of recombination with more active radicals and facilitates the termination reaction.^{65,66} For example, the well-studied and very bulky SG-1 nitroxide radical is able to produce well defined acrylic prepolymers while the less sterically hindered TEMPO molecule cannot control this reaction.⁶⁷⁻⁶⁹ Another simple method of altering the rate of NMP is to increase the intensity of the NMP activation source, such as light or heat. In order to produce photo activated nitroxide mediating radicals highly conjugated double bonds or aminated photoinitiator precursors should be selected for the synthesis of the NMP photoinitiator.^{63,70}

Reversible Addition Fragmentation Chain Transfer (RAFT)

A second method of controlled radical polymerization is the RAFT process. While NMP utilizes reversible termination to control the polymerization reaction, RAFT utilizes rapid chain transfer in order to allow the propagating chains to grow at the same rate. The ease of use has allowed RAFT to become a major tool used by many polymer chemists. Further, the growing chains are never inactive which leads to most RAFT processes being faster than NMP processes.

As mentioned the RAFT mechanism occurs via rapid chain transfer involving RAFT agents. When using these agents, the growing polymer chain radical exchange occurs between a sulfur carbon double bond as shown in Mechanism 5. The propagating radical forms a new bond to the sulfur atom and the leaving group on the other sulfur

atom forms a new radical which can go on to either start a new polymer chain or to exchange with another RAFT agent, prior to RAFT equilibrium, and allow the propagating chains to begin reacting again as seen in the reaction mechanism scheme below once equilibrium is established.



Once the RAFT equilibrium has been established, the reaction will continue until the propagating chains begin to terminate.⁷¹ The RAFT agents must be selected such that the radical adduct does not immediately favor termination.⁷² Figure 1.3 below includes common general structures of RAFT agents including trithiocarbonates, dithiocarbamates, and dithiobenzoates.

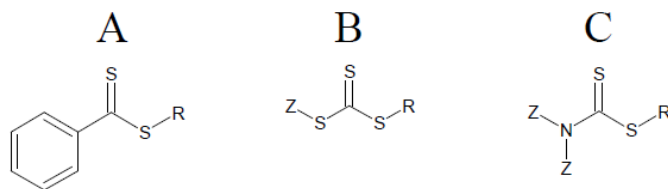


Figure 1.3. General structures of common RAFT agents dithiobenzoates (A), trithiocarbonates (B), and dithiocarbamates (C).

Basic characteristics of each type of RAFT agent that aid in their general selection are the R and Z groups as shown in Figure 1.3 where R is the initial radical leaving group and Z acts to stabilize the corresponding RAFT radical.⁷³ The dithiobenzoates tend to have the fastest chain transfer coefficients due to the high degree of resonance from the benzoate moiety.⁷⁴ On the other hand, these materials also undergo hydrolysis more readily than other agents making them slightly more difficult to use than other options.⁷⁵ For trithiocarbonates it is important to consider both the Z group, which modifies the resonance of the RAFT reaction, and R group, which is the original leaving radical

adduct from the RAFT agent. By selecting more stable radical adducts, less reactive monomers such as methyl methacrylate and styrene can be controlled while more reactive monomers like methyl acrylates require a more reactive species to reinitiate the polymerization reaction.^{71,76} Meanwhile, the Z group on a RAFT agent is meant to control the sulphur-carbon-sulphur (SCS) bond exchange rates which will affect the overall polymerization rate and also affect monomer compatibility. Faster chain transfer exchanges, such as with the dithiobenzoates, allow for the larger degrees of monomer compatibility. However, for less reactive monomers such as vinyl esters, a lower degree of chain transfer is necessary; otherwise, the chain transfer reaction will essentially dominate the overall reaction, preventing propagation completely.^{71,77} For these monomers, the dithiocarbamate family of RAFT agents are most useful. Further, dithiocarbamates can be tuned by the pH of the reaction to favor certain monomers.^{78,79}

For RAFT produced polymers, the highly conjugated double bonds in the RAFT agent frequently give these compounds a highly colored appearance ranging from yellow to red/pink appearances. If the SCS bond is removed, the color of the polymer frequently disappears post purification allowing greater application. Two primary methods of removing the RAFT agent from the polymer system include aminolysis and hydrolysis.^{75,80} The aminolysis reaction is of particular use when using trithiocarbonates as a thiol reactive group is formed which can facilitate further derivatization or polymerization. Hydrolysis meanwhile can be difficult to achieve as most common bases, such as sodium hydroxide are insoluble in most organic solutions. Further, the hydrolysis pathway to remove the RAFT agent can produce a variety of different species at the head of the polymer chain making this typically less viable.

Applications of Controlled Radical Polymerization

The ability to produce specific block copolymers through CRP has provided significant advances in a range of applications including adhesives, microelectronics, and stimuli responsive materials.^{71,81,82} These materials consist of repeating blocks of different monomer species in order to obtain specific properties. Thermoplastic elastomers, often consisting of a triblock copolymer with hard-soft-hard structure, have been of particular focus in recent years and has included the renewable sources for both monomers to produce both hard and soft segments.^{83,84} Both NMP and RAFT produced polymers are also used for surface modification of nanoparticles and other surfaces.^{85,86} In these instances the grafting from approach is most common where the NMP or RAFT agent is initially attached to the surface and the growing polymer chain grows from this initial reaction site. This CRP technique has been used for many applications including nonstick coatings from fluoro-methacrylates and temperature responsive behavior from various acrylamide monomers.^{87,88}

Controlled radical polymerization technology is also used in the development of hyperbranched copolymer materials.⁸⁹ In contrast to traditional linear copolymer thermoplastics, these materials each have multiple propagating centers tied to a central node. These materials have significantly different rheology than their linear counterparts which can significantly alter their thermomechanical properties when included in photopolymer based resins where the hyperbranched polymers raise both T_g and monomer conversion.⁹⁰ They are also used as additives in otherwise photocurable coatings in order to improve scratch resistance and anti-static properties. Another common application is the formation of nanoparticles for drug delivery.⁹⁰⁻⁹² The size of

the nanoparticle and degree of grafting can directly affect not only the loading of the drugs but also the types of drugs that can be delivered.⁹³

Photopolymer Networks

Photopolymer networks established when using conventional oligomers are often largely heterogeneous with regions of higher and lower cross-link density.^{51,13,94} These heterogeneities result in the high degree of shrinkage stress often observed in traditional photocurable systems. Pockets of high crosslinking are common in multi-functional photocurable systems as once one of the acrylate or epoxy moieties has reacted the other reactive groups are now in close proximity to the propagating center.⁹⁵ This proximity to the propagating center in turn increases the likelihood of these groups to react and thus form areas of highly crosslinked molecules. Further, these heterogeneities increase as the functionality of the monomer increases from a difunctional system to tri- or higher functionality.^{95,96} Significant efforts have been devoted to overcome the shrinkage and resultant stress via heterogeneous network structure including step-growth networks and hybrid photopolymer systems.^{97,98}

Step Growth Networks

One common method to modify and increase homogeneity of the photopolymer network is the incorporation of chain transfer materials in the form of thiols and the use of thiolene photopolymerization. The incorporation of thiols transitions the standard radical chain growth mechanism into step growth.^{99,100} Initiating radicals react with the thiol molecules to form a thiyl radical. The thiyl radical then reacts with available -enes forming a covalent sulfur carbon bond.¹⁰¹ The resulting carbon based radical will abstract a hydrogen from an available thiol molecule to form a new thiyl radical and propagate the

polymerization. The step-growth nature of these materials causes less shrinkage stress as the network formed is highly uniform and amorphous.¹⁰² Additionally, thiol-ene reactions proceed readily in oxygen as the thiyl radicals are much more difficult to quench than traditional carbon centered radicals of photopolymerization.^{103,104} While promising, these systems have yet to see wide industrial implementation due to low T_g 's and processing concerns.

Another step-growth mechanism that has been examined in recent years is the copper catalyzed azide alkyne click (CuAAC) reaction.¹⁰⁵ In photopolymerization a radical PI is used to reduce Cu (II) to Cu (I) which will then act to catalyze the formation of the cyclic azide-alkyne group. While much of the work on fully CuAAC photocurable systems is still in its infancy, these systems appear to be produce similarly amorphous networks to thiol-ene systems.^{106,107} Modifications to the monomer structure have illuminated the relationship between T_g and backbone structure and show the versatility of these systems.^{107,108} The combination of versatility in T_g and amorphous network formation suggests lower shrinkage stress than traditional photopolymer networks.

Dual Networks

Another method for controlling photopolymer network structure is to form multiple semi-independent networks. The formation of multiple networks can be achieved via several methods but in almost all instances there exists a kinetic or mechanistic difference which allows each domain to form separately.^{98,109,110} If the first network is well formed then a secondary network may form around and possibly penetrate the first.³⁴ Each domain can be formed by triggering different UV sources or other orthogonal independent reaction technology.¹¹¹ In either case, the desirable

properties from each network can be synergistically combined when some degree of phase separation is observed, as is often the case with hybrid networks.

Hybrid networks are photocurable formulations traditionally comprised of both cationically and radically cured systems. General dual/hybrid networks can be formed of systems including networks with sacrificial bonds, epoxy amine systems, and materials that utilize non-stoichiometric systems.¹¹²⁻¹¹⁴ Hybrid systems have seen broad applications in rapid prototyping where a radical network can provide the initial structure and the cationic system can provide added strength via dark cure.¹¹⁵⁻¹¹⁷ These hybrid formulations may also show reduction in shrinkage and shrinkage stress compared to single network formulations.⁵² Hybrid formulations may also increase the conversion of both acrylate and epoxy moieties as well making them especially useful in industrial applications.¹¹⁵ It should be noted that, to obtain the benefits of phase separation and increased conversion, significant formulation tuning may be required, which has limited widespread industrial applications.

In addition to hybrid networks, adaptable networks provide a separate and distinct avenue of modifying photocured networks.¹¹⁸ Adaptive networks have bonds that can undergo secondary reaction to allow for network rearrangements which may alleviate shrinkage stress or promote shape memory properties. One technique to achieve network adaptability is to utilize the reversible Diels-Alder reaction. Another method to achieve adaptable networks is to utilize specially synthesized crosslinkable monomers with trithiocarbonate moieties used in RAFT.¹¹⁹ When RAFT monomers are incorporated into a network, the developing photocured network can relax through network rearrangements, thereby lowering the shrinkage stress of these materials. Further, since RAFT mechanism

allows rearrangements via radical interactions, monomers with RAFT moieties are compatible with thiol-ene photopolymerizations as well.¹²⁰ The rearrangements can occur until the photoinitiator has been completely consumed and no new radicals can be generated.¹²⁰ With these network rearrangements a form of photoplasticity and permeability can be achieved.¹²¹

Research Plan

This work seeks to explore the use of photocurable prepolymer molecules synthesized with two different controlled radical polymerization techniques to observe the relationship between prepolymer molecule structure and the resulting photocured network. While much research has been done on the use of macromolecules and ethoxylated acrylate monomers, little research has been done exploring the key structure property relationships between much larger prepolymer architectures and the resulting network morphology. Specifically, this work will explore designed prepolymers, reactive groups located at the center or end of a prepolymer with randomly distributed reactive groups acting as a control. Both acrylic and epoxy reactive groups will be examined and deliberately placed along a prepolymer backbone to form different structures. This work will also examine how various architectures lead to novel networks and provide specific structures to the photopolymer network.

Chapter 4 will discuss the effect of prepolymer structure in cationically curable systems and the resultant differences observed on both photopolymerization kinetics and thermomechanical properties. This chapter also examines the effects of formulation and ratio of reactive groups to prepolymer molecular weight on the photocured networks.

Chapter 5 will explore differences in cationic moieties for formulation and acceleration of

cationic photopolymerization of different groups. Chapter 6 builds on this work to explore center architectures as compared to prepolymers which statistically incorporate the reactive groups with both epoxy and oxetane reactive diluents. Chapter 7 examines the differences in network behavior based on the method of prepolymer synthesis as RAFT synthetic procedures allow incorporation of dynamic network relaxation in acrylic formulations. In summary, this work aims to provide a ground work for establishing structure property relationships between prepolymer architecture, network structure, and thermomechanical properties.

References and Notes

- (1) Anakabe, J.; Zaldua Huici, A. M.; Eceiza, A.; Arbelaiz, A. *J. Appl. Polym. Sci.* **2015**, *132* (42), 426-434.
- (2) Choi, S.-H.; Lee, W. B.; Lodge, T. P.; Bates, F. S. *J. Polym. Sci. Part B Polym. Phys.* **2015**, *144*, (54) 417-421.
- (3) Decker, C.; Viet, T. *Macro Chem. and Phys.* **2001**, *200* (2) 2204–2216.
- (4) Garate, H.; Goyanes, S. *Macromolecules*, **2014**, *47* (21), 7416–7423.
- (5) Odian, G. *Principles of Polymerization*, 4th ed.; 2004.
- (6) Fernández-d'Arlas, B.; Eceiza, A. *J. Polym. Sci. Part B Polym. Phys.* **2015**, *54* (7) 747-759.
- (7) Nguyen, L.-T. T.; Truong, T.; Tran Nguyen, H.; Le, L.; Nguyen, V. Q.; Le, T. Van; Luu, A. T. *Polym. Chem.* **2015**, *10*, (4) 124-132.
- (8) Kunwong, D.; Sumanochitraporn, N.; Kaewpirom, S. **2011**, *33* (2), 201–207.
- (9) <http://www.cdc.gov/niosh/topics/isocyanates/> (accessed Jan 1, 2016).
- (10) Bonart, R.; Germany, W. *Polymer*, **1979**, *20* (7), 1389–1403.
- (11) Stempfle, F.; Schemmer, B.; Oechsle, A.-L.; Mecking, S. *Polym. Chem.* **2015**, *6* (40), 7133–7137.
- (12) Zander, Z. K.; Wang, F.; Becker, M. L.; Weiss, R. A. *Macromolecules* **2016**, *49* (3), 926–934

- (13) Anseth, K. S.; Bowman, C. N.; Peppas, N. A. *Macromolecules* **1993**, *233*, 229–233.
- (14) Gorsche, C.; Seidler, K.; Knaack, P.; Dorfinger, P.; Koch, T.; Stampfl, J.; Moszner, N.; Liska, R. *Polym. Chem.* **2016**, *11* (11) 277-285.
- (15) Gigot, A.; Sangermano, M.; Capozzi, L. C.; Dietliker, K. *Polymer* **2015**, *68*, (54) 195–201.
- (16) Venkatraman, S.; Gale, R. *Biomaterials* **1998**, *19* (13), 1119–1136.
- (17) Marino, A.; Barsotti, J.; de Vito, G.; Filippeschi, C.; Mazzolai, B.; Piazza, V.; Labardi, M.; Mattoli, V.; Ciofani, G. *ACS Appl. Mater. Interfaces* **2015**, *7* (46), 25574–25579
- (18) Jungst, T.; Smolan, W.; Schacht, K.; Scheibel, T.; Groll, J. *Chem. Rev.* **2015**, *116* (3), 1496–1539
- (19) Ligon, S. C.; Husár, B.; Wutzel, H.; Holman, R.; Liska, R. *Chem. Rev.* **2014**, *114* (1), 557–589.
- (20) Kim, S. K.; Owusu-adom, K.; Guymon, C. A. *Polymer* **2009**, *50* (1), 363–364.
- (21) Szczepanski, C. R.; Pfeifer, C. S.; Stansbury, J. W. *Polymer* **2012**, *53* (21), 4694–4701.
- (22) Anseth, K. S.; Bowman, C. N. *Macromolecules*, **1992**, *48* (12) 489-502.
- (23) Park, H. Y.; Kloxin, C. J.; Abuelyaman, A. S.; Oxman, J. D.; Bowman, C. N. *Dent. Mater.* **2012**, *28* (11), 1113–1119.

- (24) Szczepanski, C. R.; Stansbury, J. W. *Eur. Polym. J.* **2015**, *67*, 314–325.
- (25) Anseth, K. S.; Walker, T. A.; Bowman, C. N. *Polymer* **1995**, *54*, (3), 166–182.
- (26) Penczek, S. *J. Polym. Sci. Part A Polym. Chem.* **2000**, *38*, (4) 1919–1933.
- (27) Crivello, J. V.; Lam, J. H. W. *J. Org. Chem.* **1978**, *43* (15), 3055–3058.
- (28) Crivello, J. V. *J. Polym. Sci. Part A Polym. Chem.* **2014**, *52*, (5), 432–441.
- (29) Verstegen, E. J. K.; Kloosterboer, J. G.; Lub, J. J. *Appl. Polym. Sci.* **2005**, *98* (4), 1697–1707.
- (30) Sasaki, H. *Oxetane Proj.* **2001**, *1*, (1) 11–15.
- (31) Sangermano, M.; Malucelli, G.; Bongiovanni, R.; Priola, A. *Eur. Polym. J.* **2004**, *40* (2), 353–358.
- (32) Dillman, B.; Jessop, J. L. P. *J. Polym. Sci. Part A Polym. Chem.* **2013**, *51* (9), 2058–2067.
- (33) Sipani, V.; Scranton, A. B. *J. Polym. Sci. Part A Polym. Chem.* **2003**, *41*, (8) 2064–2072.
- (34) Decker, C.; Viet, T.; Decker, D. *Macromolecules* **2001**, *42*, 5531–5541.
- (35) Sangermano, M.; Razza, N.; Crivello, J. V. *Macromol. Mater. Eng.* **2014**, *299* (7), 775–793.
- (36) Sprenger, S. *J. Appl. Polym. Sci.* **2013**, *130* (3), 1421–1428.
- (37) Owusu-Adom, K.; Guymon, C. A. *Polymer* **2008**, *49* (11), 2636–2643.

- (38) Bomze, D.; Knaack, P.; Liska, R. *Polym. Chem.* **2015**, *54* (6) 8161–8167.
- (39) Ligon, S.; Schwentenwein, M.; Gorsche, C.; Stampfl, J.; Liska, R. *Polym. Chem.* **2015**, *54* (8) 257–286.
- (40) Jo, B.; Arceneaux, A.; Willard, K. *Radtech* **2010**, 1–8.
- (41) Sipani, V.; Kirsch, A.; Scranton, A. B. *J. Polym. Sci. Part A Polym. Chem.* **2004**, *42* (17), 4409–4416.
- (42) Scognamillo, S.; Alzari, V.; Nuvoli, D.; Mariani, A. *J. Polym. Sci. Part A Polym. Chem.* **2010**, *48* (11), 2486–2490.
- (43) Pei, Y.; Sugita, O. R.; Quek, J. Y.; Roth, P. J.; Lowe, A. B. *Eur. Polym. J.* **2015**, *62*, 204–213.
- (44) Huang, S.; Shen, J.; Li, N.; Ye, M. *J. Appl. Polym. Sci.* **2014**, *62* (9) 132-140
- (45) Chatterjee, S.; Sen Gupta, S.; Kumaraswamy, G. *Chem. Mater.* **2016**, *28* (6), 1823–1831
- (46) Pandey, S.; Mishra, S. P.; Kolli, B.; Kanai, T.; Samui, A. B. *J. Polym. Sci. Part A Polym. Chem.* **2012**, *50* (13), 2659–2668.
- (47) Dorner, F.; Boschert, D.; Schneider, A.; Hartleb, W.; Al-Ahmad, A.; Lienkamp, K. *ACS Macro Lett.* **2015**, 1337–1340.
- (48) Zhang, C.; Su, G.; Chen, H.; Sun, Y.; Song, H.; Tong, L. *J. Appl. Polym. Sci.* **2014**, *41303*.

- (49) Belon, C., Allonas, X., Croutxé-barghorn, C. and Lalevée, J. *Journ. Polym. Sci. A Polym. Chem.*, **2010**, *48*, (9), 2462–2469.
- (50) Eric Dietz, J.; Peppas, N. A. *Polymer* **1997**, *38* (15), 3767–3781.
- (51) Singh, A.; Kuksenok, O.; Johnson, J.; Balazs, A. C. *Polym. Chem.* **2016** *16* (23) 320-329.
- (52) Mucci, V.; Arenas, G.; Duchowicz, R.; Cook, W. D.; Vallo, C. *Dent. Mater.* **2009**, *25* (1), 103–114.
- (53) Chiu, C.-W.; Huang, T.-K.; Wang, Y.-C.; Alamani, B. G.; Lin, J.-J. *Prog. Polym. Sci.* **2013**, *39* (3), 443–485.
- (54) Geng, K.; Tsui, O. K. C. *Macromolecules* **2016**, *49* (7), 2671–2678
- (55) Xiao, L.; Isner, A. B.; Hilt, J. Z.; Bhattacharyya, D. *J. Appl. Polym. Sci.* **2012**, *155* 58390.
- (56) Chen, M.-H. *J. Dent. Res.* **2010**, *89* (6), 549–560.
- (57) Jaranilla-tran, E. *Radtech Conf.* **2014**.
- (58) Destarac, M. *Macromol. React. Eng.* **2010**, *4* (3-4), 165–179.
- (59) González-Blanco, R.; Cunningham, M. F.; Saldívar-Guerra, E. *J. Polym. Sci. Part A Polym. Chem.* **2015**, *54* (4) 49–62. .
- (60) Amir, E. R.; Bondi, D. H. S. *Polymer*, **2012**, *52* (9) 945–969.
- (61) Gryn'ova, G.; Lin, C. Y.; Coote, M. L. *Polym. Chem.* **2013**, *4* (13), 3744

- (62) Hawker, C. J.; Bosman, a W.; Harth, E. *Chem. Rev.* **2001**, *101* (12), 3661–3688.
- (63) Telitel, S.; Telitel, S.; Bosson, J.; Spangenberg, A.; Lalevée, J.; Morlet-Savary, F.; Clément, J.-L.; Guillaneuf, Y.; Gigmes, D.; Soppera, O. *Adv. Mater. Interfaces* **2014**, *1* (5), 30-36.
- (64) Delaittre, G.; Rieger, J.; Charleux, B. *Macromolecules* **2011**, *44* (3), 462–470.
- (65) Abreu, C. M. R.; Mendonça, P. V.; Serra, A. C.; Noble, B. B.; Guliashvili, T.; Nicolas, J.; Coote, M. L.; Coelho, J. F. J. *Macromolecules* **2016**, *49* (2), 490–498
- (66) Bertin, D.; Gigmes, D.; Marque, S. R. a; Tordo, P. *Chem. Soc. Rev.* **2011**, *40* (5), 2189–2198.
- (67) Hoogenboom, R.; Popescu, D.; Steinhauer, W.; Keul, H.; Möller, M. *Macromol. Rapid Commun.* **2009**, *30* (23), 2042–2048.
- (68) Yoshida, E. *Colloid Polym. Sci.* **2010**, *288* (8), 901–905.
- (69) Guillaneuf, Y.; Versace, D. L.; Bertin, D.; Lalevée, J.; Gigmes, D.; Fouassier, J. P. *Macromol. Rapid Commun.* **2010**, *31*, 1909–1913.
- (70) Huix-Rotllant, M.; Ferré, N. *J. Phys. Chem. A* **2014**, *118* (25), 4464–4470.
- (71) Mayadunne, R. T. A.; Rizzardo, E.; Chiefari, J.; Krstina, J.; Moad, G.; Postma, A.; Thang, S. H. *Macromolecules* **2000**, *33* (2), 243–245.
- (72) Poly, J.; Cabannes-Boué, B.; Hebinger, L.; Mangin, R.; Sauvage, A.; Xiao, P.; Morlet-Savary, F.; Lalevée, J. *Polym. Chem.* **2015** *14* (6) 502-512.

- (73) Moad, G.; Rizzardo, E.; Thang, S. H. *Living Radical Polymerization by the RAFT Process*; 2005; Vol. 58.
- (74) Sidoruk, A.; Buback, M.; Meiser, W. *Macromol. Chem. Phys.* **2013**, *214* (15), 1738–1748.
- (75) Chen, M.; Moad, G.; Rizzardo, E. *J. Polym. Sci. Part A Polym. Chem.* **2009**, *47* (23), 6704–6714.
- (76) St Thomas, C.; Maldonado-Textle, H.; Cabello-Romero, J. N.; Macossay, J.; Zhang, X.; Esturau-Escofet, N.; Guerrero-Santos, R. *Polym. Chem.* **2014**, *5* (8), 3089-3097.
- (77) Mayadunne, R. T. a; Moad, G.; Rizzardo, E. *Tetrahedron Lett.* **2002**, *43*, 6811–6814.
- (78) Stace, S. J.; Moad, G.; Fellows, C. M.; Keddie, D. J. *Polym. Chem.* **2015**, *6* (40), 7119–7126.
- (79) Xing, H.; Wan, D.; Qiu, J.; Wang, Y.; Ma, L.; Jiang, Z.; Tang, T. *Polymer*, **2014**, *54* (14) 341-349.
- (80) Willcock, H.; O'Reilly, R. K. *Polym. Chem.* **2010**, *1*, (11), 149–157.
- (81) Can, A.; Zhang, Q.; Rudolph, T.; Schacher, F. H.; Gohy, J.-F.; Schubert, U. S.; Hoogenboom, R. *Eur. Polym. J.* **2015**, *69*, 460–471.
- (82) Hu, H.; Choo, Y.; Feng, X.; Osuji, C. O. *Macromol. Rapid Commun.* **2015**, *43*, (5) 234-240.

- (83) Zhang, J.; Li, T.; Mannion, A. M.; Schneiderman, D. K.; Hillmyer, M. A.; Bates, F. S. *ACS Macro Lett.* **2016**, *16* (3) 407–412.
- (84) Spontak, R. J.; Pate, N. P. *Polymer* **2000**, *5*, 334–341.
- (85) Guo, Y.; Liu, J.; Zetterlund, P. B. *Macromolecules* **2010**, *43* (14), 5914–5916.
- (86) Rowe, M. D.; Hammer, B. a. G.; Boyes, S. G. *Macromolecules* **2008**, *41* (12), 4147–4157.
- (87) Noy, J.-M.; Koldevitz, M.; Roth, P. J. *Polym. Chem. Part A Polym. Chem.* **2014** *54* (6) 590-596.
- (88) Li, L.; Luo, T.; Kiick, K. L. *Macromol. Rapid Commun.* **2014**, *42* (4) 1–6.
- (89) Santiago, D.; Fabregat-Sanjuan, A.; Ferrando, F.; De la Flor, S. *J. Polym. Sci. Part B Polym. Phys.* **2016**, *56* (4) 678-683.
- (90) Foix, D.; Ramis, X.; Serra, a.; Sangermano, M. *Polymer* **2011**, *52* (15), 3269–3276.
- (91) Yang, J.; Li, L.; Jing, Z.; Ye, X.; Wu, C. *Polymer* **2014** *55* (14), 2229–2236.
- (92) Li, J.; Su, Z.; Xu, H.; Ma, X.; Yin, J.; Jiang, X. *Macromolecules* **2015**, *48* (15), 2379–2386..
- (93) Wei, X.; Luo, Q.; Sun, L.; Li, X.; Zhu, H.; Guan, P.; Wu, M.; Luo, K.; Gong, Q. *ACS Appl. Mater. Interfaces* **2016**, *44* (5), 1235-1244.
- (94) Malo de Molina, P.; Lad, S.; Helgeson, M. E. *Macromolecules* **2015**, *48* (9), 169–176.

- (95) Andrzejewska, E. *Prog. Polym. Sci.* **2001**, *26*, 605–665.
- (96) Crivello, J. V. *J. Polym. Sci. Part A* **2006**, *45* (19) 6435–6448.
- (97) Campos, L. M.; Killops, K. L.; Sakai, R.; Paulusse, J. M. J.; Damiron, D.; Drockenmuller, E.; Messmore, B. W.; Hawker, C. J. *Macromolecules* **2008**, *41* (19), 7063–7070.
- (98) Crivello, J. V. *J. Polym. Sci. Part A Polym. Chem.* **2007**, *45* (21), 3759–3769.
- (99) Grim, J. C.; Marozas, I. A.; Anseth, K. S. *J. Control. Release* **2015** *219* 91-105 .
- (100) Senyurt, A. F.; Wei, H.; Phillips, B.; Cole, M.; Nazarenko, S.; Hoyle, C. E.; Piland, S. G.; Gould, T. E. *Macromolecules* **2006**, *39* (19), 6315–6317.
- (101) Hoyle, C. E.; Lee, T. Y.; Roper, T. *J. Polym. Sci. Part A Polym. Chem.* **2004**, *42* (21), 5301–5338.
- (102) Hoyle, C. E.; Bowman, C. N. *Angew. Chem. Int. Ed. Engl.* **2010**, *49* (9), 1540–1573.
- (103) Jasinski, F.; Rannée, A.; Schweitzer, J.; Fischer, D.; Lobry, E.; Croutxé-Barghorn, C.; Schmutz, M.; Le Nouen, D.; Criqui, A.; Chemtob, A. *Macromolecules* **2016**, *49* (4), 1143–1153.
- (104) An, S. Y.; Lee, D. G.; Hwang, J. W.; Kim, K. N.; Nam, J. H.; Jung, H. W.; Noh, S. M.; Oh, J. K. *J. Polym. Sci. Part A Polym. Chem.* **2014**, *51* (8) 435-450.
- (105) Arslan, M.; Yilmaz, G.; Yagci, Y. *Polym. Chem.* **2015** *14* (4) 540-545.

- (106) Baranek, A.; Song, H. B.; McBride, M.; Finnegan, P.; Bowman, C. N. *Macromolecules* **2016**, *49* (4), 1191–1200
- (107) Song, H. B.; Baranek, A.; Bowman, C. N. *Polym. Chem.* **2015** *14* (7) 320-329.
- (108) McBride, M. K.; Gong, T.; Nair, D. P.; Bowman, C. N. *Polymer* **2014**, *51* (6) 430-437.
- (109) Lin, Y.; Stansbury, J. W. *Polymer* **2003**, *44* (17), 4781–4789.
- (110) Ge, X.; Ye, Q.; Song, L.; Misra, A.; Spencer, P. *Macromolecules* **2015**, *48* (6) 856–872.
- (111) Killops, K. L.; Campos, L. M.; Hawker, C. J. *J. Am. Chem. Soc.* **2008**, *130* (15), 5062–5064.
- (112) Mc Aninch, I. M.; Palmese, G. R.; Lenhart, J. L.; La Scala, J. J. *J. Appl. Polym. Sci.* **2015**, *132* (8), 256-264.
- (113) Burkhart, A.; Fischer, J.; Mondrzyk, A.; Ritter, H. *Macromol. Chem. Phys.* **2014**, *215* (5), 421–425.
- (114) An, S. Y.; Noh, S. M.; Nam, J. H.; Oh, J. K. *Macromol. Rapid Commun.* **2015**, *8* (4) 123-131.
- (115) Cai, Y.; Jessop, J. L. P. *Polymer* **2006**, *47* (19), 6560–6566.
- (116) Bayramoğlu, G.; Kahraman, M. V.; Kayaman-Apohan, N.; Güngör, A. *Prog. Org. Coatings* **2006**, *57* (1), 50–55.

- (117) Park, Y.-J.; Lim, D.-H.; Kim, H.-J.; Park, D.-S.; Sung, I.-K. *Int. J. Adhes. Adhes.* **2009**, *29* (7), 710–717.
- (118) Kloxin, C. J.; Bowman, C. N. *Chem. Soc. Rev.* **2013**, *42* (17), 7161–7173.
- (119) Fenoli, C. R.; Bowman, C. N. *Polym. Chem.* **2014**, *5* (1), 62.
- (120) Fenoli, C. R.; Wydra, J. W.; Bowman, C. N. *Macromolecules* **2014**, *47* (3), 907–915.
- (121) Meng, Y.; Fenoli, C. R.; Aguirre-Soto, A.; Bowman, C. N.; Anthamatten, M. *Adv. Mater.* **2014**, *26* (37), 6497–6502.

CHAPTER 2

OBJECTIVES

Significant improvements to the thermomechanical properties and network phase separation have been observed when large macromolecules have been incorporated into acrylate networks. This work investigates the inclusion of specifically placed photoreactive groups to covalently bind the prepolymers into the polymer networks. By strategically placing the photocurable groups, significant changes in network morphology and thermo-mechanical properties could be realized. Several steps, including the specialized synthesis of reactive prepolymers, have prevented the investigation of reactive group placement on thermoset morphology. Controlled radical polymerization (CRP) is one such method that has been employed in this research to probe the relationships between reactive group placement and macroscopic physical properties. Therefore, we hypothesize that by governing the prepolymer architecture controllable thermomechanical properties could be obtained.

Within the photopolymerization field, network heterogeneity has attracted a great amount of interest due to its correlation to high shrinkage stress and other limitations such as high brittleness. Tailored network heterogeneities lead to important thermomechanical properties, like T_g and moduli, in epoxy and acrylic systems. The primary goal of the following dissertation is to establish structure-property relationships between the placement of reactive groups in prepolymer structures to produce unique network morphologies and thermomechanical properties. This research accomplishes this overall goal through the following objectives:

1. Utilize Nitroxide-Mediated Polymerization (NMP) to synthesize prepolymer molecules with epoxide reactive groups either randomly distributed or placed only at the prepolymer ends.
2. Identify key variables and effects of copolymerization of terpene oxide with cationically curable resins on polymerization kinetics.
3. Establish CRP synthesis-structure-property relationships correlating prepolymer structure and synthetic route to the thermo-mechanical properties exhibited by photocured systems.
4. Control the polymerization of methacrylate monomers via nitroso compounds to synthesize prepolymers with epoxide reactive groups located in the center or randomly distributed along a highly aliphatic prepolymer.

The first objective is accomplished in Chapter 4 by utilizing nitroxide radicals to control the polymerization of butyl acrylate and to place epoxide groups at strategic locations, namely concentrated at the ends or randomly distributed along the prepolymer backbone. The potential for the prepolymer structure to induce different morphology is characterized via dynamic mechanical analysis and mechanical testing. Further, the effects of prepolymer structure on network structure is also shown with regard to concentration and number of reactive groups on the structured prepolymers.

The second objective is examined in Chapter 5 and uses nitroso compounds that are better suited to the controlled polymerization of methacrylate monomers. This study investigates the effect of concentrating the reactive prepolymer blocks in the center of the prepolymer and how this placement modifies the resulting network morphology. The

presence of non-reactive end block with greater flexibility and potential for self-association, may provide a different means of controlling network heterogeneity.

Chapter 6 examines synthesis of similar prepolymers via different methods and how the method alters the photopolymerization kinetics and macroscopic behavior. In addition to nitroxide mediated polymerization (NMP), reversible addition-fragmentation chain transfer (RAFT) polymerization is used as another controlled radical polymerization technique capable of generating end and randomly functionalized prepolymers. Specifically, the role of the active RAFT agent is contrasted with the residual inactive NMP agent regarding the role of each agent in network heterogeneity formation and resulting thermomechanical properties.

The work presented in Chapter 7 revolves around the second objective which utilizes design of experiments to predict and model the external factors that affect monomer conversion and rate of polymerization of common cationic monomers. These tests are used to identify which factors are most important to cationic photopolymerization and how to formulate epoxide and oxetane monomers to maximize the rate of polymerization. Terpene oxides are also identified as novel additives to rapidly form the tertiary oxonium ion propagating centers and are characterized for their effects on cationic photopolymerization kinetics as well as resulting thermomechanical properties.

The accomplishment of these goals will provide a fundamental understanding of the impact of prepolymer structure on network/property relationships. As the next generation of photocurable materials will require enhanced thermomechanical properties, architected prepolymers provide a blueprint for their design. Characterization of the

network morphology has demonstrated how prepolymer structure influences the formation of heterogeneities and provides the groundwork for architected prepolymers to be implemented into a wide range of academic and industrial applications. Overall, this work demonstrated the utility of using controlled radical polymerization to generate novel oligomers with control over local composition differences in photocured thin films, thereby allowing unique network morphology and thermo-mechanical properties and future advances in the photopolymerization materials.

CHAPTER 3

MATERIALS AND METHODS

This chapter describes the materials and methods used in the synthesis of novel prepolymers, the photopolymerization of the resins which incorporate the prepolymers, and the thermomechanical and microscopic characterization of the resulting thin films. General polymerization procedures for the synthesis of the prepolymers are presented in the first part of this chapter. Monomers and photoinitiators used in the formulation of the photocurable resins are presented followed by the characterization methods used.

Prepolymer Synthesis

For prepolymers made using the nitroxide SG-1 (BlocBuilder RC-50, 1-(diethoxyphosphinyl)-2,2-dimethylpropyl 1,1-dimethylethyl nitroxide) the following general guidelines were followed. End functionalized prepolymers were synthesized utilizing the alkoxyamine NMP agent Blocbuilder RC-50. A 1/4/13 molar ratio of Blocbuilder RC-50/3,4-epoxycyclohexylmethyl methacrylate/butyl acrylate was diluted to 50% by mass with propyl acetate. A second feed consisting entirely of butyl acrylate was then added followed by a third feed identical to the first. Randomly functionalized prepolymers were synthesized with a single feed, composed of BlocBuilder RC-50/3,4-epoxycyclohexylmethyl methacrylate/butyl acrylate at a molar ratio of 1/8/64 diluted to 50% by mass with propyl acetate. In both procedures, the reactor was sparged for one hour with nitrogen before the vessel was then heated to 110°C.

Lauryl methacrylate based prepolymers require less stable nitroxides in order to control the reaction. Methyl-2-methyl-3-nitro-2-nitrosopropionate (NMMA) was identified as a nitroso compound which forms a compatibly stable nitroxide radical in the

presence of a thermal initiator and was synthesized as described in the literature.¹ Center functionalized prepolymers were synthesized utilizing the nitroso-agent NMMA. A 1/2/40 molar ratio of NMMA/AIBN/LMA was diluted to 50% by mass with propyl acetate. A second feed consisting of a 3/1 molar ratio of LMA/METH-B was then added followed by a third feed identical to the first. Randomly functionalized prepolymers were synthesized with a single feed, composed of NMMA/AIBN/METH-B/LMA at a molar ratio of 1/2/20/140 diluted to 50% by mass with ethyl acetate. In both procedures, the reactor was sparged for one hour with nitrogen before the vessel was then heated to 90°C. All feeds were allowed to reach approximately 85% conversion, as determined by targeted molecular weight. Once the desired molecular weight was achieved, residual monomer and solvent were removed via rotary evaporation for one hour at 55°C.

DBTTC was synthesized as described in the literature and used to synthesize prepolymers via the RAFT technique.^{2,3} RAFT synthesized end and randomly functionalized prepolymers were synthesized using dibenzyl trithiocarbonate (DBTTC). A 1/8/26 molar ratio of DBTTC/3,4-epoxycyclohexylmethyl methacrylate/butyl acrylate was diluted to 50% by mass with propyl acetate. A second feed consisting entirely of butyl acrylate was then added to produce the middle non-reactive block. Randomly functionalized prepolymers were synthesized with a single feed, composed of DBTTC/3,4-epoxycyclohexylmethyl methacrylate/butyl acrylate at a molar ratio of 1/8/64 diluted to 50% by mass with propyl acetate.

All feeds were allowed to come to approximately 85% conversion, as determined by gas chromatography using a Shimadzu GC-17A or by observed molecular weight via GPC, before the subsequent feeds were added. Once the desired final molecular weight

was achieved, residual monomer and solvent were removed via rotary evaporation for one hour at 55°C. Molecular weight and polydispersity index (PDI) of prepolymers were measured using a size exclusion chromatography setup including a refractive index detector (Shimadzu RID-10A). Additionally, a flow rate of 1 mL/min ethyl acetate through a PLgel Mixed-D column and was used for experimental analysis. Figure 2.1 below shows the molecular structures of all chemicals used in the synthesis and photopolymerization of the thin films.

Film Formation and Characterization

To formulate prepolymer/monomer mixtures, high viscosity prepolymers were diluted to 50 wt% in acetone if necessary. Lower molecular weight monomers were then added and mixed via vortexing. Diaryliodonium hexafluoroantimonate photoinitiator, (PC-2506) (2 wt%) and isothioxanthone photosensitizer (1 wt%) were incorporated shortly before the polymerization for cationic systems and 0.5 wt% 2,2-dimethoxy-2-phenylacetophenone (DMPA, Ciba) was used for radical systems.

Photopolymerization behavior of prepolymer/monomer mixtures was examined utilizing a Perkin Elmer Diamond differential scanning calorimeter (DSC7) modified with a medium pressure mercury arc lamp (photo-DSC). 3 to 3.5 mg of formulations were placed into DSC pans. Photopolymerization profiles were compared using the evolved polymerization heat per unit mass of photocurable resin during the polymerization. Rates of photopolymerization were measured at irradiation intensities indicated in the following chapters. Photopolymerization profiles were compared using the evolved polymerization heat per unit mass of photocurable resin during the polymerization to

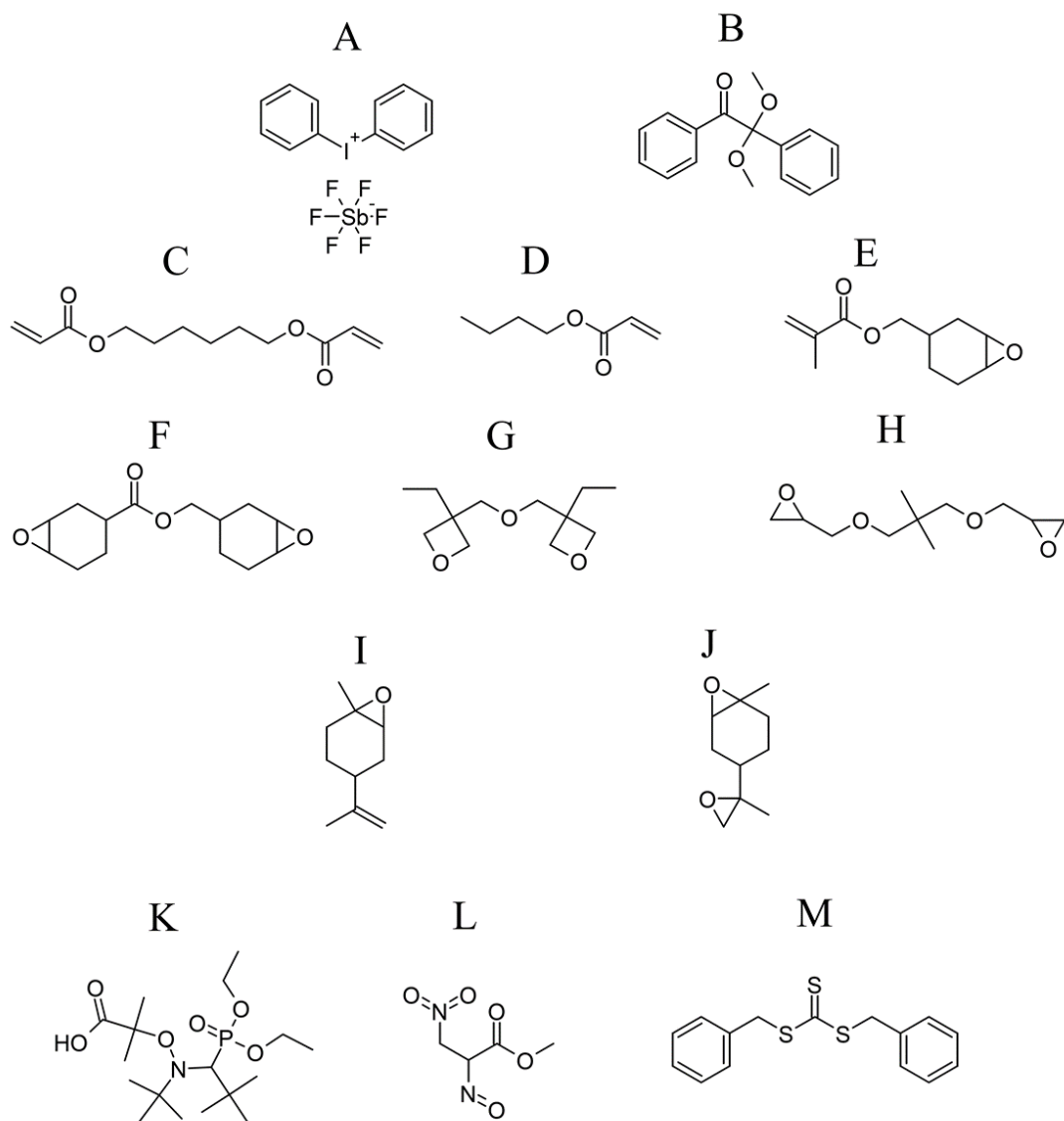


Figure 2.1. Molecular structures of chemicals used in this work. Shown are diaryl iodonium hexafluoroantimonate (PC-2506, A), 2,2-dimethoxyphenyl acetophenone (DMPA, B), 1,6 hexanediol diacrylate (HDDA, C), butyl acrylate (BA, D), cycloaliphatic epoxide methacrylate (METH-B, E), 3,4-Epoxy cyclohexylmethyl 3,4-epoxycyclohexanecarboxylate (EEC, F), bis[2,2-dihydroxymethyl] butyl ether (DOX, G), Neopentyl diglycidyl ether (NPGDGE, H), Limonene Monoxide (LMO, I), Limonene Dioxide (LDO, J), (1-(diethoxyphosphinyl)-2,2-dimethylpropyl 1,1-dimethylethyl nitroxide) (SG-1, K), Methyl-2-methyl-3-nitro-2-nitrosopropionate (NMMA, L), Dibenzyl trithiocarbonate (DBTTC, M).

determine the normalized polymerization rate according to equation 1.

$$\frac{R_p}{[M_0]} = \frac{Q \cdot MW}{m \cdot n \cdot \Delta H_p} \quad (1)$$

Where R_p is the extensive rate of

polymerization, $[M_0]$ is monomer concentration, Q is heat flow, MW is the monomer

molecular weight, m is sample mass, n is number of reactive groups per molecule, and ΔH_p is the enthalpy of polymerization as indicated in the individual chapters. Real time infrared spectroscopy was performed using a Thermo Nicolet nexus 670. One mg of sample was placed on a sodium chloride plate covered with 15 μm spacer beads and sandwiched with an additional sodium chloride plate. The laminate nature of this testing geometry prevents oxygen and water from diffusing into the system. Analysis was performed at ambient temperature and atmosphere.

Dynamic mechanic analysis (DMA, Q800 DMA TA Instruments) was conducted to investigate the effect of polymer architecture on ultimate mechanical and visco-elastic properties of cured polymers. To fabricate rectangular films, two thick glass plates covered by amorphous polyvinylidene fluoride films (PVDF, Teflon® AF, Dupont) were used. Adhesive tape spacers (150 μm thick) were attached on each edge of the bottom plate to control the film thickness. Approximately 3g of liquid sample mixture was placed on the bottom glass plate, the liquid samples were then tightly pressed using the upper glass plate and secured using binder clips. Filled molds were irradiated as indicated in the individual chapters using a UV lamp (250-500 nm) for cationic systems or at 365 nm^{-1} for radical systems. To measure the modulus and glass transition temperature of the samples, the temperature of films was increased from -100°C to 150°C at a heating rate of $3^\circ\text{C}/\text{min}$. DMA tensile mode was utilized under constant strain at a frequency of 1 Hz. Young's modulus and tensile properties were evaluated at 30°C in tensile mode with a force rate of 1.0 N/m. Young's Modulus was calculated using the slope of the stress-strain curve in the early linear regime (less than 10% strain).⁴ Creep tests were performed by applying an

onset stress for ten minutes and measuring the subsequent strain. Strain recovery was recorded for 30 minutes after the stress was removed.

Morphologies of films prepared as described above were analyzed utilizing an Asylum Research mfp3d atomic force microscope (AFM) and analyzed with the provided Igor software. Phase images were obtained in tapping mode at a rate of 1 Hz.

References and Notes

- (1) Detrembleur, C.; Jérôme, C.; De Winter, J.; Gerbaux, P.; Clément, J.-L.; Guillaneuf, Y.; Gimes, D. *Polym. Chem.* **2014**, *5* (2), 335.
- (2) Keddie, D. J.; Moad, G.; Rizzardo, E.; Thang, S. H. *Macromolecules* **2012**, *45* (13), 5321–5342.
- (3) Mayadunne, R. T. a; Moad, G.; Rizzardo, E. *Tetrahedron Lett.* **2002**, *43*, 6811–6814.
- (4) Callister, W. D.; Rethwisch, D. G. *Material Science and Engineering*, 9th ed.; Wiley: New York, 2013.

CHAPTER 4

EFFECTS OF DIRECTED ARCHITECTURE IN EPOXY FUNCTIONALIZED PREPOLYMERS FOR PHOTOCURABLE THIN FILMS*

Cationic photopolymerization has become increasingly important in thin-film applications for advantages including no oxygen inhibition and rapid polymerization rates. Photocurable cationic thin film properties are often modulated by incorporation of oligomeric and prepolymer materials, but little work has directly examined the effect of prepolymer structure and reactive group placement on the thermomechanical properties of the final material. To explore the role of molecular architecture, epoxy functionalized butyl acrylate gradient copolymers were synthesized with reactive groups in end segments or randomly distributed along the prepolymer chain. Polymerized end functionalized formulations exhibit moduli almost double that of random functionalized oligomer formulations. Additionally, inclusion of end functionalized prepolymers decrease creep of resulting thin films by a factor of 10. Further, decreasing the concentration of the crosslinking diluent in end functionalized prepolymer systems results in amorphous networks with significantly lower mechanical strength. Increasing reactive groups at the ends of prepolymers produces stronger materials without affecting tensile elongation at break. These properties indicate that structured oligomers facilitate formation of continuous hard domains with high crosslink density with inclusions of soft, flexible domains of low crosslink density. This work demonstrates that the prepolymer architecture governs network formation and ultimate properties.

*Scholte et Al *Journ. Poly Sci. Part A*, **2017**, 55, 144–154

Introduction

Photopolymerization has received increasing attention both academically and industrially due to fast polymerization rates and minimal volatile organic components. Recent research has focused on the synthesis of new monomers, light-activated controlled radical polymerization, and novel photoinitiators and reactions.¹⁻³ Monomer chemistry in photopolymerization is predominantly (meth)acrylate and radical based due to the availability of compatible photoinitiating molecules. With the development of iodonium and sulfonium salt initiators and different properties, cationic photopolymerization of epoxy and oxetane monomers has become of significant interest.⁴⁻⁸

Photocured thin-film materials, both cationically and radically cured, are typically highly crosslinked.⁹ This large degree of crosslinking provides high tensile modulus, hardness, and durability, but also generates heterogeneities in the network, especially those involving formulations with multifunctional monomers.¹⁰ Unfortunately, these network heterogeneities lead to a number of disadvantages including pronounced shrinkage stress and broad glass transition temperatures.¹¹ Ongoing research on novel photopolymerizable materials aims to avoid these disadvantages by utilizing either photoinitiated copper catalyzed azide alkyne “click” reaction or thiol-ene/yne chemistry.¹² The step growth polymerization mechanism of thiol-ene/ynes leads to much more uniform networks with less shrinkage stress and more narrow range glass transition temperatures.

Film formation and properties of industrial photocured materials are largely governed through incorporation of large reactive prepolymer molecules. These molecules significantly reduce the change in free-volume that occurs during polymerization and

control basic thermomechanical characteristics.^{13,14} Controlled radical polymerization provides opportunities to produce large prepolymers with defined structures that could further modulate these thermomechanical properties. For example, reversible addition-fragmentation chain transfer (RAFT) polymerization is a popular means to produce controlled polymer structure; however, the common trithiocarbonate and dithioethers RAFT agents remain reactive after the polymerization reaction allowing network rearrangements during the photopolymerization.¹⁵ Nitroxide-mediated polymerization (NMP), another method of controlled radical polymerization, utilizes thermally reversible termination to control the propagation mechanism thereby providing control over molecular weight. In contrast to RAFT, the thermally reversible termination of NMP is not susceptible to network rearrangement in the presence of other radical sources, as the majority of nitroxides are only active at elevated temperatures.¹⁶ Thus, as photopolymerization is commonly performed at ambient temperatures, the use of NMP prevents the rearrangements that could change network structure during polymerization as likely would be the case for RAFT systems.

Synthesis via controlled radical polymerization has been used to form controlled structure block copolymers for a large variety of applications.¹⁷⁻²⁰ For example, simple modification of soft rubbery or hard glassy blocks of thermoplastic block copolymers allows significant control of thermomechanical properties.^{21,22} By increasing the length of the low T_g soft block, the polymer becomes much more flexible and impact resistant while with higher hard/glassy block compositions, the material becomes much more stiff and brittle.¹⁸ Gradient copolymers have also been studied, which allow for a statistical incorporation of two or more monomers.^{23,24} Incorporating a homopolymer segment of

butyl acrylate, a low T_g monomer, in a thermoplastic polystyrene material alters the thermomechanical properties by significantly increasing the strain at break and strain recovery as compared to traditional block copolymers.²⁵ In these gradient thermoplastics, the domains are not necessarily distinct, but do show evidence of regions with different properties at the nanoscale. Additionally, these block and gradient copolymers, when incorporated into a crosslinking matrix, may produce interpenetrating networks (IPN) or dual network materials.²⁶⁻²⁹

This research aims to determine the effect of various prepolymer architectures, controlled and defined by the placement of reactive epoxide moieties within a crosslinked network, to change structure and modulate final thin film properties. Here, we examine the role of reactive group placement in a prepolymer for cationically photopolymerizable systems and the effects of prepolymer architecture in network and morphological properties. NMP was used to synthesize butyl acrylate prepolymers with epoxide functionalities located at both ends of the polymer chains or with the epoxide functionalities incorporated statistically along the butyl acrylate backbone. The molecular weight and number of functional groups were modulated to tune the network structures. Photo-induced reaction rate behavior was determined as a function of prepolymer structure. Thermo-mechanical properties including T_g , modulus, and creep behavior were examined for both end and randomly functionalized systems to probe the effect of the prepolymers on ultimate network structure. Atomic force microscopy was also utilized to examine the existence of domains with localized properties induced by placement of polymerizable groups. We hypothesize that the prepolymer molecular structure,

specifically with regard to reactive group placement, will provide a facile method to control photocurable material characteristics.

Experimental

Materials

Neopentyl diglycidyl ether (NPGDGE, Sigma Aldrich), 3,4-epoxycyclohexylmethyl 3,4-epoxycyclohexanecarboxylate (EEC, Sigma Aldrich), isothioxanthone (ITX, Sigma Aldrich), and PC-2506 (Polysset), a diaryliodonium hexafluoroantimonate photoinitiator, were used as received. Butyl acrylate and 3,4-epoxycyclohexylmethyl methacrylate were provided by Avery Dennison. Blocbuilder RC-50 (1-(diethoxyphosphinyl)-2,2-dimethylpropyl 1,1-dimethylethyl nitroxide) was obtained from Arkema.

End functionalized prepolymers were synthesized utilizing the alkoxyamine NMP agent Blocbuilder RC-50. A 1/4/13 molar ratio of Blocbuilder RC-50/3,4-epoxycyclohexylmethyl methacrylate/butyl acrylate was diluted to 50% by mass with propyl acetate. A second feed consisting entirely of butyl acrylate was then added followed by a third feed identical to the first. Randomly functionalized prepolymers were synthesized with a single feed, composed of BlocBuilder RC-50/3,4-epoxycyclohexylmethyl methacrylate/butyl acrylate at a molar ratio of 1/8/64 diluted to 50% by mass with propyl acetate. Schemes 4.1A and 4.1B show representations of the synthesis of end and randomly functionalized molecules, respectively.

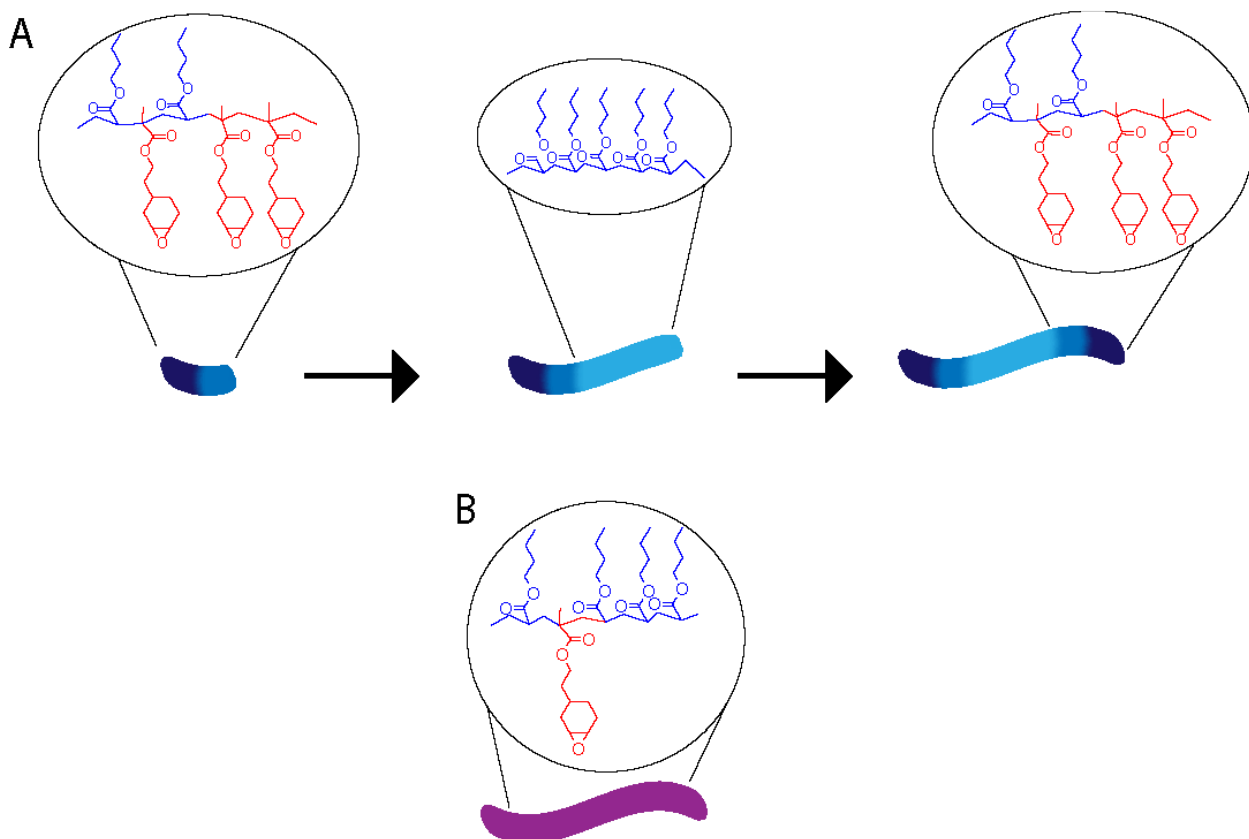
In both procedures, the reactor was sparged for one hour with nitrogen before the vessel was heated to 110°C. All feeds were allowed to come to approximately 85% conversion, as determined by gas chromatography using a Shimadzu GC-17A, before the

subsequent feeds were added. Once the desired molecular weight was achieved, residual monomer and solvent were removed via rotary evaporation for one hour at 55°C.

Molecular weight and polydispersity index (PDI) of prepolymers were measured using a size exclusion chromatography setup including a refractive index detector (Shimadzu RID-10A). Additionally, a flow rate of 1 mL/min ethyl acetate through a PLgel Mixed-D column and was used for experimental analysis. Table 4.1 summarizes the properties of the prepolymer molecules used in this study. Due to high concentrations of the epoxy functional methacrylate monomer, PDI's are above what would typically be considered a controlled radical polymerization with very defined and monodisperse molecular weight. Of much greater interest for this work is control over reactive group placement and approximate molecular mass in a batch feed process which is readily enabled by the “living” nature of the highly stable nitroxide radical.

Table 4.1 Prepolymers used in this study

Sample Name	Epoxy Location	Average # of Reactive Groups	M _n	PDI
End 13k8	End	8	11400	2.33
End 16k8	End	8	15900	1.60
End 20k16	End	16	23400	1.50
Random 13k8	Random	8	15100	1.64
Random 20k16	Random	16	19800	2.10



Scheme 4.1 Synthetic procedures for making architected prepolymers. Scheme 4A shows the feeds for an end functional prepolymer and 4B for a randomly functional prepolymer.

Methods

To formulate prepolymer/monomer mixtures, high viscosity prepolymers were diluted to 50 wt% in acetone. Lower molecular weight monomers were then added and mixed via vortexing. Diaryliodonium hexafluoroantimonate photoinitiator, (PC-2506) (2 wt%) and isothioxanthone photosensitizer (1 wt%) were incorporated shortly before the polymerization.

Photopolymerization behavior of prepolymer/monomer mixtures was examined utilizing a Perkin Elmer Diamond differential scanning calorimeter (DSC7) modified with a medium pressure mercury arc lamp (photo-DSC). 3 to 3.5 mg of formulations in acetone were placed into DSC pans and the acetone was removed in a vacuum oven at

60°C. Photopolymerization profiles were compared using the evolved polymerization heat per unit mass of photocurable resin during the polymerization. Rates of photopolymerization were measured at an irradiation intensity of 60-70mW/cm².

Dynamic mechanic analysis (DMA, Q800 DMA TA Instruments) was conducted to investigate the effect of polymer architecture on ultimate mechanical and visco-elastic properties of cured polymers. To fabricate rectangular 6 x 25 mm and 0.15 mm thick films, two thick glass plates, covered by amorphous polyvinylidene fluoride films (PVDF, Teflon® AF, Dupont) for easy release, were used. Adhesive tape spacers (150 µm thick) were attached on each edge of the bottom plate to control the film thickness. Approximately 3g of liquid sample mixture were placed on the bottom glass plate and dried for 30 minutes in a vacuum oven at 60°C to remove acetone. The dried liquid samples were then tightly pressed using the upper glass plate and secured using binder clips. Filled molds were irradiated for 30 minutes using a UV lamp (250-500 nm) at an irradiation intensity of 13.5 mW/cm². To measure the modulus and glass transition temperature of the samples, the temperature of films was increased from -100°C to 150°C at a heating rate of 3°C/min. DMA tensile mode was utilized under constant strain at a frequency of 1 Hz. Young's modulus and tensile properties were evaluated at 30°C in tensile mode with a force rate of 1.0 N/m. Young's Modulus was calculated using the slope of the stress-strain curve in the early linear regime (less than 10% strain).³⁰ Creep tests were performed by applying an onset stress of 4 MPa for ten minutes and measuring the subsequent strain. Strain recovery was recorded for 30 minutes after the 4 MPa stress was removed.

Morphologies of films prepared as described above were analyzed utilizing an Asylum Research mfp3d atomic force microscopy (AFM) and analyzed with the provided Igor software. Phase images were obtained in tapping mode at a rate of 1 Hz.

Results and Discussion

Network formation in traditional photopolymerizable formulations frequently leads to micro- and nanogel heterogeneities within the network that limit the applications of these materials due to increased shrinkage stress. Network heterogeneities arise from fast reaction kinetics and gelation, leading to areas of higher and lower crosslink densities.^{6,8} This phenomenon results in much different relaxation times leading to networks with broad glass transition networks. Incorporation of prepolymers significantly improves overall thin film properties. Alterations in size and functionality of the prepolymers allows further tuning of network structure and thermomechanical property characteristics, such as modulus and T_g . Even with the importance of prepolymer structure, reactive group placement in the prepolymer has yet to be explored in detail.^{10,21} This study examines the impact of molecular architecture, based on placement and number of epoxide reactive groups on reaction kinetics and resulting photocured network properties. Prepolymers, comprised primarily of poly(butyl acrylate), are investigated with epoxy moieties either randomly incorporated or concentrated at the ends leaving large nonreactive middle. The effect of altering the ratio of reactive diluent to prepolymer and the subsequent changes in crosslink density are also determined.

Based on the chemical similarities of the highly functionalized tail ends and the reactive diluents, it is possible for the prepolymer architecture to effect the local reactive group concentration before and during polymerization. Prior research has focused on the

effects of reactive group proximity on the photopolymerization kinetics via lyotropic liquid crystal templating.³¹ In these systems, monomers segregate within the nanostructured system into polar and nonpolar regions, bringing the reactive monomer species into closer proximity. This proximity, in turn, yields increases in the rate of polymerization.³² If the prepolymer architectures induce different local reactive group concentrations in these photocurable formulations, the kinetics of the photopolymerization reaction may also show differences based on the prepolymer molecular structure. Difunctional glycidyl ether (NPGDGE) and cycloaliphatic epoxy (EEC) monomers were incorporated as reactive diluents and reacted with both architected and random prepolymers, using a common diaryl iodonium cationic photoinitiator, to investigate the effect of prepolymer architecture on reaction behavior. Figures 4.1A and 4.1B display the heat flow during photopolymerization, normalized by sample mass, for the formulations utilizing NPGDGE and EEC as reactive diluents, respectively. The difference in heat flow when utilizing the glycidyl ether reactive diluent is seen in Figure 4.1A, where almost double the heat flow is observed for the formulation utilizing end functionalized prepolymers as compared to the randomly functionalized formulation. Figure 4.1B shows the differences in heat flow when utilizing the cycloaliphatic epoxide reactive diluent where a small but reproducible difference is observed, with the end functionalized prepolymers showing a greater maximum heat flow. These results are consistent with the possibility that the highly reactive chain ends are affecting the relative local reactive group concentrations prior to and/or during photopolymerization implying that regions with higher and lower cross-link density may be induced. While the differences in rate are not as significant when EEC is used as the

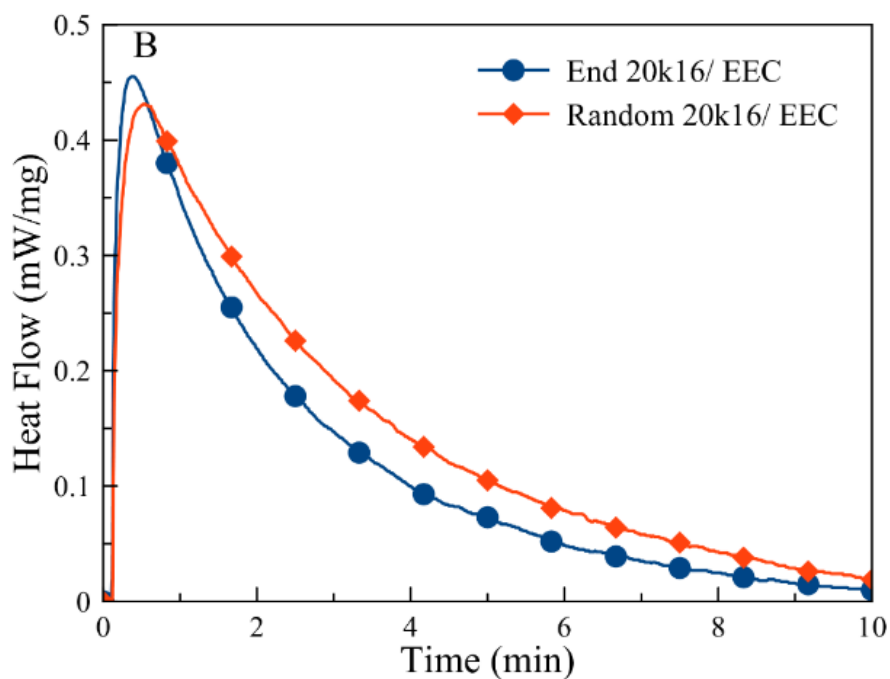
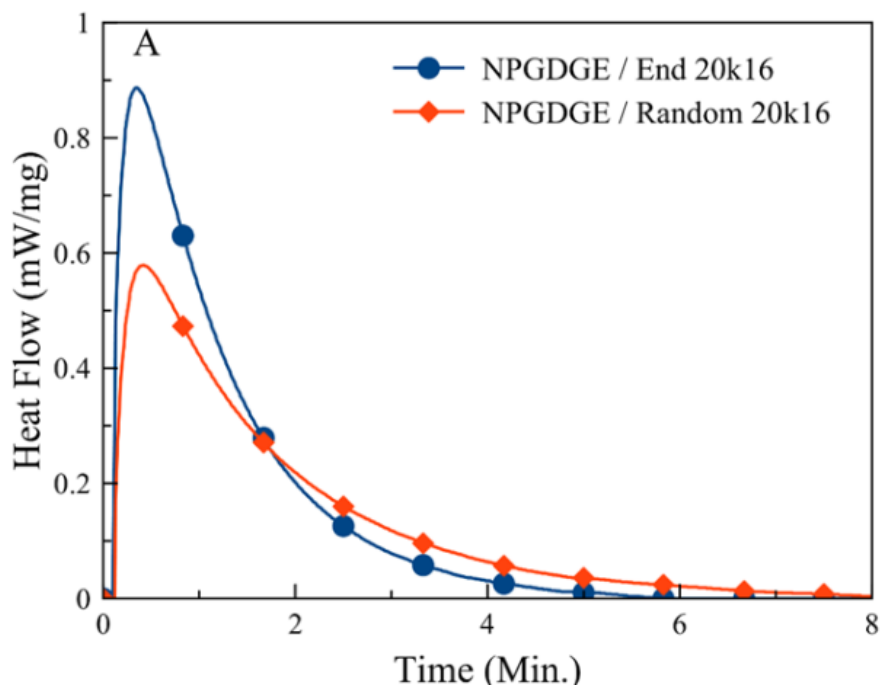


Figure 4.1. Normalized heat flow as a function of time during photopolymerization of formulations using end 20k16 (—●—) and random 20k16 (—◊—) 70 wt% oligomer species using NPGDGE (A) and EEC (B) as reactive diluents and photopolymerized at 65 mW/cm². 2 wt% PC-2506 and 1wt% ITX were used as a photoinitiators.

reactive diluent, it was chosen for further thermomechanical property testing. The reactive group for both EEC and 3,4-epoxycyclohexylmethyl methacrylate is a cycloaliphatic epoxide, which leads to tack free thin films and apparent full cure. On the other hand, the reactive group for NPGDGE is a glycidyl ether. Systems cured with NPGDE are quite tacky, suggesting an incomplete cure with the two different functional groups, making further analysis untenable.

If the reactive groups of the end functionalized prepolymers do concentrate or segregate within the photocurable resin during reaction, it is plausible that the resulting network structure would be much different than one formed utilizing the randomly functionalized prepolymer. In fact, the closer proximity of the functional end groups and possible segregation may lead to the formation of multiple domains within the network with much different localized properties, such as glass transition and storage modulus, resulting in dual network-like behavior.²⁷ Dynamic mechanical analysis (DMA) is one method for detecting the presence of multiple domains in highly crosslinked systems with heterogeneities. The presence of multiple domains within the photocured thermoset may provide dual network-like behavior as observed by multiple T_g 's and unique mechanical properties. Figure 4.2A shows the storage modulus as a function of temperature of photocured formulations using either end or randomly functionalized prepolymers. The storage modulus of the polymer network incorporating randomly functionalized prepolymers shows a broad single decrease in the modulus characteristic of photocured thermosets with a wide range of relaxation times. In contrast, for materials formulated with the end architected prepolymer, two distinct decreases in storage modulus are observed as the temperature increases, indicating the possible presence of domains with

different properties. The decrease at lower temperatures could be attributed to transitions related to non-reactive butyl acrylate segments in the end functionalized prepolymer. The second and broader transition at higher temperatures could then be due to highly crosslinked regions formed from the reactive segments of the end 20k16 prepolymer molecule and the reactive diluent EEC. The fact that this decrease is much greater than the initial decrease suggests that the highly crosslinked, domain is dominating properties of the polymer network.

The loss factor, $\tan(\delta)$, gives further information regarding the polymer network and its corresponding glass transitions. Peaks in $\tan(\delta)$ vs temperature plots are a specific measure of the glass transition temperature in polymeric materials. This technique can be used to probe for network heterogeneities by observing broad $\tan(\delta)$ peaks or perhaps multiple $\tan(\delta)$ maxima if domains with different properties are present. Figure 4.2B shows the effect of prepolymer architecture on $\tan(\delta)$ for both random and end functionalized systems. The random 20k16 prepolymer formulations experience a broad glass transition occurring at 51°C, characteristic of photopolymerized thermosets. These broad glass transitions are the result of a relative continuous distribution of network heterogeneities with regions of high and low crosslinking. On the other hand, the end 20k16 prepolymer/EEC formulation shows two $\tan(\delta)$ maxima indicating these formulations have multiple and distinct glass transitions. As with the storage modulus results, the first maxima is likely due to the predominantly butyl acrylate homopolymer and the second broader peak is due to the highly functionalized end segments of the prepolymer molecules crosslinking with the reactive monomer diluent. The differences in

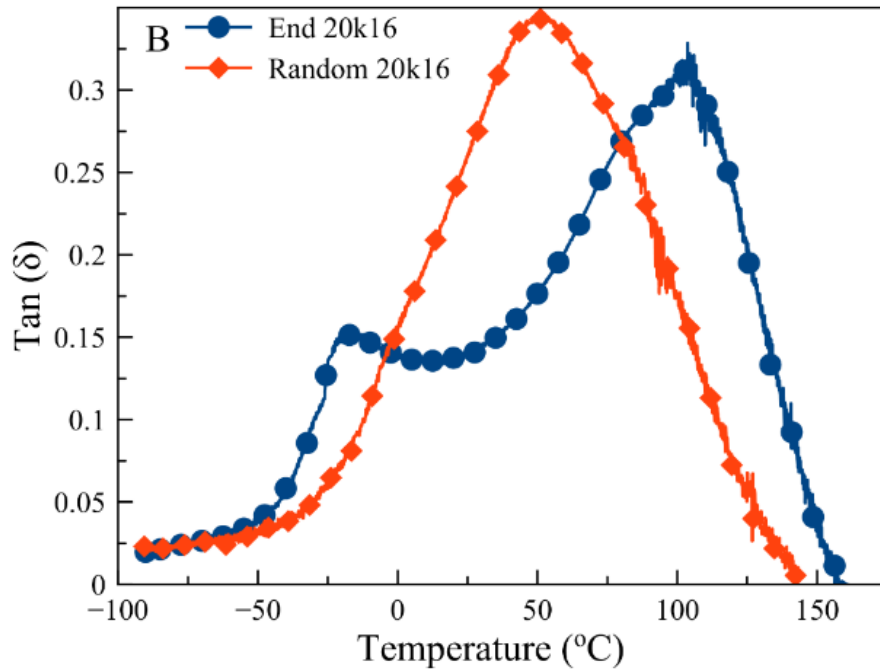
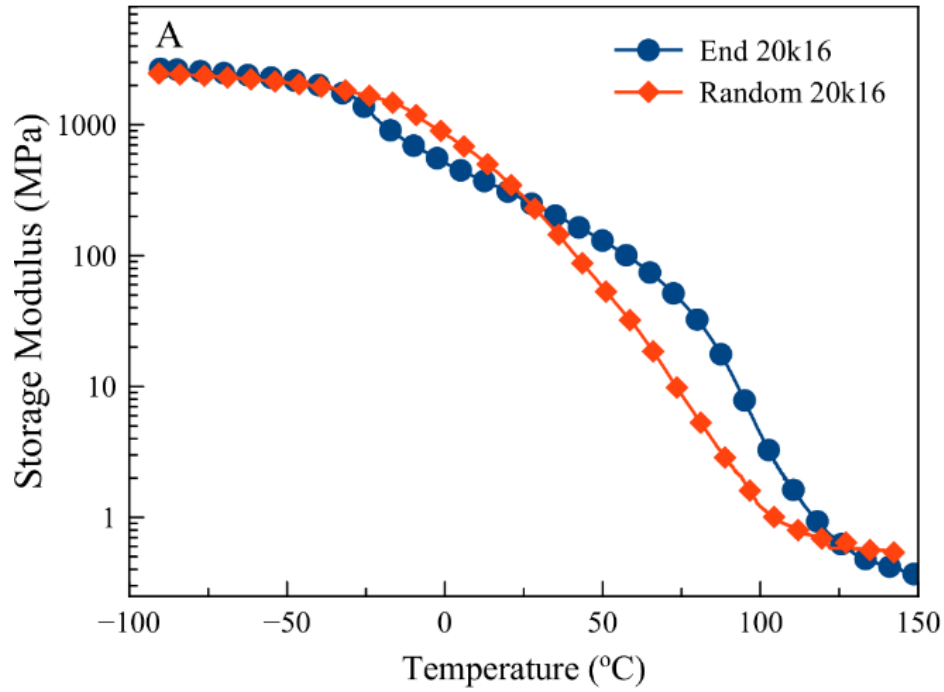


Figure 4.2. Storage modulus and Tan (δ) profiles as a function of temperature of end 20k16 (—●—) and random 20k16 (—◊—) oligomer species formulated with 70 wt% EEC. All samples were photopolymerized with 2 wt% PC-2506 and 1wt% ITX at 13.5 mW/cm² for 30 minutes.

both the storage modulus and $\tan(\delta)$ as a function of temperature for both formulations show the pronounced effect of the prepolymer architecture. Incorporating a distinct nonreactive segment into the prepolymer molecule appears to allow a secondary domain to form, in this case consisting primarily of soft poly (butyl acrylate) with little crosslinking.

With multiple $\tan(\delta)$ maxima for materials photocured with end functionalized prepolymers, it is reasonable to believe that these materials will exhibit different properties than materials formulated with the randomly functionalized prepolymers which show a single, albeit broad, glass transition.³⁴ To probe the changes in mechanical properties, Figure 4.3 shows the stress-strain plots for end and random 70 wt% prepolymer formulations. The moduli of materials utilizing randomly functionalized prepolymers behave as would be expected of a traditional photo-cured thermoset, i.e. a relatively constant slope is observed with increasing strain until break. On the other hand, the materials containing end 20k16 oligomers, when subjected to tensile stress show an almost 90% increase in initial slope and corresponding modulus, as observed through 10% strain compared to the randomly functionalized formulations. The end 20k16 material then appears to yield to some degree, and continues to deform at a similar rate to the randomly functionalized materials.

The initial large modulus in the end 20k16 material may be due to the highly crosslinked high T_g domains resisting strain. Subsequently, it is possible that as the material begins to yield, this lower resistance to continued stress may be due to the lightly crosslinked, softer domains. The size of the softer domains would likely decrease via

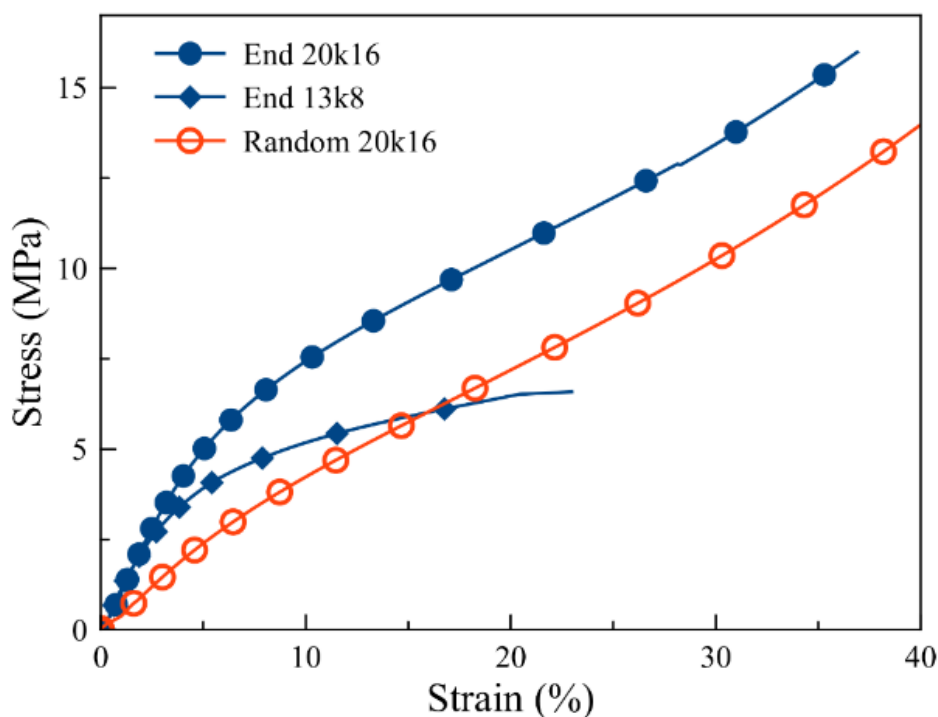


Figure 4.3. Stress-strain behavior in tensile mode at 30°C of end 20k16 (—●—), end 13k8 (—□—), and random 20k16 (—○—) oligomer species formulated with 30 wt% EEC. All samples were photopolymerized with 2 wt% PC-2506 and 1wt% ITX at 13.5 mW/cm² for 30 minutes.

smaller butyl acrylate segments present in the End 13k8 formulation. With smaller soft domains the overall flexibility and ultimate elongation of these materials will be limited. The smaller 13k8 end functional formulation shows a more pronounced difference in their ability to resist strain when compared to its larger 20k16 counterparts. The end 13k8 prepolymer has a similar functional group concentration, but with half the molecular weight and half the average number of functional groups on each end as the end 20k16 prepolymer. Formulations with the smaller end functional material shows a similar initial modulus but begin to yield at much lower strain. The modulus after yielding and the elongation at break are both significantly lower as well. The smaller lengths of reactive and non-reactive segments limit the size of high T_g domains, which form and provide

greater mechanical stability to the system. Meanwhile, for both formulations using the larger and smaller end prepolymer, both high and low modulus regimes are observed in Figure 4.3. This behavior provides further evidence that a high T_g , highly crosslinked domain is the first to deform within the polymer network, which leads to a larger initial modulus as compared to films using randomly functionalized oligomers. The end functional materials also appear to yield, which is consistent with the presence of a secondary softer domain allowing the materials to elongate to greater strain after yielding before break. The shorter butyl acrylate segments in the end 13k8 formulations also likely contribute to the lower elongation of these materials.

The evidence of hard and soft domains, resistant to initial strain with inclusions of a soft domain that allows further elongation, is consistent with dual network formation. It is reasonable to believe that dual networks will respond strongly to different stress rates with significantly greater resistance to strain. Creep, or deformation due to rapid onset and continued application of a stress, is one technique that can provide additional knowledge regarding network structure and behavior. Figure 4.4A shows the results of creep tests using 4 MPa of constant stress to demonstrate effects of molecular architecture in resisting sudden stresses. In formulations consisting of 60 wt% prepolymer, end functional material systems resist strain to a much greater degree. In fact, these materials only allow approximately 3% strain versus over 30% strain for systems incorporating randomly functionalized oligomers. As the concentration of prepolymer increases in the formulation to 70 wt%, the effect of architecture becomes even more pronounced. Formulations using random prepolymers prematurely broke on

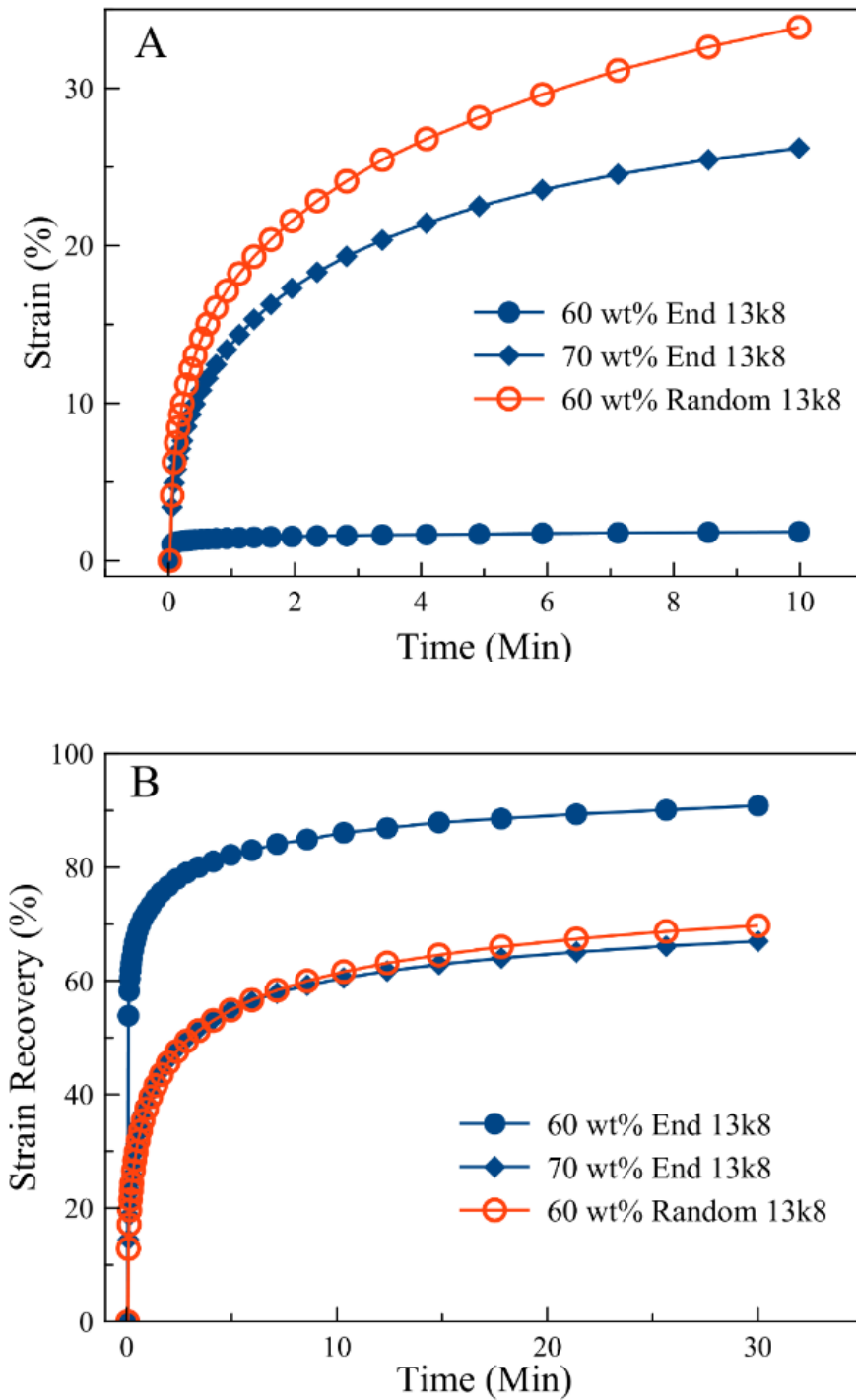


Figure 4.4. Creep test at 30°C using constant application of 4 MPa of Stress on end 13k8 at 60 wt% (●), 70 wt% (◆), and 60 wt% random 13k8 (○) oligomer species formulated with 40 wt% EEC. All samples were photopolymerized using 2 wt% PC-2506 and 1wt% ITX at 13.5 mW/cm² for 30 minutes.

repeated trials, while the end functionalized materials exhibit strains of approximately 25% after 10 minutes similar to the behavior of the random oligomer systems at lower concentrations. The creep behavior provides further evidence that a highly crosslinked, high T_g domain formed from the reactive diluent and the functionalized portions of the end 13k8 prepolymers is present. Given the significant resistance to rapid stress, this domain is likely well distributed, if not continuous, within the system.

Further information regarding the nature of these polymer networks may be found through examination of the strain recovery. Figure 4.4B shows the strain recovery of these samples after the 4 MPa stress was removed. The 60 wt% systems containing the end functionalized prepolymer molecules recovered almost 90% of the strain, meaning that each sample exhibited less than 1% net deformation. Conversely, formulations utilizing the random prepolymers show only 60% recovery. Formulations using random prepolymers experience nearly 15% permanent deformation, an increase of two orders of magnitude as compared to the end prepolymer formulations. The samples containing 70 wt% end functionalized oligomer recover a similar percent strain. In both systems that utilize the end functionalized prepolymer significantly less permanent deformation from sudden stresses is observed indicating that the hard domains with high cross-link density significantly resist plastic deformation while random systems with more typical network structure allows significant and unrecoverable plastic deformation. The lower response to sudden stresses and greater recovery to these stresses are consistent with a highly crosslinked, high T_g domain being more dominant and continuous in the overall polymer network.

Given the evidence of multiple domains from the thermomechanical properties, atomic force microscopy (AFM) was utilized to detect direct evidence of mechanical dissimilarities as seen in Figure 4.5. The phase micrographs of photopolymerized formulations containing 70 wt% end and random functionalized materials are seen in Figures 4.5A and 4.5B, respectively. Neither polymer system appears to display distinct well-ordered domains via self-association common to thermoplastic block copolymers. At the same time, the materials containing end functionalized oligomers show 4 times the difference in phase contrast as compared to the materials containing the random 13k8 prepolymer with much greater evidence of domains with significantly different properties. This much greater contrast is likely due to the presence of different network regions throughout the material with higher concentration domains of butyl acrylate (low T_g), compared to domains of highly crosslinked EEC (high T_g) and prepolymer reactive groups. On the other hand, the random samples exhibit more homogenous and amorphous surface morphology, as witnessed by lower degree of phase contrast. These differences are consistent with the formation of distinct domains with different mechanical properties from end functional materials based on prepolymer architecture.

The overall composition, especially of prepolymer in photocurable systems, will have large effects on the thermomechanical properties, including T_g and mechanical strength. To determine the effects of different levels of end functionalized prepolymer on final material properties, formulations were examined with varying prepolymer content. Figure 4.6A shows the effect of increasing the end 20k16 prepolymer content while decreasing the concentration of the reactive diluent on the storage modulus. Up to 80

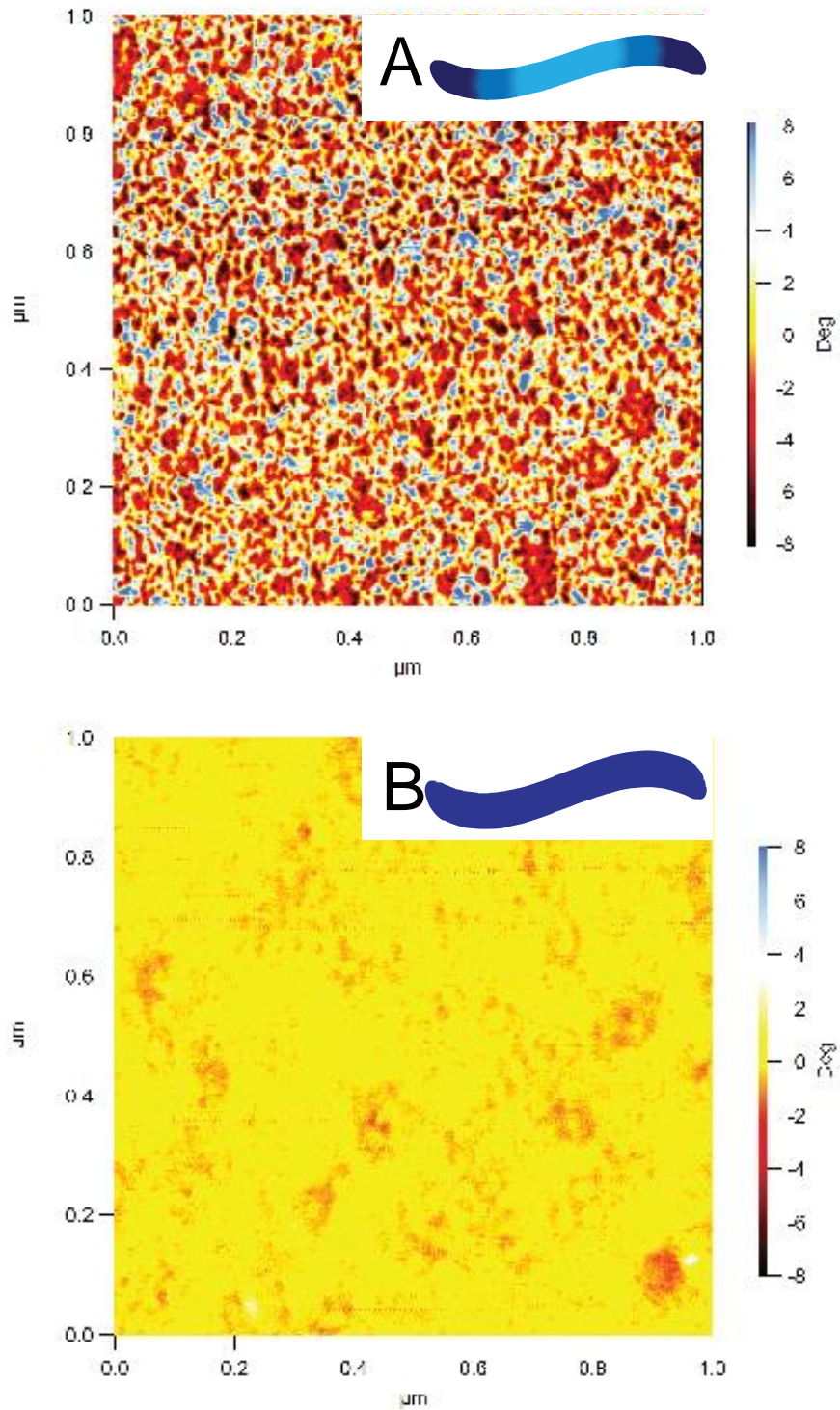


Figure 4.5. AFM Phase images of 70 wt% end 13k8 (A) and random 13k8 (b) oligomers formulated with 30 wt% EEC. All samples were photopolymerized using 2 wt% PC-2506 and 1wt% ITX at 13.5 mW/cm² for 30 minutes 2 wt% PC-2506 and 1wt% ITX at 13.5 mW/cm² for 30 minutes.

wt% end functionalized prepolymer can be added to the formulation before a significant effect on the glassy plateau of the polymer network is observed. The 90 wt% system exhibit a pronounced decrease in the glassy modulus, roughly a third of other formulations, and repeatedly broke at temperatures above 50°C. These findings suggest that the reactive diluent provides much of the highly crosslinked hard domain present in the formulations using 60-80 wt% end functionalized prepolymer. At lower concentrations of the end functionalized prepolymer molecule, the beginning of the glassy plateau extends to nearly -25°C. These results suggest that the butyl acrylate segments are significantly influenced by the highly crosslinked EEC network and the functional portions of prepolymer, as a sharp glass transition at -54°C is not observed, which would be expected if neat butyl acrylate alone were examined. As the concentration of butyl acrylate in the highly crosslinked domains increases, via more cycloaliphatic epoxy prepolymer moieties reacting with the small reactive diluent, the second drop in modulus occurs at lower temperatures. This occurs at 100°C in the 60 wt% system and decreases by nearly 20°C for both the 70 and 80 wt% systems. Further, the slope between the two decreases is lower for low prepolymer content systems appearing almost flat in the 60 wt% systems. These results suggest that the butyl acrylate rich regions are becoming more dominant in the polymer network and that prepolymer structure may provide an additional avenue for tailoring properties, like stiffness and T_g .

The changes observed in the storage modulus behavior suggest that thermomechanical properties and possibly network domains can be readily tuned by modifying the prepolymer/reactive diluent ratio. Specifically, the glass transition, as

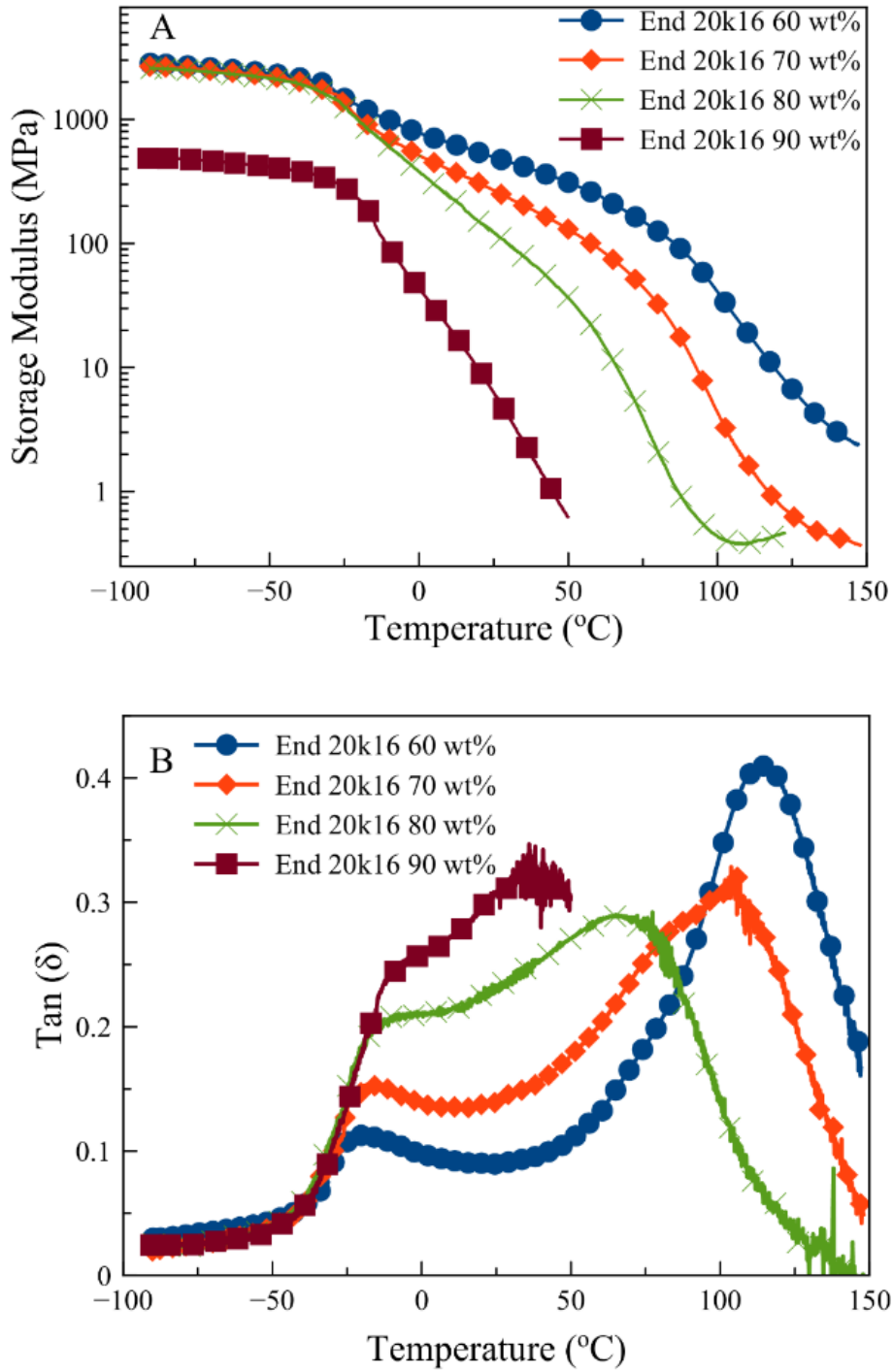


Figure 4.6. Storage modulus and Tan (δ) profiles as a function of temperature of end 20k16 with 60 wt% (—●—), 70 wt% (—◊—), 80 wt% (—×—) and 90 wt% (—◻—) oligomer species formulated with the corresponding wt% EEC. All samples were photopolymerized using 2 wt% PC-2506 and 1wt% ITX at 13.5 mW/cm² for 30 minutes.

measured by $\tan(\delta)$, of each domain may change due to different interactions between reactive diluent and prepolymer. Figure 4.6B shows the loss factor, $\tan(\delta)$, for the same formulations as a function of temperature. For all formulations using the end prepolymer, the first maxima occurs at similar but increasing temperatures. The small increase in the lower T_g is likely due to slightly greater concentrations of EEC and reactive prepolymer ends in the otherwise unreactive domains as the system becomes less defined with increasing prepolymer concentration. The peaks become more prominent as well, reflecting the increase in butyl acrylate concentration within the soft domain. Further, the increase in end reactive prepolymer lowers the apparent temperature of the secondary glass transition with decreases in cross-linking from lower concentrations of the reactive diluent and more influence from the soft butyl acrylate domains. At 60 wt% end functionalized prepolymer, the second glass transition occurs at 120°C while at 70 wt% this transition drops to 100°C. Further prepolymer content dramatically decreases this second T_g to roughly 60°C. Additionally, the second peak becomes less prominent and distinct with increasing prepolymer content. This decrease and broadening of the second $\tan(\delta)$ peak indicates more heterogeneities within the highly crosslinked, high T_g domain. These results are consistent with more butyl acrylate being incorporated within the highly crosslinked EEC domain through the crosslinking reactions with the cycloaliphatic epoxy functionalized chain ends producing a more homogeneous system with less defined hard and soft domains.

With the change in domains induced by composition of the photocurable resin, the stress-strain behavior of these materials will likely be significantly different. Figure

4.7 shows the stress–strain behavior in tensile mode of multiple formulations with various amounts of the end functionalized 20k16 prepolymer.

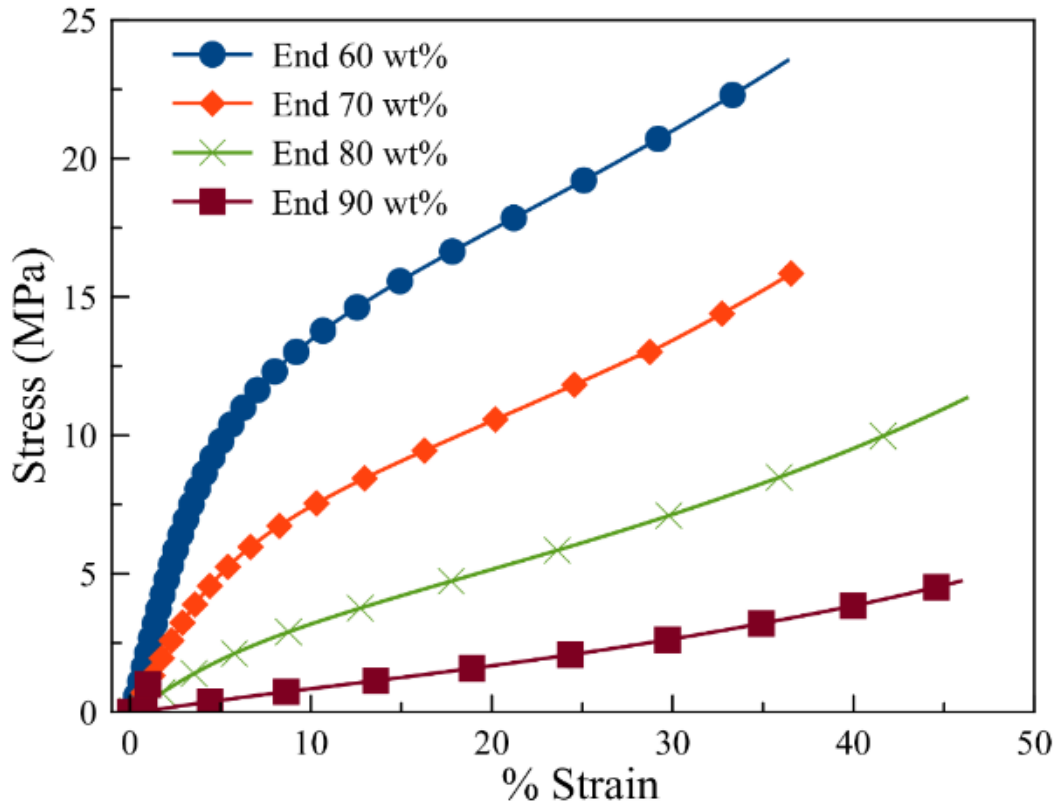


Figure 4.7. Stress-strain behavior at 30°C of with 60 wt% (—●—) 70 wt% (—◊—), 80 wt% (—×—) and 90 wt% (—◻—) end 20k16 species formulated with the corresponding wt% EEC. All samples were photopolymerized using 2 wt% PC-2506 and 1wt% ITX at 13.5 mW/cm² for 30 minutes.

Films with lower concentrations of the prepolymer exhibit multiple, distinct moduli, consistent with dual network materials. In the 60 wt% prepolymer system the highly crosslinked domain provides a large initial modulus. The modulus of the highly crosslinked domain, as indicated by the initial slope of these materials, is nearly halved as the prepolymer content increases to 70 wt%. As the prepolymer content continues to increase to 80 wt%, the initial modulus decreases again to roughly one fifth of the modulus observed in the 60 wt% system. At 90 wt% prepolymer concentration, the

system no longer exhibits multiple moduli, though the high concentration of butyl acrylate in the network allows these materials to have the highest elongation at break. These results further confirm that the initial modulus results from to the deformation of the highly crosslinked domain. Additionally, as the hard domain appears to deform at early strains, the highly crosslinked domains are likely continuous within the network. As the amount of prepolymer increases and the reactive diluent decreases, both the size and continuity of the hard domains decrease resulting in lower modulus and behavior approaching that of single domain polymer networks.

While the thermomechanical properties of photocurable resins can be altered by the concentration of the end functionalized prepolymer, another key method to control and modulate the polymer networks of these materials is to control the domain size and interactivity of the different networks. Increasing the rubbery or soft portion may make the material more elastic, while increasing the hard domain of the same material can increase modulus and abrasion resistance. In order to test similar properties as they relate to these end functionalized systems, a prepolymer was synthesized with lower concentration of reactive groups. Figure 4.8A shows the storage moduli for end 20k16 and end 16k8 prepolymer formulations at 60 wt% with 40% EEC reactive diluent added. The initial decrease in the storage modulus with increased temperature due to the predominantly butyl acrylate domain is observed in both formulations beginning at -25°C . This decrease is more pronounced in the 16k8 system, likely due to the longer butyl acrylate chain to reactive end segment ratio. The higher temperature transition, corresponding to the highly cross-linked domains formed with reactive chain ends and the EEC monomer, also occurs at lower temperatures for the end 16k8 as compared to

end 20k16. As there is likely more butyl acrylate within the functionalized ends of the 16k8 prepolymer, it is consistent that the EEC rich domains within these samples are softer and contain fewer crosslinks resulting in a lower modulus. Figure 4.8B, meanwhile, shows $\tan(\delta)$ as a function of temperature for these same materials. The first peak, again corresponding to a glass transition of the butyl acrylate rich domain, is more pronounced in the lower functionality species. The prominence of this peak is consistent with the longer butyl acrylate segment occupying more volume within the network, as compared to the more highly functionalized system. The second glass transition at higher temperatures, due to the highly crosslinked domain, is broader and occurs at a lower temperature for the 16k8 system. These results suggest a wider variety of relaxation times in the domain, compared to the higher functionality prepolymer. Further, the greater prominence of the first $\tan(\delta)$ peak combined with the lower, broader second $\tan(\delta)$ appears to show that the longer uninterrupted chains in the 16k8 prepolymers increase the distribution and properties of network heterogeneities. Meanwhile, the greater number of reactive groups on the 20k16 prepolymers and corresponding increase in domain size and continuity induce an increase in the second T_g of almost 25°C.

The stress-strain behavior will also be likely be affected by the decrease in functionality as the network now incorporates more of the soft butyl acrylate and has fewer reactive sites for crosslinking. Figure 4.9 shows the tensile stress-strain behavior of materials fabricated with 60 wt% end 20k16 or end 16k8 prepolymer and 40 wt% EEC reactive diluent. The photocured material incorporating the 20k16 prepolymer has a significantly greater modulus through 10% deformation, almost five times greater than

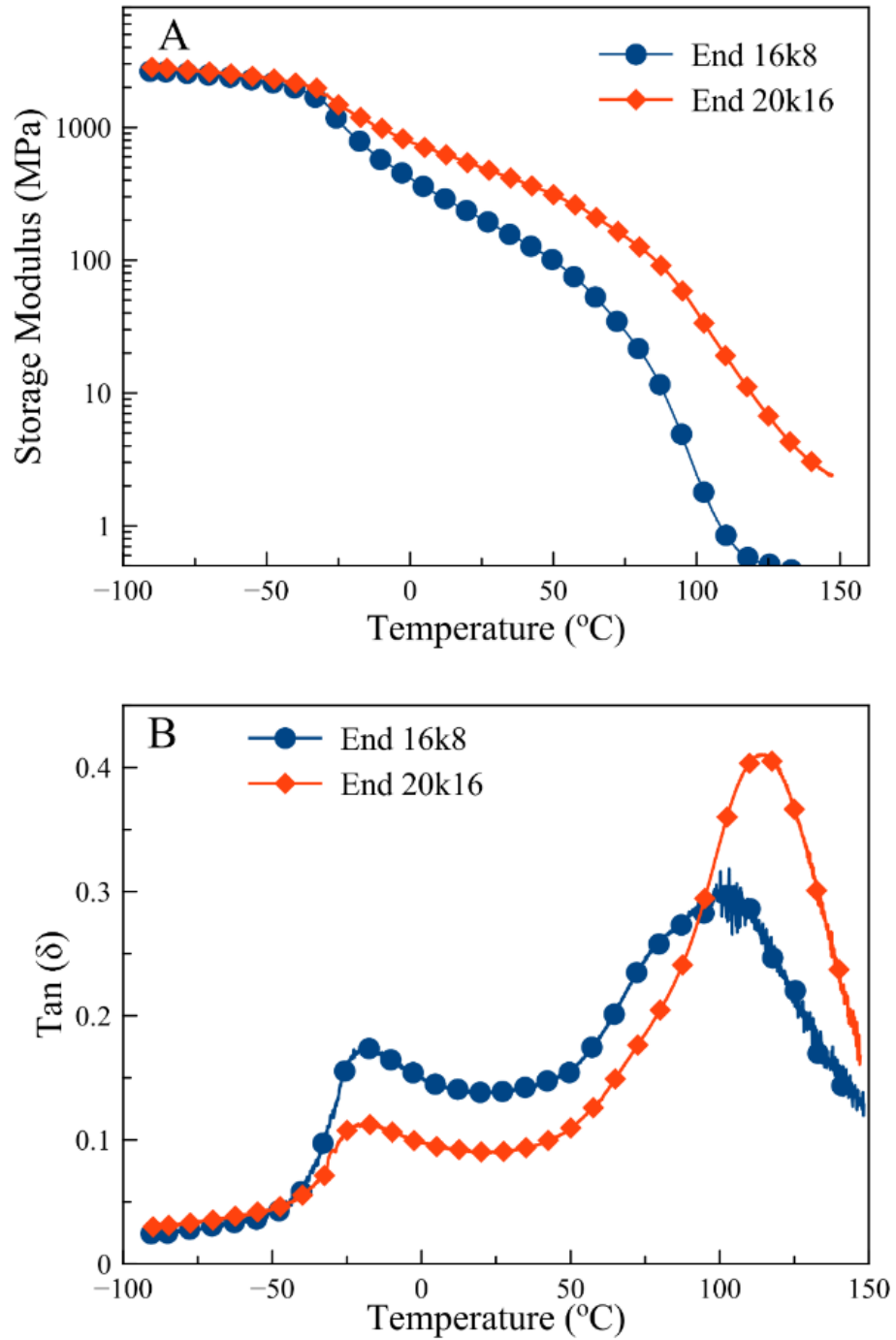


Figure 4.8. Storage modulus and Tan (δ) profiles as a function of temperature of end 16k8 % (—●—) and end 20k16 (—□—) oligomer species formulated with 40 wt% EEC. All samples were photopolymerized using 2 wt% PC-2506 and 1wt% ITX at 13.5 mW/cm² for 30 minutes.

the formulation incorporating the 16k8 formulation. Both of these materials appear to exhibit two moduli, as observed in other end functional prepolymers, although the transition is much more difficult to observe in the lower functionality system. The sharp transition in the 20k16 system show the impact of the greater number of reactive groups

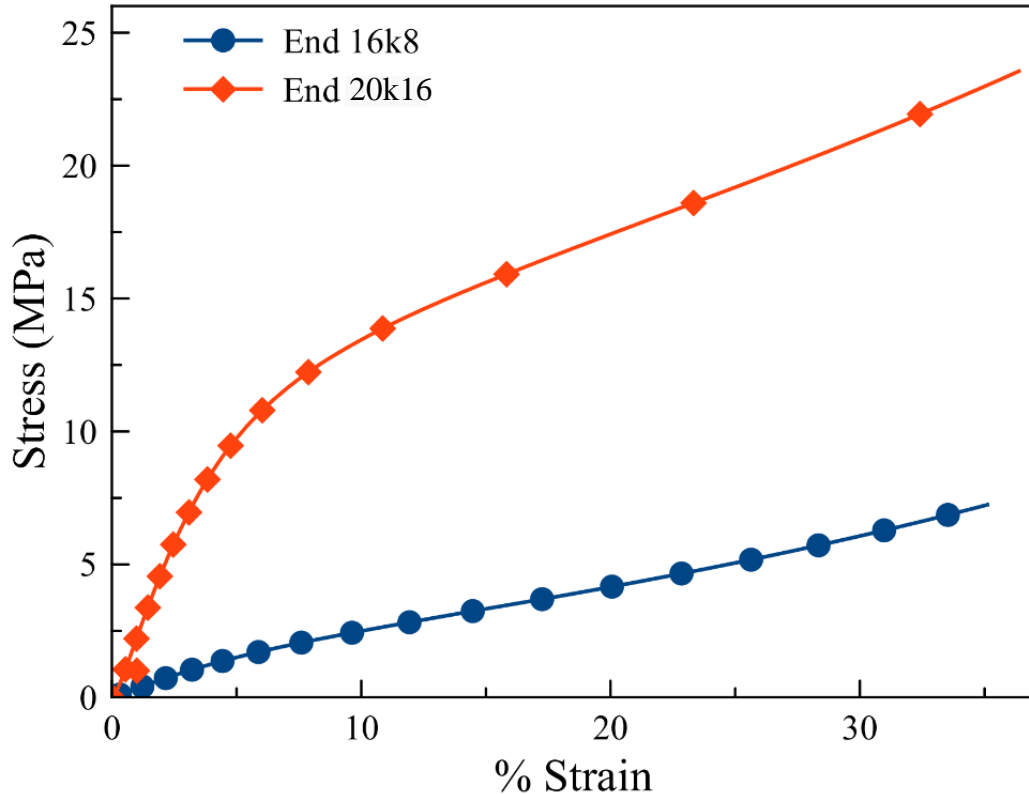


Figure 4.9. Stress-strain behavior at 30°C of 60 wt% end 16k8 (—●—) and end 20k16 (—◊—) species formulated with 40 wt% EEC. All samples were photopolymerized using 2 wt% PC-2506 and 1wt% ITX at 13.5 mW/cm² for 30 minutes.

that increases the overall crosslinking and the ability to resist strain. Interestingly, the presence of more butyl acrylate does not increase the elongation at break. Both materials exhibit almost 35% strain at break, even though the 20k16 materials require roughly 4 times the stress to break. Further, the slope of the secondary deformation, from roughly

10% to break, is larger for the 20k16 system. This difference in slope seems to indicate that there may be more cross-linking even in the otherwise nonreactive butyl acrylate domains. These results highlight the significant effect of both molecular architecture and the number of reactive groups in establishing the architecture in the resulting photopolymer networks.

Conclusions

Herein we report the use of architected reactive prepolymers to tune the properties of a photocured epoxy thermoset. Nitroxide-mediated polymerization is used to synthesize reactive oligomers with multiple blocks to isolate reactive groups in end segments or to synthesize randomly reactive copolymers. Formulations with end functionalized prepolymers exhibit greater rates of reaction than random analogues, suggesting a higher local concentration of epoxy moieties during photopolymerization. These higher rates indicate that the local reactive groups from the prepolymer and reactive monomer diluent segregate to form regions of higher crosslink densities. Thermomechanical analysis shows that end functionalized prepolymer systems form networks with multiple glass transitions, while randomly functionalized systems appear to form an amorphous network with a single, but broad, T_g . These results emphasize the importance of reactive group placement during polymer synthesis and photocurable network formation. Additionally, the segregation of reactive groups at the ends of the prepolymer molecule facilitates significant increases to the modulus and a 10-fold decrease of creep and greater creep recovery. The surface morphology of these materials via AFM show a higher range of in and out of phase behavior, suggesting that the hard, highly crosslinked and the longer, non-reactive butyl acrylate backbones provide greater

contrast. Increasing the end functionalized prepolymer content leads to a more homogenous material and a lower degree of segregation between the domains, resulting in decreases in both the initial modulus and the overall toughness of the materials. Furthermore, a decrease in the number of functional groups along the oligomer backbone induces a broadening and lowering of the T_g from the highly crosslinked regions indicating less distinction between domains and decreases in the continuity of the hard domain observed in end functional formulations. Higher functionality prepolymer systems exhibit a higher T_g , greater evidence of highly crosslinked areas which leads to a large initial modulus and more apparent dual network behavior. When formulated with end functionalized prepolymers, final polymer networks incorporate both continuous hard and highly crosslinked domains with inclusions of soft domains that facilitates increased modulus and elongation at break. Overall, this work demonstrates the importance of prepolymer molecular architecture on network morphology and thermomechanical properties.

References and Notes

- 1 H.Y. Park, C.J. Kloxin, A.S. Abuelyaman, J.D. Oxman, and C.N. Bowman, *Macromolecules*, **2012**, *45*, 5640-5646.
- 2 W. Xi, H. Peng, A. Aguirre-Soto, C.J. Kloxin, J.W. Stansbury, and C.N. Bowman, *Macromolecules*, **2014**, *47*, 6159-6165.
- 3 C. Dietlin, S. Schweizer, P. Xiao, J. Zhang, F. Morlet-Savary, B. Graff, J.-P. Fouassier, and J. Lalevée, *Polym. Chem.*, **2015**, *6*, 3895–3912.
- 4 J. V Crivello, and J.H.W. Lam, *J. Polym. Sci. Part A Polym. Chem.*, **1980**, *18*, 2697–2714
- 5 J. V Crivello, B. Falk, and M.R. Zonca, *J. Polym. Sci. Part A Polym. Chem.*, **2004**, *42*, 1630–1646.
- 6 J. V. Crivello and J.H.W. Lam, *Macromolecules*, **1977**, *10*, 1307–1315.
- 7 J. V Crivello, *Adv. Polym. Sci.*, **1984**, *62*, 3-47.
- 8 J. V. Crivello and J.H.W. Lam, *J. Org. Chem.*, **1978**, *43* 3055–3058.
- 9 K.S. Anseth, K.J. Anderson, and C.N. Bowman, *Macromol. Chem. Phys.*, **1996**, *197*, 833–848.
- 10 K.S. Anseth and C.N. Bowman, *J. Polym. Sci. Part B Polym. Phys.* **1995**, *33*, 1769-1780.
- 11 K.S. Anseth, C.N. Bowman, and N.A. Peppas, *Poly. Bull.*, **1993**, *31*, 229–233.
- 12 M.K. McBride, T. Gong, D.P. Nair, and C.N. Bowman, *Polymer*, **2014**, *55*, 5880-5884.

- 13 C.R. Szczepanski and J.W. Stansbury, *Eur. Polym. J.*, **2015**, 67 314–325.
- 14 C.R. Szczepanski, C.S. Pfeifer, and J.W. Stansbury, *Polymer*, **2012**, 53 4694–4701.
- 15 C.R. Fenoli, J.W. Wydra, and C.N. Bowman, *Macromolecules*, **2014**, 47 907–915.
- 16 L. Tebben and A. Studer, *Angew. Chem. Int. Ed. Engl.*, **2011**, 50, 5034–68.
- 17 M. Destarac, *Macromol. React. Eng.*, **2010**, 4 165–179.
- 18 N. Agudelo, A.M. Elsen, H. He, B.L. López, and K. Matyjaszewski, *J. Polym. Sci. Part A Polym. Chem.*, **2015**, 53 228-238.
- 19 G. Delaittre, J. Rieger, and B. Charleux, *Macromolecules*, **2011**, 44, 462–470.
- 20 H. Shen, G. Quintard, J. Chen, and M. Taha, *J. Appl. Polym. Sci.*, **2014**. 132, 41295
- 21 C. Decker and T.N.T.H.I. Viet, *J. Appl. Polym. Sci.*, **77**, 1999, 1902–1912
- 22 Y. Rao, J. Munro, S. Ge, and E. Garcia-Meitin, *Polymer*, **2014**, 55, 6076–6084.
- 23 C. Chen, J. Liu, F. Sun, and J.W. Stansbury, *J. Polym. Sci. Part A Polym. Chem.*, **2014**, 52, 2830–2840.
- 24 L. Wang and L.J. Broadbelt, *Macromolecules*, **2009**, 42, 7961–7968.
- 25 Y. Guo, X. Gao, and Y. Luo, *J. Polym. Sci. Part B Polym. Phys.*, **2015**, 53, 860–868.
- 26 A. Gigot, M. Sangermano, L.C. Capozzi, and K. Dietliker, *Polymer*, **2015**, 68, 195–201.

- 27** M. Sangermano, D. Foix, G. Kortaberria, and M. Messori, *Prog. Org. Coatings*, **2013**, 76 1191–1196.
- 28** M. Sangermano, W.D. Cook, S. Papagna, and S. Grassini, *Eur. Polym. J.*, **2012**, 48, 1796–1804
- 29** S. Ponyrko, J. Kovářová, L. Kobera, and L. Matějka, *J. Appl. Polym. Sci.*, **2014**, 131. 40899
- 30** W.D. Callister and D.G. Rethwisch, *Material Science and Engineering*, 9th ed. Wiley, New York, 2013.
- 31** B.S. Forney and C. A. Guymon, *Macromolecules*, **2006**, 39, 8502-8510.
- 32** M. A. DePierro and C.A. Guymon, *Macromolecules*, **2006**, 39, 617–626.
- 33** J.D. Clapper and C.A. Guymon, *Macromolecules*, **2007**, 40, 1101–1107.

CHAPTER 5
PHOTOPOLYMERIZATION RATE AND PREPOLYMER EPOXIDE
LOCATION ON NETWORK MORPHOLOGY

Introduction

Photopolymerization has been a prominent technology for a wide array of coatings and adhesives applications and particular interest 2D and 3D printing.¹⁻³ Cationic photopolymerization is one method that has received significant attention due to unique reaction kinetics and thermomechanical properties. Cationic systems utilize photoacid generators to create superacids to initiate a ring opening polymerization reaction.⁴⁻⁶ In the past decade, heterocyclic four-membered oxetanes have gained interest in cationic photopolymerization as a method to modify resins.⁷⁻⁹ Traditionally, oxetane monomers have been characterized by a long induction period, which limits their broader industrial and academic applications.¹⁰⁻¹² The induction period usually requires incorporation of a comonomer to accelerate the overall photopolymerization reaction, though the resulting thin films are highly crosslinked with little control over the resulting network heterogeneities.^{4,13,14}

Formulations that have been examined to overcome the network heterogeneities and accompanying shrinkage stress in highly crosslinked films include thiol-epoxy and thiol-acrylate systems.^{15,16} These thiol-x formulations are frequently referred to as click chemistries due to their rapid reactions with high yields at and under moderate conditions.^{17,18} Unfortunately, both thiol-acrylate and thiol-epoxy reactions suffer from low glass transitions and poor long term stability, which limits their widespread industrial applications.^{18,19} Ternary mixtures of thiol-epoxy-acrylate monomers have also been

examined.²⁰ These systems show promise to combine multiple networks within a single polymer system with tunable mechanical properties through the manipulation of each network.²¹ Other photoinduced click reactions, including copper catalyzed azide alkyne reaction and diels-alder systems have also been examined.²²⁻²⁴ The networks generated by these click reactions are formed via a step polymerization mechanism similar to the thiol-x reactions and produce highly regular networks without the heterogeneities of traditional cationic or radical photopolymer formulations. The lack of heterogeneities can lead to decreased shrinkage stress during the photopolymerization reaction.²²

Another method that is used to control the heterogeneities of photocured networks is to incorporate large prepolymers and oligomers that are >10,000 Da in size.^{25,26} Interest in these systems stems from controlling the relative free volume change as a method of both limiting shrinkage stress with an added benefit of potentially generating multiple domains within the thermosetting network.²⁷ Both reactive and non-reactive prepolymers have been examined for their ability to modify the polymer network morphology and structure.²⁸ Multiple phases and domains have been detected with properties that can be modified via the selection of prepolymer backbone.^{25,28} Research has also shown that if the prepolymers are made via a reversible addition fragmentation chain transfer (RAFT) method, or if a RAFT adduct is present, the shrinkage stress can be lowered significantly if the controlling agent is left active.²⁹ The combination of free volume transition and rapid bond rearrangement inherent to these systems demonstrate the promise of utilizing prepolymer additives to reduce shrinkage stress and tune network morphology in the field of photocurable thin films.

The present study aims to expand on the use of architected prepolymers synthesized via stable free radical polymerization by establishing methodologies to use methacrylate monomers in the center functionalized prepolymer backbones. Nitroso-compounds were synthesized with epoxy groups located either in the center or statistically distributed along the prepolymer backbone. The role of a terpene oxide accelerant and its interactions with the two architectures on both conversion profile and thermomechanical properties, including T_g and stress strain, were examined. Network differences were probed with atomic force microscopy and resulting differences in surface properties were characterized via water contact angle of these films. We hypothesize that the center prepolymer architecture will promote the backbone monomer characteristics via the formation of heterogeneities and, thus, tune macroscopic properties.

Experimental

Materials

Bis[(2,2-dihydromethyl) butyl] ether (DOX, Toagosei), and PC-2506 (Polysset), a diaryliodonium hexafluoroantimonate photoinitiator, were used as received. Lauryl methacrylate (LMA, Sigma Aldrich) and 3,4-epoxycyclohexylmethyl methacrylate (METH-B, Toagosei) were used as obtained. Methyl-2-methyl-3-nitro-2-nitrosopropionate (NMMA) was synthesized as described in the literature.³⁰

Center functionalized prepolymers were synthesized utilizing the nitroso-agent NMMA. A 1/2/40 molar ratio of NMMA/AIBN/LMA was diluted to 50% by mass with propyl acetate. A second feed consisting of a 3/1 molar ratio of LMA/METH-B was then added followed by a third feed identical to the first. Randomly functionalized

prepolymers were synthesized with a single feed, composed of NMMA/AIBN/METH-B/LMA at a molar ratio of 1/2/20/140 diluted to 50% by mass with ethyl acetate. In both procedures, the reactor was sparged for one hour with nitrogen before the vessel was then heated to 90°C. All feeds were allowed to reach approximately 85% conversion, as determined by targeted molecular weight. Once the desired molecular weight was achieved, residual monomer and solvent were removed via rotary evaporation for one hour at 55°C.

Molecular weight and polydispersity index (PDI) of prepolymers were measured using a size exclusion chromatography setup including a refractive index detector (Shimadzu RID-10A). Additionally, a flow rate of 1 mL/min ethyl acetate through a PLgel Mixed-D column and was used for experimental analysis. Table 5.1 summarizes the properties of the prepolymer molecules used in this study.

Table 5.1 Prepolymers used in this study

Sample Name	Epoxy Location	Number of Reactive Groups	M _n	PDI
Center	Center	20	40,000	1.24
Random	Random	20	38,800	1.44

Methods

To formulate prepolymer/monomer mixtures, lower molecular weight monomers were added to weighed out prepolymer content and mixed via vortexing. Diaryliodonium hexafluoroantimonate photoinitiator, (PC-2506) (2 wt%) was incorporated shortly before the polymerization.

Real-time infrared spectroscopy was performed using a Thermo Nicolet nexus 670. One mg of sample was placed on a sodium chloride plate covered with 15 μm spacer

beads and sandwiched with an additional sodium chloride plate. The laminate nature of this testing geometry prevents oxygen and water vapor from diffusing into the system. Analysis was performed at ambient temperature and atmosphere. Oxetane and epoxide conversions were determined by monitoring the decrease of the absorbance bands at 980 cm^{-1} and 790 cm^{-1} , respectively. Photopolymerization reaction analysis was performed using an irradiation intensity of 25 mW/cm^2 .

Dynamic mechanic analysis (DMA, Q800 DMA TA Instruments) was conducted to investigate the effect of polymer architecture on ultimate mechanical and visco-elastic properties of cured polymers. To fabricate rectangular $6 \times 25\text{ mm}$ and 0.15 mm thick films, two thick glass plates, covered by amorphous polyvinylidene fluoride films (PVDF, Teflon® AF, Dupont) for easy release, were used. Adhesive tape spacers ($150\text{ }\mu\text{m}$ thick) were attached on each edge of the bottom plate to control the film thickness. Approximately 3 g of liquid sample mixture were placed on the bottom glass plate. The liquid samples were then tightly pressed using the upper glass plate and secured using binder clips. Filled molds were irradiated for 10 minutes using a UV lamp ($250\text{-}500\text{ nm}$) at an irradiation intensity of 25 mW/cm^2 . To measure the modulus and glass transition temperature of the samples, the temperature of the films was increased from -100°C to 150°C at a heating rate of $3^\circ\text{C}/\text{min}$. DMA tensile mode was utilized under constant strain at a frequency of 1 Hz . Young's modulus and tensile properties were evaluated at 30°C in tensile mode with a force rate of 1.0 N/m . Young's Modulus was calculated using the slope of the stress-strain curve in the early linear regime (less than 10% strain).³¹

Morphologies of films prepared, as described above, were analyzed utilizing an Asylum Research mfp3d atomic force microscopy (AFM) and analyzed with the provided Igor software. Phase images were obtained in tapping mode.

Results and Discussion

The use of multifunctional monomers and prepolymers gives rise to a crosslinked network that can be used to tune various properties such as glass transition temperature and modulus. One way to tune these properties is to control the network architecture and local heterogeneous structure. Most common photocurable resins utilize basic prepolymer structure to tune thermomechanical properties. However, recent work from our group shows that larger oligomers with defined structures can be used to obtain networks that are difficult to achieve via conventional photopolymerization. These unique network structures are generated by placing reactive epoxy or acrylate groups chiefly at the end of a butyl acrylate prepolymer synthesized via NMP or RAFT methods. This work examines the placement of epoxide functionalities located at the center of a lauryl methacrylate prepolymer to determine how this new architecture may be used to tune thermomechanical properties and network heterogeneities formed during the photopolymerization reaction. We hypothesize that the long aliphatic tails will disrupt the polymer network and produce highly heterogeneous materials.

Based on the polymerization kinetics observed using prepolymers with tailored functionality and structure, it is plausible that a higher concentration of epoxy reactive groups may cause an increase in the photopolymerization and potentially conversion rates for these samples. One indirect measure to determine if photocurable resins may have differences in their reaction kinetics is photo-DSC (pDSC). Figure 5.1 shows the pDSC

profiles for the center and random prepolymer formulations both with and without LDO studied in this chapter. Differences in the reaction profiles of heat evolved as a function of time show significant differences. Both of the center formulations appear to have little or no inhibition, while the formulation that uses both the random formulation and LDO appears to have a significant inhibition time. Furthermore, the shape of the pDSC profiles indicates the presence of potential complexities in the reaction. Traditional pDSC profiles most closely resemble the random/DOX profile, while the other profiles indicate there may be secondary reactions occurring or that the oxetane monomers and the epoxide groups may be reacting on different time scales. The differences in molecular structure appear to be causing segregation of monomers prior to photopolymerization inducing unique reaction profiles for all but the Random/DOX prepolymer formulation.

To further characterize the reaction kinetics for the photopolymerization of the architected prepolymer formulations, real time FTIR was used to determine if the epoxy moieties attached to the prepolymer are reacting differently in the resins than the reactive oxetane diluent. Figure 5.2A and 5.2B display the oxetane and epoxide conversion, respectively, for resins both with and without a terpene oxide accelerant for both center and randomly functionalized prepolymer formulations. The inclusion of a terpene oxide accelerant appears to greatly affect the oxetane conversion when used in combination with either type of prepolymer architecture. When included in the center functionalized prepolymer, a brief induction period is observed followed by a rapid polymerization with a final oxetane conversion of near 80%. When LDO is not included, no induction period is seen while the overall conversion of the oxetane moiety is low. These results suggest that terpene oxides may be sequestered with the other epoxy

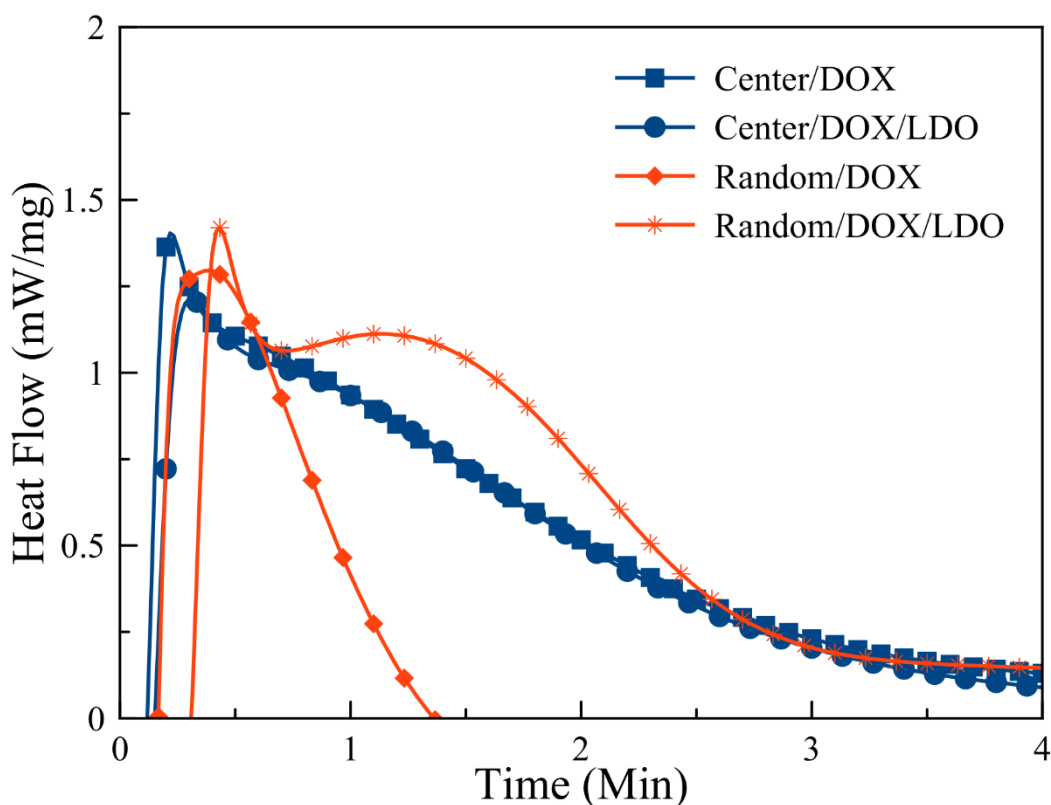


Figure 5.1. Photo-DSC (PDSC) profiles for center and randomly functionalized prepolymer/DOX formulations with and without LDO. Photopolymerizations were initiated with 2 wt% PC-2506 using 280-400 nm light at 25 mW/cm².

groups and thus may require diffusion before reacting with the reactive DOX monomer diluent. The epoxy conversion for the center functionalized prepolymer materials suggests that some diffusion limiting event is occurring. The center formulation without LDO appears to have a relatively smooth conversion profile typical of a standard uniform photoreactive formulation. On the other hand, the inclusion of a small amount of terpene oxide appears to induce two stages of epoxide conversion. The first occurs from 0 to approximately 17% epoxide conversion. The second regime may result as the limonene dioxide becomes less diffusionally limited than the epoxides incorporated onto the

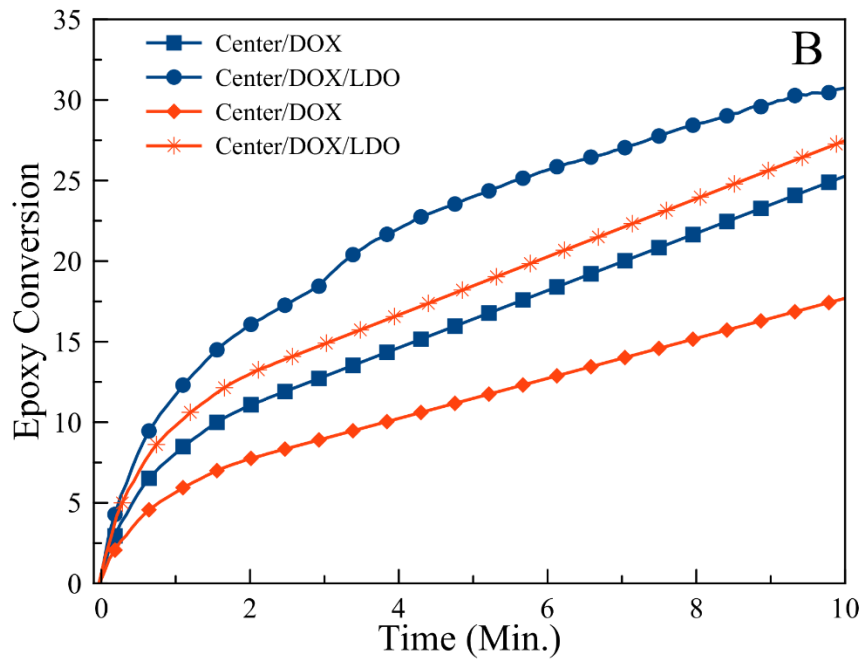
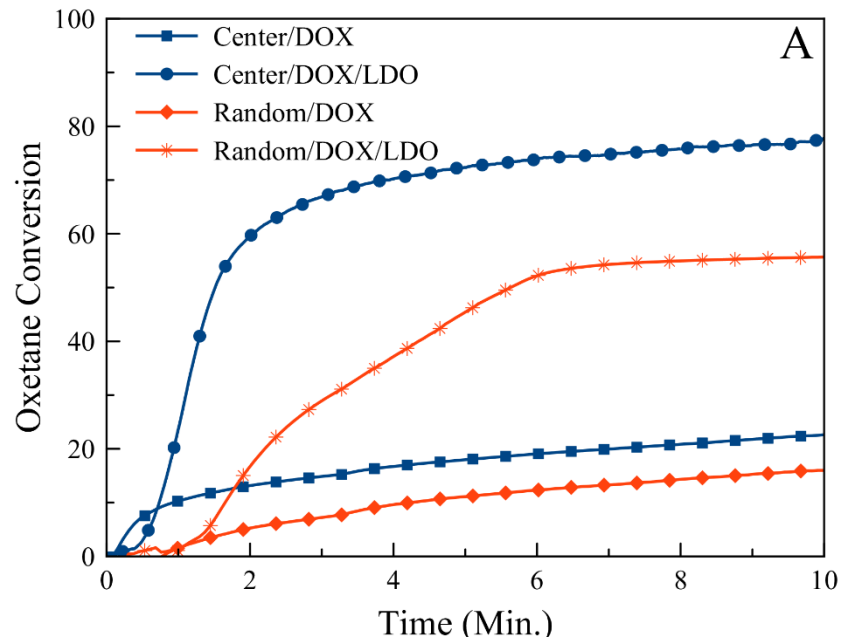


Figure 5.2 Functional group conversion profiles for oxetane (A) and epoxide (B) groups in 60 wt% prepolymer formulations. Photopolymerizations were initiated with 2 wt% PC-2506 using 280-400 nm light at 25 mW/cm².

prepolymer backbone. The randomly functionalized samples meanwhile display lower conversions for both the oxetane and epoxy monomers. The random formulation without the terpene oxide accelerant shows very low conversions similar to those seen in the center functional materials, though the higher proximity of epoxide groups on the center functionalized prepolymers may account for the greater rate of epoxide conversion. Additionally, the greater concentration of epoxy groups located in the middle of the prepolymer may also aid in the acceleration of the oxetane reaction, as compared to the randomly functionalized control. The oxetane formulations show inhibition times when LDO is included in the formulation. Once LDO is incorporated, a small induction time of a few seconds is observed for the center functionalized materials, compared to approximately 45 seconds for the random prepolymer system. Further, it is possible that the architecture of these materials accounts for the lower overall conversion for the randomly functionalized formulation as the center functionalized prepolymers cause stronger segregation of reactive diluents prior photopolymerization. Additionally, the random prepolymer/LDO formulation also has a lower epoxy conversion during the illumination period, which may again be a result of the differences in potential local reactive group concentrations between the two architectures. Together, these results suggest that the center functionalized prepolymers may be causing some degree of separation between the large prepolymers and smaller reactive oxetane monomers. The separation between the two may thus affect the morphologies of the photocured networks.

The reaction kinetics indicate that specific domains may be forming with the differently functionalized prepolymers and the reactive diluent, similar to what is

observed for end functionalized prepolymers. As such, it is reasonable to believe that differences in the polymer network are induced as well. Dynamic mechanical analysis (DMA) was utilized to determine the moduli and glass transition of these materials. Figure 5.3 shows the storage modulus (A) and $\tan(\delta)$ (B) for center and randomly functionalized formulations. The storage moduli for both the center and randomly functionalized materials exhibit broad transitions from the glassy to rubbery states. For samples without the terpene oxide accelerant, these transitions begin roughly 20°C lower than those systems that incorporate LDO as an accelerant. Since significantly greater photopolymerization conversions for both the oxetane and epoxide moieties are observed when LDO is utilized; the resulting films may be stiffer with more heterogeneity within the network. Greater conversion would result in a higher glassy plateau and increases the temperature at which these films undergo their glass transition. Further, with or without LDO present, the center functionalized formulations display a broader transition, as compared to their randomly functionalized counterparts. It is possible that the differences in transition are due to the long aliphatic tails of the center functionalized prepolymers protruding into the network resulting in a much larger distribution of relaxation times. Additionally, between the combination of higher reactive group density and larger oxetane conversion, it appears that these materials have a larger rubbery modulus indicating a network with a potentially higher relative crosslink density. To gain further insight into the network structure of the polymer network, the $\tan(\delta)$ values of the polymers and corresponding glass transition temperatures (T_g) were determined. Figure 5.3B shows $\tan(\delta)$ as a function of temperature for the random and center functionalized prepolymers both with and without LDO.

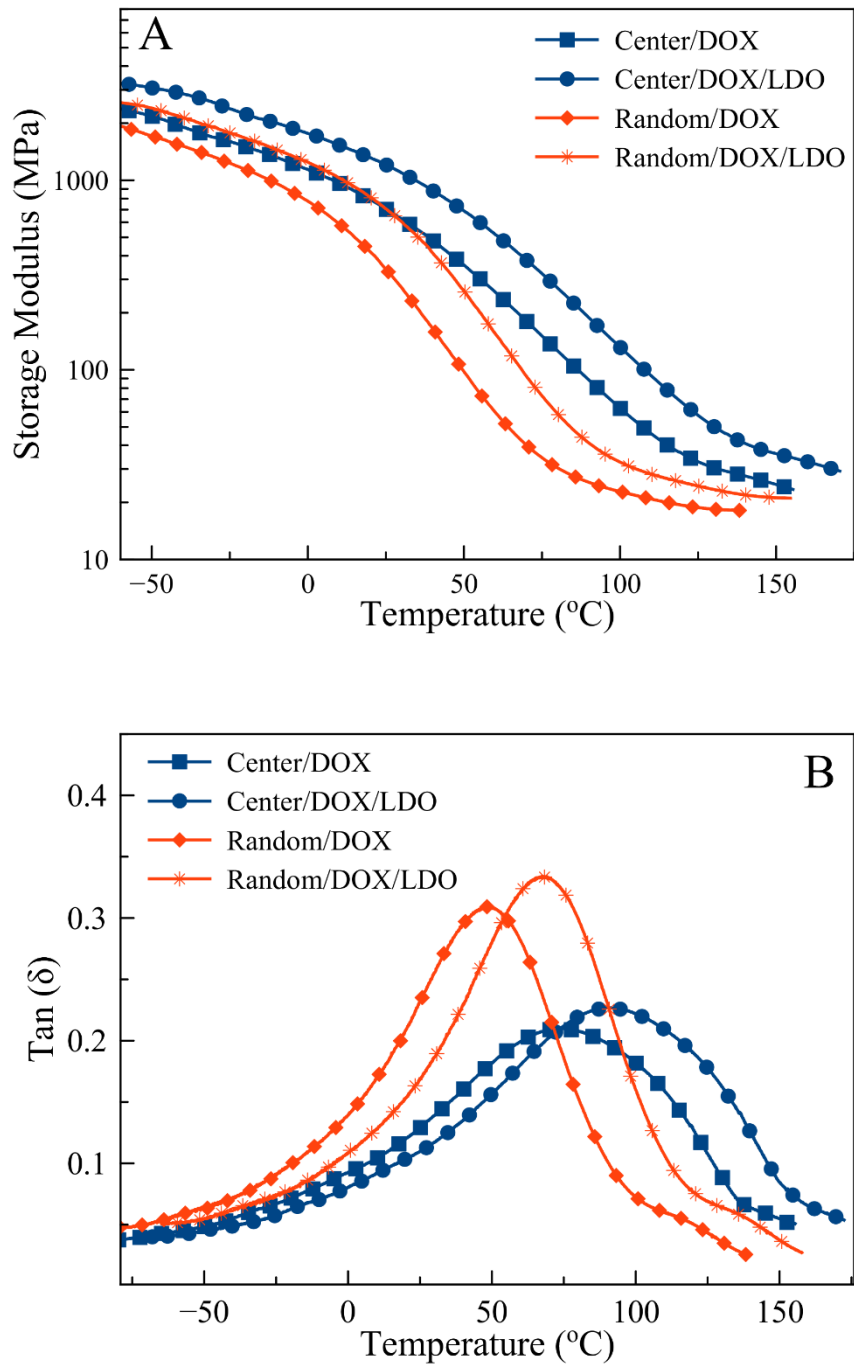


Figure 5.3. Storage modulus(A) and the tan (δ) (B) profiles as a function of temperature for both center and random prepolymer formulations with and without a terpene oxide accelerant. All samples were photopolymerized using 2 wt% IHA under standard room temperature conditions at 25 mW/cm² for 10 min. All samples were annealed at 60°C for 24 hours.

The randomly functionalized materials have a lower overall T_g than the center functionalized materials and show a narrower $\tan(\delta)$ distribution. When LDO is incorporated into the formulation it is likely that the higher degree of photopolymerization generates greater heterogeneities via greater polymerization of the smaller difunctional oxetane monomers. The higher degree of heterogeneities is also apparent from the full width at half max of the $\tan(\delta)$ peaks. The formulations utilizing randomly functionalized prepolymers are nearly half the value of the center functionalized formulations. The significant breadth of the center functional prepolymer $\tan(\delta)$ peaks suggests that there are significantly more diverse local molecular relaxations in the center functional prepolymer networks. The resulting oxetane polymerizations would account for the increase in the T_g for both prepolymer systems. When LDO is not incorporated in these systems, the center functionalized species still exhibits a higher T_g with a much broader distribution of relaxation times. The difference in network structure is plausible if the longer aliphatic ends of center prepolymers are creating much more diverse microenvironments throughout the network. These thermomechanical results indicate that the non-reactive segments of the prepolymer introduce greater overall network heterogeneity and, thus, produce broader glass transition materials.

As the glass transitions of these materials appear to be greatly affected by the structure of the prepolymer incorporated into the network, it is likely the different formulations will exhibit different stress-strain behavior. To probe the effect of the network heterogeneity differences on mechanical properties, Figure 5.4 shows the stress-strain behavior of these formulations in tensile mode. Center functionalized materials

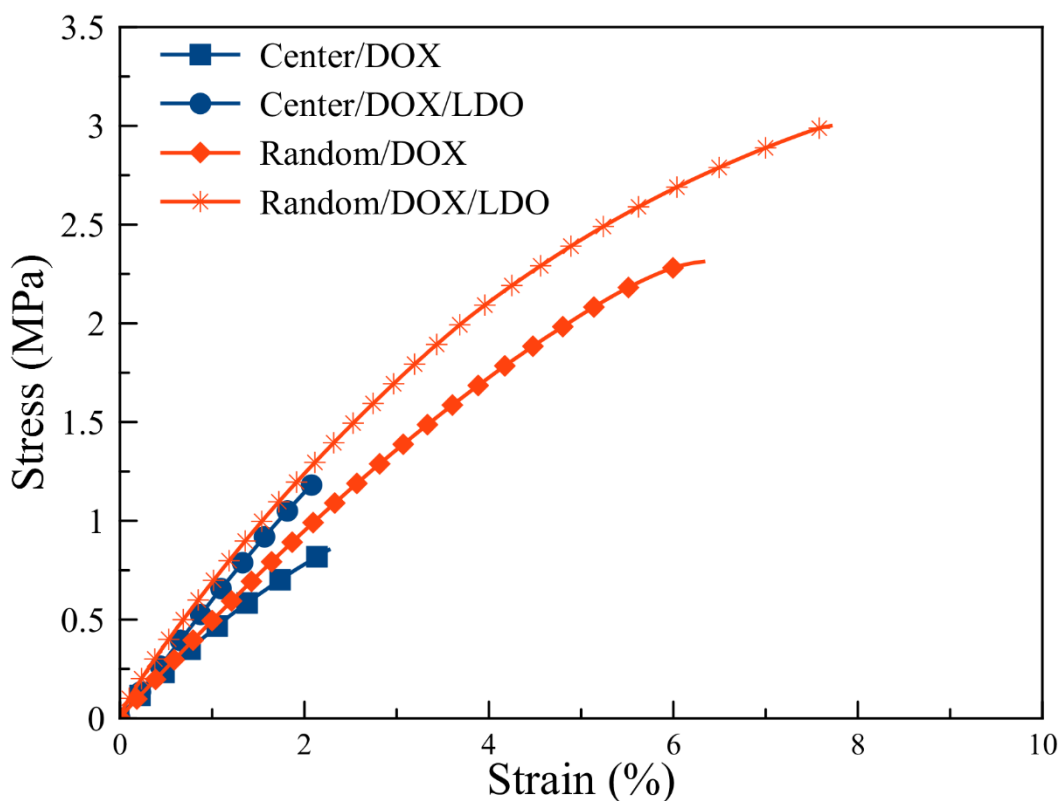


Figure 5.4. Stress-strain behavior in tensile mode at 30°C for both center and randomly functionalized prepolymers formulated with and without LDO as an accelerant. All samples were photopolymerized using 2 wt% IHA under standard room temperature conditions at 25 mW/cm² for 10 min. All samples were annealed at 60°C for 24 hours.

exhibit surprising behavior given their high T_g . It appears that the aliphatic homopolymer at the end of each prepolymer chain within the network under mines much of its integrity under tensile testing, especially as compared to their randomly functionalized counterparts. It appears that the greater distribution of reactive groups along the prepolymer backbone allows a more homogenous network with greater interactions between the prepolymer and reactive diluent. Additionally, when LDO is incorporated, the modulus of each formulation increases by more than 50% for the center functional resin and 25% for the randomly functionalized resin. The increase in modulus is again consistent with not only the incorporation of a higher T_g monomer but also with

potentially greater oxetane conversion. Interestingly, the randomly functionalized systems undergo more than twice the elongation of the center functional materials. The difference in elongation at break may be consistent the lauryl methacrylate homopolymers disrupting the network. The soft aliphatic segments may be forming pockets within the network, though are not covalently bound, and thus act to decrease the actual mechanical properties of these films. The presence of the lauryl methacrylate blocks at the ends of center functionalized prepolymers appear to greatly affect the network structure and thus decrease the mechanical properties of these films.

Typically enhanced conversion would lead to enhanced thermomechanical properties. To determine if these contradictory results are due to changes in polymer network structure, AFM was used to characterize the microenvironment of the photopolymer networks. Figure 5.5 shows the phase images for center and random prepolymer formulation with and without LDO. Figures 5.5A and 5.5B show the nanoscale domains of the center functionalized formulations while figures 5.5C and 5.5D show the nanoscale domains of the randomly functionalized prepolymer formulations. Figures 5.5A and 5.5B show distinct, large black areas suggesting there is a strong contrast in the morphology within the film. Figure 5.5B shows roughly half the black areas of figure 5.5A, suggesting that the use of LDO as an accelerant is directly affecting the morphology of the films allowing less time for the aliphatic tails to reptate and assume relaxed configurations within the network. The random prepolymers both with and without LDO show much lower in and out of phase behavior, consistent with more homogenous networks. The formulation without LDO appears to have almost 60% more contrast in their in and out of phase behavior compared to the accelerated counterpart

formulation. Moreover, the immediate contrast between the two formulations based on prepolymer architecture used in the formulation further corroborates our hypothesis that the larger aliphatic tails are serving to disrupt network formation. One aspect that should be noted is the domain sizes of the nanoscale features. For the center functionalized materials, domains and features on the order of hundreds of microns can be easily observed and contrasted to the rest of the photo-crosslinked network. On the other hand, the randomly functionalized samples show very small scale differences that could easily be attributed to simple small differences behaviors across the surface of the material.

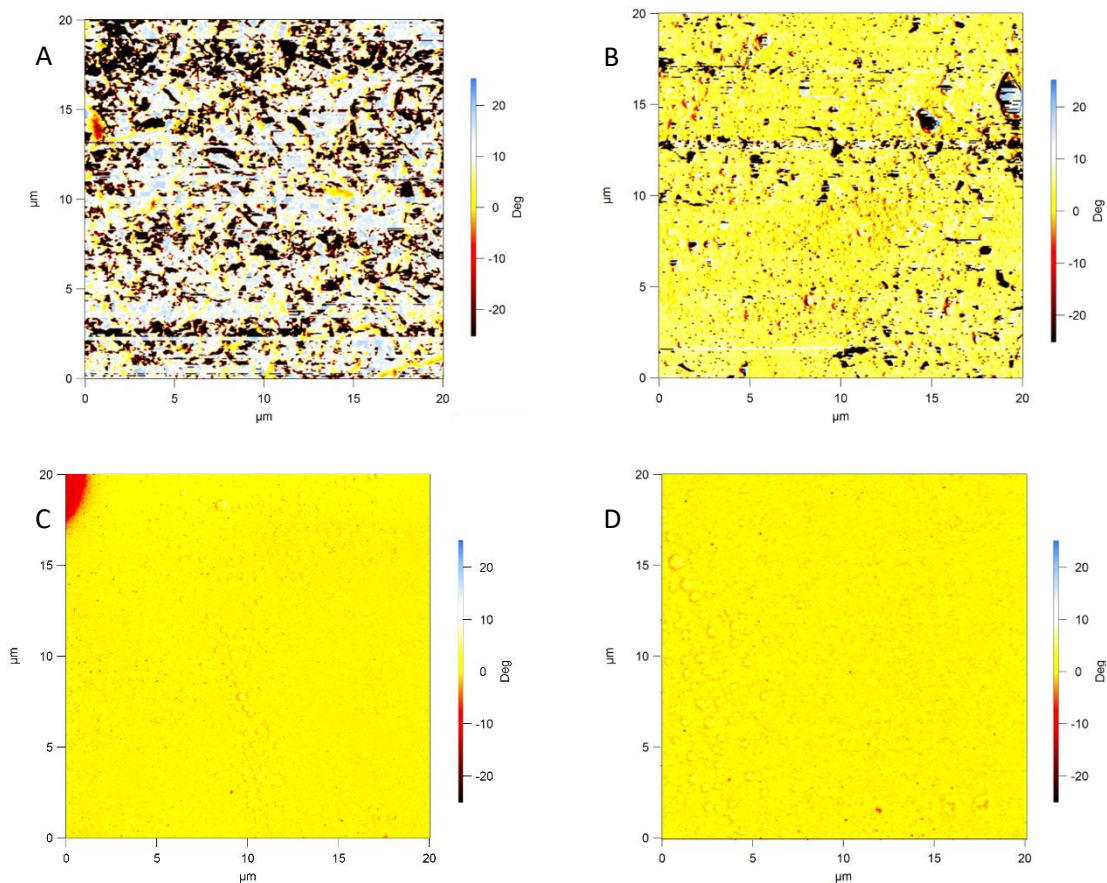


Figure 5.5. AFM Phase images of 60 wt% center (A and B) and random (C and D) prepolymers formulated with 40 wt% DOX. Figure 5.5B and 5.5D incorporate 5 mol% LDO. All samples were photopolymerized using 2 wt% PC-2506 at 25 mW/cm² for 10 minutes. All samples were annealed at 60°C for 24 hours.

The randomly functionalized materials would not be expected to show much in or out of phase behavior, though the formulation without LDO does appear to have slightly higher in and out of phase behavior. The two center functionalized formulations meanwhile show a much more pronounced acceleration effect. As a significantly greater amount of the oxetane diluent is converting when LDO is included, these tails have less time to diffuse or move in the network. The increase in phase contrast when using the center functionalized materials, compared to their randomly functionalized controls, further confirms the increase in heterogeneities and architected prepolymers abilities to govern network morphology.

Given the apparent differences in morphology throughout the network, it is plausible to believe that the two formulations would have different surface properties as well. To measure differences in surface properties, the water contact angle is shown in Figure 5.6 for polymerized formulations. The center functionalized formulations exhibit higher contact angles, suggesting that the aliphatic nature of the prepolymer backbone is being expressed much more at the surface of these materials. The formulation without LDO accelerant shows the greatest contact angle, consistent with the AFM phase images. When LDO is incorporated into the center functional formulation, a small change in the water contact angle is observed with further decreases in the randomly functionalized formulations. The increased aliphatic character of the networks, as observed in the AFM images, may explain why the center functionalized prepolymers increase the water contact angle becoming more hydrophobic. The increased concentration of long aliphatic chains changes the relative polarity at the surface of the polymer system, producing films

that are more hydrophobic without altering the concentration of lauryl methacrylate in the network.

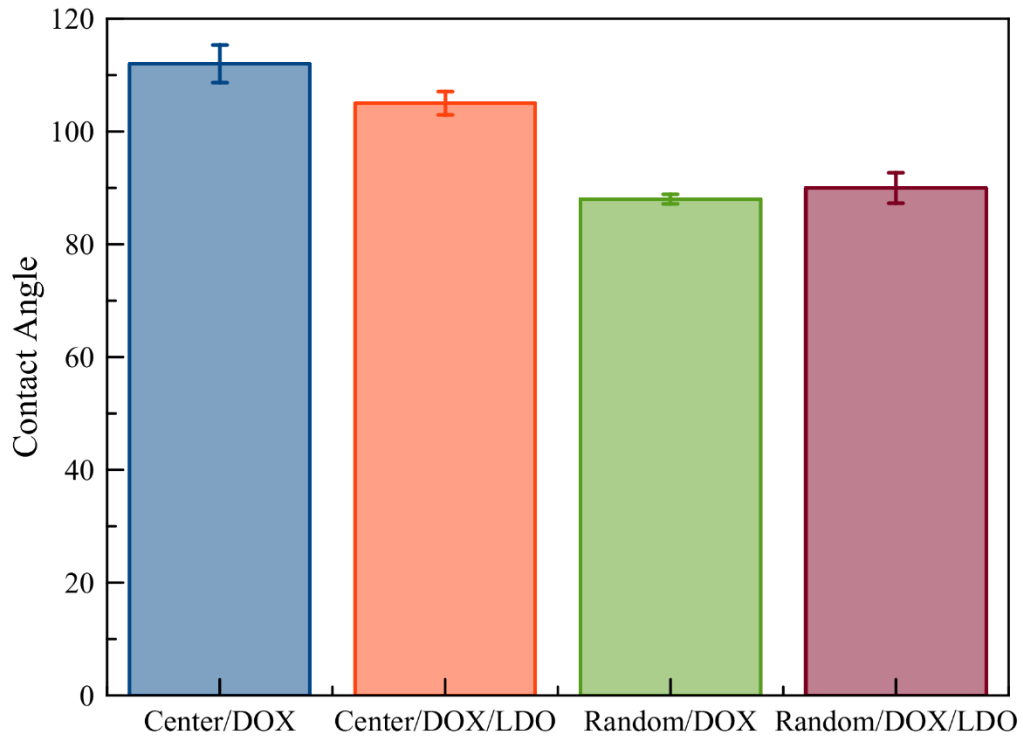


Figure 5.6. Water contact angle measurements for lauryl methacrylate/ oxetane thin films. All samples were photopolymerized using 2 wt% PC-2506 at 25 mW/cm² for 10 minutes. All samples were annealed at 60°C for 24 hours.

Conclusions

Here we report the utilization of center functionalized prepolymers in comparison to randomly functionalized prepolymers to modify polymer networks. Nitroso compounds were identified for compatible polymerization of methacrylate groups in order to modify and control the placement of cycloaliphatic epoxy reactive groups. The combination of a center architecture and longer aliphatic tails shows higher conversion

for both oxetane and epoxy groups. When LDO is included in the photopolymer resin as a method to increase the rate of oxetane conversion, diffusionally limited reactions between the oxetanes and the center functional prepolymer appear to occur. Further, prepolymer molecules with the cycloaliphatic groups concentrated in the center provide materials with a higher glass transition and apparent crosslink density, as indicated by the rubbery modulus. The center functionalized materials show a wider $\tan(\delta)$ peak compared to the random functional prepolymers due to the aliphatic tails disrupting network formation and increasing network heterogeneity. The resulting disruptions in network integrity also account for the lower modulus and elongation at break for the center functionalized formulations. AFM phase images show that the polymer networks utilizing the center functional prepolymers appear to have segregated regions rich in the aliphatic lauryl methacrylate that may weaken the resulting polymer network. On the other hand, these regions of lauryl methacrylate present in the polymer network do modify the surface properties. Center functionalized prepolymer formulations exhibit greater hydrophobicity, which is further tuned by the inclusion of a terpene oxide accelerant. In summary, this work demonstrates that the use of center functionalized prepolymers may produce highly heterogeneous networks with direct control over surface properties which may be further modified by the rate of photopolymerization.

References and Notes

- (1) Webster, I. *Int. J. Adhes. Adhes.* **1997**, *17* (1), 69–73.
- (2) Crivello, J. V. *J. Photopolym. Sci. Technol.* **2007**, *20*, 599–603.
- (3) Decker, C. *Macromol. Rapid Commun.* **2002**, *23* (18), 1067–1093.
- (4) Jang, M.; Crivello, J. V. *J. Polym. Sci. Part A Polym. Chem.* **2003**, *41* (19), 3056–3073.
- (5) Crivello, J. V.; Lee, J. L.; Corporate, G. E. **1990**, *28*, 479–503.
- (6) Crivello, J. V.; Reichmanis, E. *Chem. Mater.* **2014**, *26* (1), 533–548.
- (7) Christ, E.-M.; Müller, S. S.; Berger-Nicoletti, E.; Frey, H. *J. Polym. Sci. Part A Polym. Chem.* **2014**, *52*, (11) 3267-3279.
- (8) Bulut, U.; Crivello, J. V. *J. Polym. Sci. Part A Polym. Chem.* **2005**, *43* (15), 3205–3220.
- (9) Crivello, J. V. *J. Polym. Sci. Part A Polym. Chem.* **2014**, *52*, (4) 1230-1242.
- (10) Verstegen, E. J. K.; Kloosterboer, J. G.; Lub, J. *J. Appl. Polym. Sci.* **2005**, *98* (4), 1697–1707.
- (11) Torron, S.; Johansson, M. *J. Polym. Sci. Part A Polym. Chem.* **2015**, *53*, 2258–2266.
- (12) Crivello, J. V. *Polymer* **2015**, *64*, 227–233.
- (13) Crivello, J. V. *J. Polym. Sci. Part A Polym. Chem.* **2015**, *53* (4), 594–601.
- (14) Sasaki, H. *Oxetane Proj.* **2001**, 11–15.
- (15) Jin, K.; Heath, W. H.; Torkelson, J. M. *Polymer* **2015**, *81*, 70–78.
- (16) Grim, J. C.; Marozas, I. A.; Anseth, K. S. *J. Control. Release* **2015**, *215*, 910-921.

- (17) Lee, T. Y.; Carioscia, J.; Smith, Z.; Bowman, C. N. *Macromolecules* **2007**, *33* (10)1473–1479.
- (18) Hoyle, C. E.; Bowman, C. N. *Angew. Chem. Int. Ed. Engl.* **2010**, *49* (9), 1540–1573.
- (19) Fang, Y.; Ha, H.; Shanmuganathan, K.; Ellison, C. J. *ACS Appl. Mater. Interfaces* **2016**, *8* (17), 11050–11059.
- (20) Carioscia, J. a; Stansbury, J. W.; Bowman, C. N. *Polymer* **2007**, *48* (6), 1526–1532.
- (21) Lan, T.; Torkelson, J. M. *Polymer* **2015**, *64*, 183–192.
- (22) Xi, W.; Scott, T. F.; Kloxin, C. J.; Bowman, C. N. *Adv. Funct. Mater.* **2014**, *29*, (12) 8902-8932.
- (23) Berg, G. J.; Gong, T.; Fenoli, C. R.; Bowman, C. N. *Macromolecules* **2014**, *47* (10), 3473–3482.
- (24) Baranek, A.; Song, H. B.; McBride, M.; Finnegan, P.; Bowman, C. N. *Macromolecules* **2016**, *49*, (6) 540-548.
- (25) Jon P. Scholte, Soon Ki Kim, Christopher L. Lester, and C. A. G. *J. Polym. Sci. Part a-Polymer Chem.* **2016**. (In Press)
- (26) Szczepanski, C. R.; Darmanin, T.; Guittard, F. *ACS Appl. Mater. Interfaces* **2016**, *8* (5), 3063–3071.
- (27) Szczepanski, C. R.; Stansbury, J. W. *Eur. Polym. J.* **2015**, *67*, 314–325.
- (28) Szczepanski, C. R.; Pfeifer, C. S.; Stansbury, J. W. *Polymer (Guildf)*. **2012**, *53* (21), 4694–4701.

- (29) Fenoli, C. R.; Wydra, J. W.; Bowman, C. N. *Macromolecules* **2014**, 47 (3), 907–915.
- (30) Detrembleur, C.; Jérôme, C.; De Winter, J.; Gerbaux, P.; Clément, J.-L.; Guillaneuf, Y.; Gimes, D. *Polym. Chem.* **2014**, 5 (2), 335.
- (31) Callister, W. D.; Rethwisch, D. G. *Material Science and Engineering*, 9th ed.; Wiley: New York, 2013.

CHAPTER 6

EFFECT OF ACRYLATE GROUP PLACEMENT AND SYNTHETIC ROUTE ON PHOTOPOLYMER NETWORK FORMATION

Abstract

Photopolymerization has been enabled in several applications in recent years due to new chemistries and processing techniques. However, the resulting network morphology in materials generated via photopolymerization, especially those using acrylate monomers, is difficult to control, limiting the range of thermo-mechanical properties. The network morphology and resulting properties are typically tuned by incorporating large prepolymer molecules. While effects of functional groups in these prepolymers have been studied, little work has examined the role of functional group placement on photopolymer network formation. To investigate the effect of prepolymer structure, prepolymers were synthesized with reactive groups located at chain ends or randomly distributed along the prepolymer backbone using two different controlled radical polymerization (CRP) techniques, nitroxide mediated polymerization (NMP) and reversible addition fragmentation chain transfer (RAFT) polymerization. The CRP method used to prepare the prepolymer influences photopolymerization kinetics with RAFT formulations showing lower conversions and rates of polymerization. Interestingly, photopolymerized networks also exhibit different glass transition behavior based on their synthetic method. Both synthetic routes show dual T_g behavior with RAFT prepared end functional prepolymer systems showing higher T_g though with less defined $\tan(\delta)$ peaks. Further, the network relaxations, which occur in the presence of a RAFT agent, produced films with twice the elongation at break and similar moduli for end

functionalized prepolymers as compared to NMP prepolymer formulations. Incorporation of randomly functionalized prepolymers prepared via RAFT meanwhile show a modulus over three times that of the NMP random formulation. Additionally, RAFT formulations show less than one percent permanent deformation during creep tests. Shrinkage stress results reveal that a combination of end functionalized prepolymer architecture and RAFT synthesis reduce shrinkage stress by an order of magnitude over random NMP prepolymer systems. Overall these results indicate that both synthetic route and prepolymer architecture play significant roles in network morphology and thermomechanical properties.

Introduction

Recently, photopolymerization has received significant attention due to a variety of inherent advantages including spatial and temporal control. Being able to manipulate formation of polymeric materials, like photocurable resins, with the illumination source has allowed significant advances in coatings, adhesives and 3D printing technologies.^{1,2} Although photopolymerization has facilitated many advances, the resulting networks have historically been plagued by both large network heterogeneities and shrinkage stress, especially those formed utilizing traditional (meth)acrylate chemistries.^{3,4} In these systems the change in free volume combined with network heterogeneities induces substantial shrinkage stress.^{5,6} These networks also have little to no defined structure, typically characterized by a broad array of relaxation times and broad glass transition temperatures.⁷ The combination of broad glass transition and brittleness originating from high crosslinking has limited the broader application of photopolymerization.⁸

Research has focused on inducing multiple phases to control network morphology in photocurable systems.^{9,10} For example, lyotropic liquid crystals have been utilized to compatibilize blends and induce specific structures in photocurable hydrogels.^{11,12,13} Other work has focused on step-growth photopolymerizations, such as the thiol-ene and photoinduced CuAAC click reactions.¹⁴⁻¹⁶ The amorphous, highly regular networks formed by a step-growth mechanism show lower shrinkage stress than acrylic systems and exhibit much narrower T_g distributions indicating a greater homogeneity in the network.¹⁶⁻¹⁸ Thiol-ene systems have shown promise in adhesives for which their inherently low T_g is desirable; however, the films produced by these systems are often not robust enough for many other applications without post treatment or fillers to increase the mechanical properties.^{19,14} Ongoing work examining photoinduced CuAAC has also shown potential in producing network control, but the presence of copper and required synthesis of the monomers again limits broader application of these materials.^{20,21}

A potential method to control structure in photocurable networks is the use of controlled radical polymerization, specifically nitroxide mediated polymerization (NMP) and reversible addition-fragmentation polymerization (RAFT) to produce reactive prepolymers.²²⁻²⁵ Both of these methods have been utilized extensively to synthesize block copolymers and hyperbranched materials for stimuli responsive materials.²⁶⁻²⁹ NMP utilizes reversible termination to control the propagation step of a polymerization reaction, which maintains control of the molecular weight.²⁶ On the other hand, RAFT uses rapid chain transfer in order to limit the number of propagating chains for control.³⁰ Interestingly, the rearrangements inherent to RAFT based reaction have been utilized to change network properties. RAFT adducts have been incorporated into small molar mass

acrylate functionalized monomers that significantly limit the shrinkage stress experienced in traditional acrylate and thiol-ene systems.³¹ The presence of RAFT moieties also allows for some degree of photoplasticity and permeability, allowing a network to become selectively permeable during illumination to activate the RAFT chain transfer mechanism.^{32,33} The ability for NMP and RAFT to both synthesize reactive prepolymers may allow for the larger molecules to have similar properties to the smaller monomers mentioned above while governing network formation.³⁴

Previously, we have combined NMP with butyl acrylate and epoxy-functionalized methacrylate monomers to produce architected prepolymers.³⁵ By locating the epoxide reactive groups at the ends of the prepolymer molecules a continuous hard domain appeared to be formed. The pockets of butyl acrylate significantly alter the resulting thermomechanical properties of the epoxide network by having “soft” domains incorporated into the continuous hard domain. On the other hand, the randomly functionalized prepolymers display no evidence of different domains forming. The continuous hard domain of the end functional formulations also allow for a higher modulus material without a compromise in elongation. Moreover, the end functional formulations exhibit an order of magnitude decrease in creep and intricate nanoscale morphology.

In the present study, end and randomly functionalized prepolymers were utilized to further understand the role prepolymer architecture plays in photopolymerization kinetics and network morphology. In addition, these prepolymers were synthesized via NMP and RAFT polymerization mechanisms. The role of reactive group placement and synthetic route on photopolymerization kinetics and conversion was examined with RT-

FTIR. Thermomechanical properties such as T_g , creep, and modulus, were investigated to determine the effects of network structure on thermo-mechanical properties. Shrinkage stress was investigated to provide additional knowledge regarding the effect of prepolymer architecture and potential RAFT rearrangements. This work aims to demonstrate that prepolymer architecture and CRP method provide facile means to control and tune resulting photopolymer networks.

Experimental

Materials

1,6 Hexanediol diacrylate (HDDA, Sartomer) and 2,2-dimethoxy-2-phenylacetophenone (DMPA, Ciba) were used as received. Butyl acrylate and 3,4-epoxycyclohexylmethyl methacrylate were provided by Avery Dennison. Blocbuilder RC-50 (1-(diethoxyphosphinyl)-2,2-dimethylpropyl 1,1-dimethylethyl nitroxide) and Blocbuilder DB (dibenzyl trithiocarbonate) were obtained from Arkema.

End functionalized prepolymers were synthesized utilizing the alkoxyamine NMP agent Blocbuilder RC-50. A 1/4/13 molar ratio of Blocbuilder RC-50/3,4-epoxycyclohexylmethyl methacrylate/butyl acrylate was diluted to 50% by mass with propyl acetate. A second feed consisting entirely of butyl acrylate was then added, followed by a third feed identical to the first. Randomly functionalized prepolymers were synthesized with a single feed, composed of BlocBuilder RC-50/3,4-epoxycyclohexylmethyl methacrylate/butyl acrylate at a molar ratio of 1/8/64 diluted to 50% by mass with propyl acetate. In both procedures, the reactor was sparged for one hour with nitrogen before the vessel was then heated to 110°C. All feeds were allowed to reach approximately 85% conversion, as determined by gas chromatography using a





Shimadzu GC-17A, before the subsequent feeds were added. Once the desired molecular weight was achieved, residual monomer and solvent were removed via rotary evaporation.

RAFT synthesized end and randomly functionalized prepolymers were synthesized using dibenzyltrithiocarbonate (DBTTC). A 1/8/26 molar ratio of DBTTC/3,4-epoxycyclohexylmethyl methacrylate/butyl acrylate was diluted to 50% by mass with propyl acetate. A second feed consisting entirely of butyl acrylate was then added to produce the middle non-reactive block. Randomly functionalized prepolymers were synthesized with a single feed, composed of DBTTC/3,4-epoxycyclohexylmethyl methacrylate/butyl acrylate at a molar ratio of 1/8/64 diluted to 50% by mass with propyl acetate.

Molecular weight and polydispersity index (PDI) of prepolymers were measured using size exclusion chromatography with a refractive index detector (Shimadzu RID-10A). A flow rate of 1 mL/min ethyl acetate through a PLgel Mixed-D column (Agilent) was used for experimental analysis. Table 6.1 summarizes the structure characteristics of the prepolymer molecules used in this study. Due to high concentrations of the epoxy functional methacrylate monomer, PDI's are greater than what would typically be considered a controlled radical polymerization. Of much greater interest than the molecular weight distribution for this work is control over reactive group placement and approximate molar mass in a batch feed process which is readily enabled by the "living" nature of the nitroxide and RAFT mechanisms. After the prepolymers were synthesized, Hycat 2000S catalyst was added at a concentration of 1 part per hundred of the polymer. Acrylic acid was then added at a 10:1 molar concentration relative to the cycloaliphatic

epoxide monomer on the prepolymer backbone to produce the reactive acrylate moieties. The reaction was heated to 70°C and allowed to proceed overnight to completion.

Table 6.1 Prepolymers used in this study

Sample Name	Acrylate Location	Number of Reactive Groups	M _n	PDI
N-End 	End	8	11400	2.33
R-End 	End	8	12200	1.20
N-Random 	Random	8	15100	1.64
R-Random 	Random	8	13100	1.32

Methods

Photopolymerization behavior of prepolymer/monomer mixtures was examined utilizing a RT-FTIR. Real time infrared spectroscopy was performed using a Thermo Nicolet nexus 670. 1 mg of sample was placed on a sodium chloride plate covered with 15 µm spacer beads and sandwiched with an additional sodium chloride plate. The laminate nature of this testing geometry prevents oxygen from diffusing into the system. Analysis was performed at ambient temperature and atmosphere. Acrylate conversion was determined by monitoring the decrease of the absorbance band at 810 cm⁻¹.

Dynamic mechanic analysis (DMA, Q800 DMA TA Instruments) was conducted to investigate the effect of polymer architecture on ultimate mechanical and visco-elastic

properties of cured polymers. To fabricate rectangular 6 x 25 mm and 0.15 mm thick films, two thick glass plates, covered by amorphous polyvinylidene fluoride films (PVDF, Teflon® AF, Dupont) for easy release, were used. Adhesive tape spacers (150 µm thick) were attached on each edge of the bottom plate to control the film thickness. Approximately 3g of liquid sample mixture were placed on the bottom glass plate and dried for 30 minutes in a vacuum oven at 60°C to remove acetone. The dried liquid samples were then tightly pressed using the upper glass plate and secured using binder clips. Filled molds were irradiated for 10 minutes using a UV lamp (365 nm) at an irradiation intensity of 10 mW/cm². To measure the modulus and glass transition temperature of the samples, the temperature of films was increased from -70°C to 150°C at a heating rate of 5°C/min. DMA tensile mode was utilized under constant strain at a frequency of 1 Hz. Young's modulus and tensile properties were evaluated at 30°C in tensile mode with a force rate of 1.0 N/m. Young's Modulus was calculated using the slope of the stress-strain curve in the early linear regime (less than 5% strain).³⁷ Creep tests were performed by applying an onset stress of 1 MPa for ten minutes and measuring the subsequent strain. Strain recovery was recorded for 30 minutes after the 1 MPa stress was removed. Shrinkage stress was determined using a Proto-tech shrinkage stress analyzer. 1 milligram of sample was illuminated for 10 minutes at an intensity of 10 mW/cm² at 365 nm between 2 quartz rods spaced 180° from each other. Stress is measured as the force necessary to keep rods a known distance apart.

Results and Discussion

In most photocurable resins the oligomer or prepolymer material serves to govern the bulk properties of the resulting film. These photocured resins typically display high

levels of shrinkage stress originating from network heterogeneities. Architected prepolymers may provide a means to alleviate the shrinkage stress by directing the films morphology. The effects of prepolymer structure on network formation has been recently detailed when utilizing epoxy functionalized monomers.³⁵ When the cycloaliphatic epoxy moieties are positioned at the end of a butyl acrylate prepolymer, the resulting network shows separation between the crosslinking domains and the unreactive butyl acrylate segments. The randomly functionalized materials show no significant difference in domains and behave much like a general photocured film with broad glass transitions. To investigate if this effect depends reaction mechanism and synthetic route or if similar effects are seen with other reactive groups, this work utilized end and random prepolymers with acrylate functionalities. Both end and randomly functionalized materials were made via RAFT and nitroxide controlled radical polymerization techniques. The effects of architecture and synthetic route on photopolymerization kinetics and conversion are observed via FTIR. Given past studies, it is important to characterize the photopolymer networks via dynamic mechanical analysis to observe the effect of controlling network heterogeneity formation on $\tan(\delta)$ and modulus. Additionally, as morphology can have a pronounced effect on the polymer's response to constant and rapid stress, stress-strain behavior as well as creep tests are used to characterize the networks. Lastly, as RAFT moieties have been shown to be photodynamic, the shrinkage stress of the polymer networks was also examined.

If the end-functionalized acrylate resins behave similarly to the epoxy functionalized prepolymers, differences in the photopolymerization kinetics due to segregation of the reactive groups may be observed. Additionally, the differences in

synthetic route and the continued presence of a radically reactive RAFT adduct may further alter the photopolymerization kinetics. To observe any kinetic differences, real-time FTIR was employed to monitor acrylate group conversion. Figure 6.1 shows conversion as a function of time for formulations with increasing prepolymer content when synthesized either by RAFT or NMP mechanisms. For all formulations utilizing NMP synthesized prepolymers (Figures 6.1a and 6.1c), conversion of acrylate groups achieves 90-95% within the first 90 seconds of illumination. Figures 6.1b and 6.1d show the acrylate conversion for formulations using the RAFT synthesized end and randomly functionalized prepolymers respectively. The presence of a trithiocarbonate moiety on the prepolymer backbone allows for rearrangements of the photopolymer network via reversible fragmentation and chain transfer. The chain transfer reaction competes with the polymerization reaction requiring additional time to achieve high conversions. The RAFT-synthesized end prepolymer formulations show a pronounced decrease in rate and conversion as the concentration of prepolymer is increased. At 60 and 70 wt% prepolymer the final acrylate conversion is still high approaching 90% functional group conversion. At 80 wt% of the R-End prepolymer an approximate 10% decrease in conversion is observed. This decrease in conversion is possibly due to the rearrangements preventing reaction of acrylate moieties attached to the prepolymer backbone. For the RAFT synthesized randomly functionalized (R-Random) formulations the limited conversion is more pronounced. At both the 60 and 70 wt% formulations the R-Random resins only achieve 80% conversion. The lower conversion is possibly due to the end functional materials limiting chain transfer as the trithiocarbonate groups are farther away from the reactive acrylate groups. If the propagating radicals cannot reach the

trithiocarbonate groups, then no rearrangements can occur, resulting in the formation of network heterogeneities. Above 70 wt% R-Random prepolymer appears to significantly

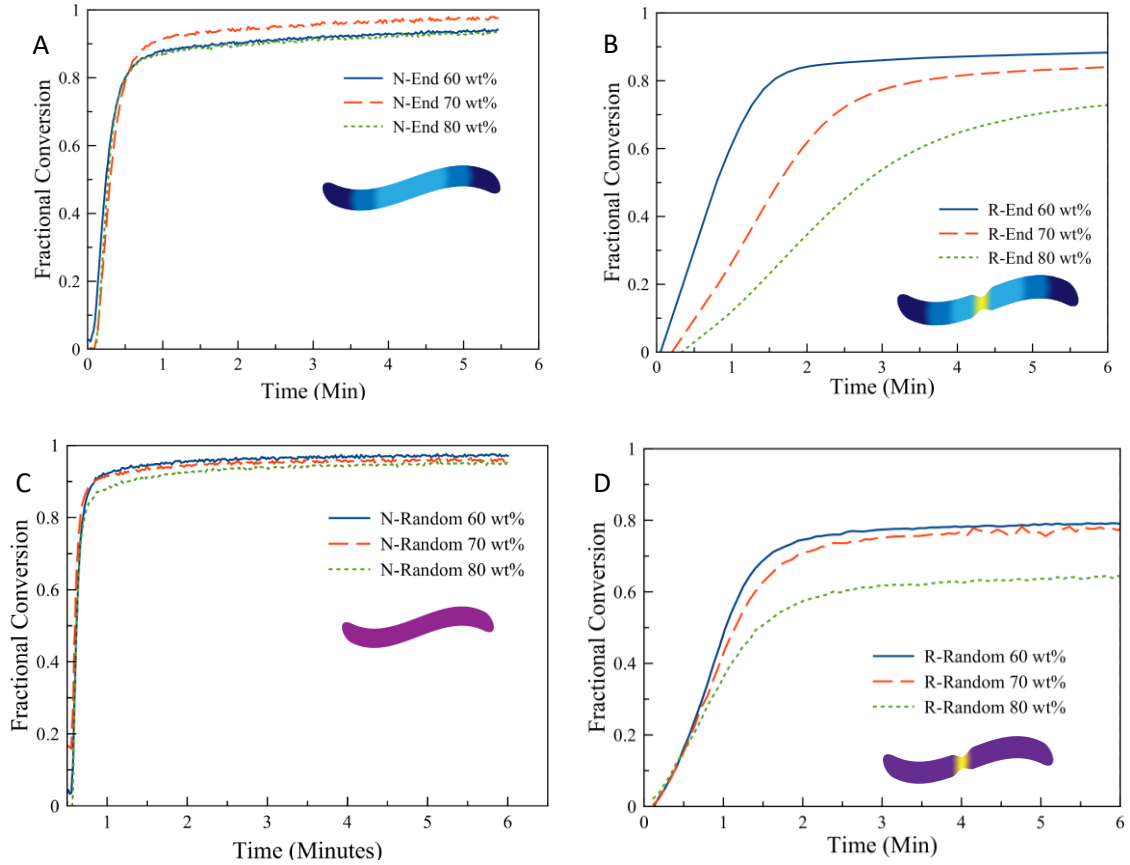


Figure 6.1. Acrylate functional group conversion of prepolymer/HDDA formulations as a function of time is shown. Figures 1A and 1C show fractional conversion for formulations utilizing nitroxide synthesized end and random structured prepolymers respectively. Figure 1B and 1D show the fractional conversion of formulations using end and randomly functionalized prepolymers synthesized via the RAFT Mechanism. Samples were photopolymerized with 0.5 wt% DMPA at 10 mW/cm².

limit the conversion with only 60% of the acrylate groups being converted. The lower conversion would make sense especially if the HDDA in the R-Random formulations are producing a homogenous network with a greater distribution of small but consistent heterogeneities. The presence of these small heterogeneities may limit the propagating radicals from reaching residual acrylate monomer. The higher conversion of R-End,

compared the R-Random prepolymer formulations, may be caused by the trithiocarbonate groups being surrounded by soft nonreactive butyl acrylate homopolymer, which will allow for additional mobility while delaying the gelation and photopolymerization kinetics. The decrease in overall conversion compared to the nitroxide formulations may be attributed to the rearrangements preferentially occurring over the polymerization of additional acrylate moieties.

With the significant changes in polymerization rate between mechanisms and architecture, it is reasonable to believe that the photocured networks will have differences in network morphology and thermomechanical properties. Figure 6.2 shows the storage modulus as a function of temperature and oligomer concentration for nitroxide and RAFT synthesized end and randomly prepolymers crosslinked with HDDA as a reactive diluent. In the NMP synthesized end formulations (Figure 6.2A) the glassy plateau extends to roughly -25°C before the storage modulus begins to decrease. A second decrease is apparent in the 60 and 70 wt% formulations at 50°C and 75°C , respectively. Conversely, the storage modulus of the 80 wt% formulation shows a broad decrease before reaching the rubbery plateau and breaking at elevated temperatures and the storage modulus for the R-End formulations behave similarly showing multiple decreases as observed in figure 6.2B. For the 60 wt% R-End prepolymer formulation, the storage modulus appears to have two decreases as well, suggesting that there are multiple domains that become mobile within the polymer network at different times. The first occurs at -25°C and is likely due to the nonreactive butyl acrylate segments being dispersed through the network. The second transition occurs at 60°C and likely is due to a more highly cross-linked network resulting from the reactive chain ends polymerizing with the HDDA

reactive diluent. For the formulations with greater than 60 wt% R-End prepolymer the secondary transition disappears, in which the storage modulus decreases over almost 100°C range beginning around -25°C before reaching their rubbery plateaus.

In both end-functionalized formulations, as the concentration of prepolymer increases the rubbery modulus value decreases slightly, suggesting that more of the low T_g butyl acrylate from the nonreactive backbones acts to soften the polymer network. Figure 6.2C and 6.2D show the storage modulus for the randomly functionalized NMP and RAFT prepolymer formulations as a function of temperature and HDDA concentration. For both formulations, the storage modulus displays a broad decrease characteristic of a heterogeneous network. Randomly functionalized prepolymers synthesized via NMP, shown in figure 6.2C, exhibit a broader more gradual transition than that observed in the RAFT synthesized randomly functionalized prepolymer formulations. The difference in the peak width indicates that the chain transfer via the RAFT moiety present in the R-Random formulations allows for rearrangements and relaxations to occur, producing a more homogenous network. These rearrangements in turn may act to provide a final network morphology with fewer heterogeneities. For the N-Random formulations, the decrease in storage modulus begins at roughly -25°C and extends to 100°C for all prepolymer concentrations. Further, as the prepolymer concentration increases the storage modulus sharply decreases, indicating that the short butyl acrylate chains are affecting the network. In the R-Random formulations the decrease in storage modulus does not occur until almost 0°C and proceeds until 75°C for all formulations. It is also important to notice the differences in the rubbery modulus, as it is closely related to the crosslink density of the photocured materials.

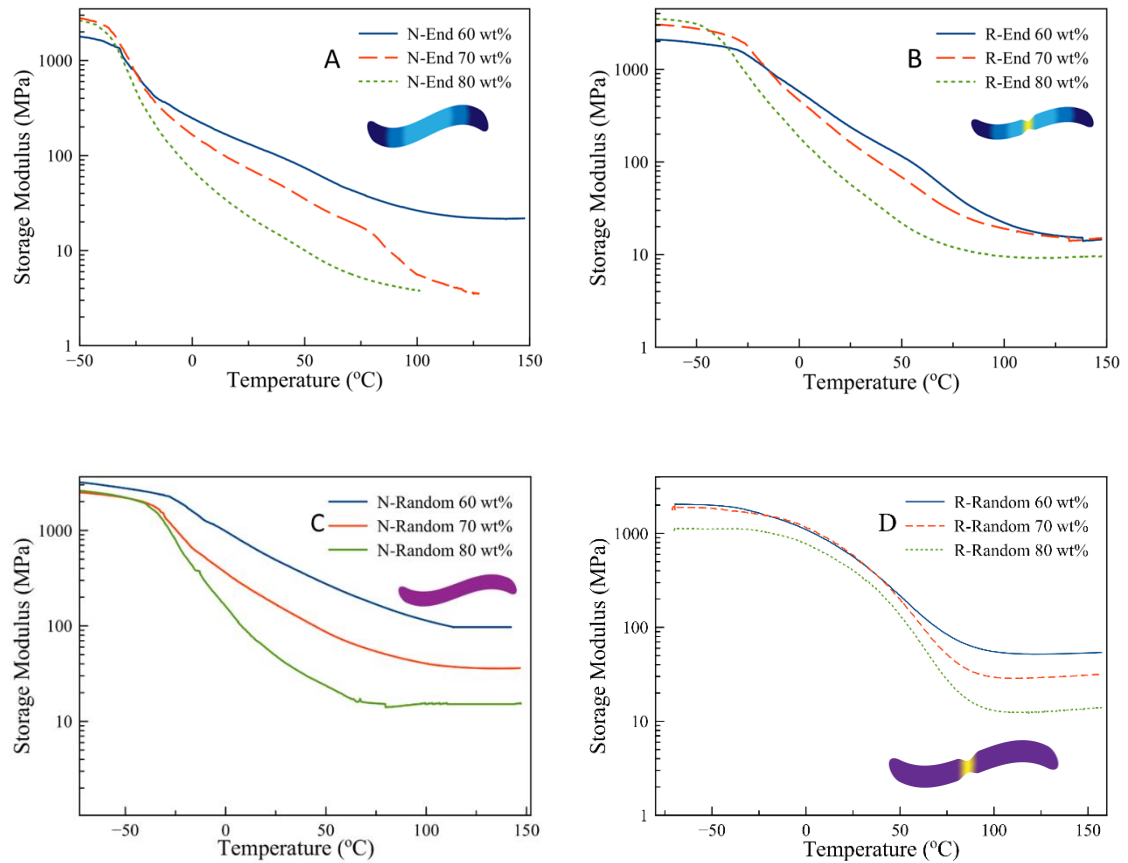


Figure 6.2. Storage modulus as a function of temperature for prepolymer/HDDA formulations. Figures 6.2A and 6.2C show the storage modulus as a function of temperature for NMP synthesized end and random prepolymers, respectively. Figures 6.2B and 6.2D show storage modulus as a function of temperature for RAFT synthesized prepolymer formulations. All samples were photopolymerized at 10 mW/cm² with 0.5 wt% DMPA for 10 minutes.

The end-functionalized species display lower rubbery modulus values, suggesting that the unreactive butyl acrylate blocks are potentially lowering overall the crosslink by creating lightly crosslinked domains. The rubbery modulus is lowest for the N-End formulations, especially at higher concentrations of prepolymers. Meanwhile, the randomly functionalized formulations show rubbery moduli almost five times that of their end-functionalized counter parts, especially at higher reactive diluent concentrations. These

differences in the rubbery modulus suggest that the photopolymer network morphology is highly tunable with prepolymer architecture.

The loss factor, $\tan(\delta)$, gives further information regarding the polymer network morphology and its corresponding glass transitions. Peaks in $\tan(\delta)$ versus temperature plots are a specific measure of the glass transition temperature in polymeric materials. This technique may be used to probe for network heterogeneities by observing broad $\tan(\delta)$ peaks or perhaps multiple $\tan(\delta)$ maxima, if domains with different properties are present as indicated by the kinetics and storage modulus data. Figure 6.3 shows the $\tan(\delta)$ values for NMP and RAFT synthesized prepolymer/HDDA formulations with changes in concentration as a function of temperature. The prepolymer-network effects are clearly visible at the 60 wt% N-End prepolymer formulations. The $\tan(\delta)$ displays two peaks, indicating that some degree of phase separation is occurring. The first and more prominent peak occurs at approximately -25°C and is likely due to the unreactive butyl acrylate backbone from the prepolymer. The second peak occurs at 75°C and is due to regions of high cross-link density produced from HDDA polymerizing with the acrylate moieties at the end of the structured prepolymer molecule. The 60 wt% R-End formulation also shows some degree of phase separation, as indicated by multiple peaks, the first of which occurs at approximately -10°C . It is possible that this transition occurs at higher temperatures than in the N-End formulation because the butyl acrylate segments are being incorporated within the network more uniformly due to the chain and network rearrangements around the trithiocarbonate groups. The second transition occurs at approximately 60°C , slightly lower than that observed in the N-End formulation. It is likely that the second transition occurs at lower temperatures again due to greater

uniformity. On the other hand, the N-Random 60 wt% formulation shows a single broad transition, spanning from -30°C to 100°C, characteristic of a heterogeneous polymer network without any distinct domains.

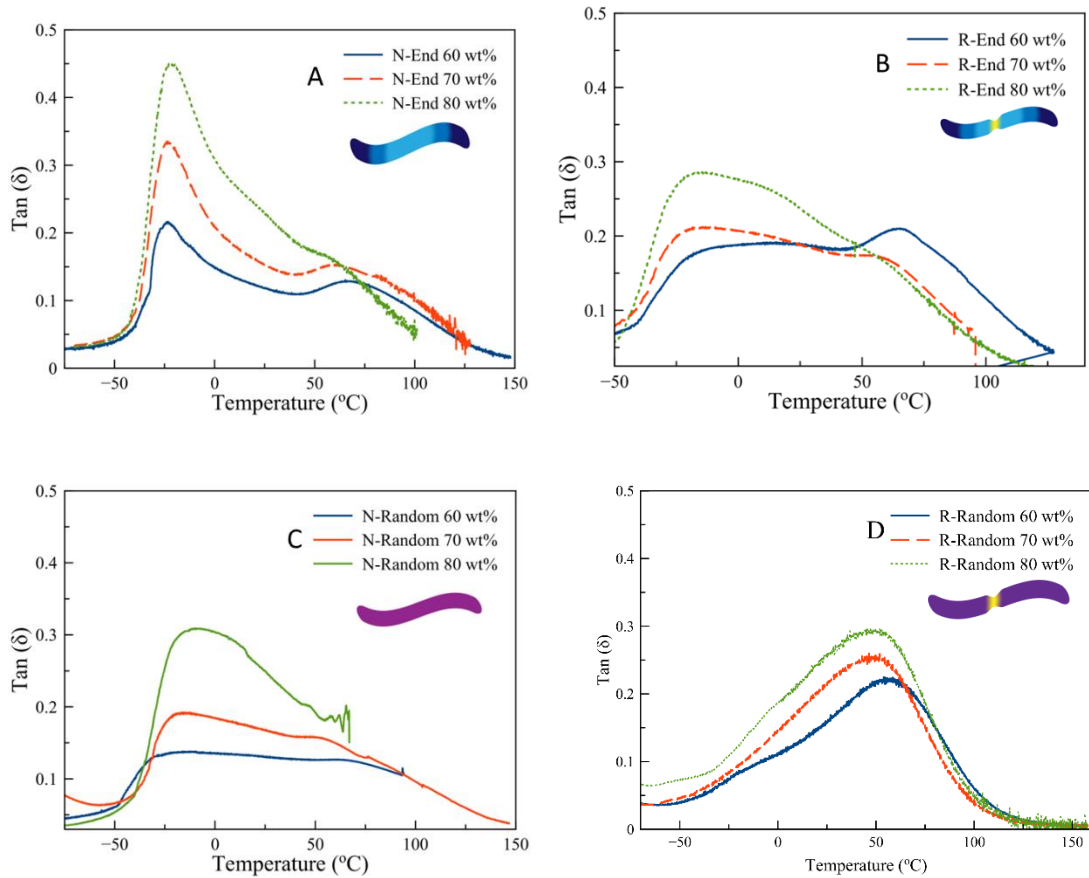


Figure 6.3 Tan (δ) profiles as a function of temperature for all prepolymer/HDDA formulations. Figures 6.3a and 6.3c show the tan (δ) as a function of temperature for NMP synthesized end and random prepolymers respectively. Figures 6.3b and 6.3d show Tan (δ) as a function of temperature for RAFT synthesized prepolymer formulations. All samples were photopolymerized at 10 mW/cm² with 0.5 wt% DMPA for 10 minutes.

The R-Random formulation shows the highest temperature T_g indicated by the tan (δ) peak at 60°C, though a single peak is still observed suggesting only one domain is prevalent in the polymer network. This higher temperature T_g may be due to HDDA heterogeneities still occurring resulting in more diverse relaxation times occurring. As

HDDA has been observed to have T_g 's as high as 80°C, it would be probable that the small groups of butyl acrylate would slightly soften the network without drastically altering the photopolymerization process or expected T_g .

The effect of increasing prepolymer concentration on network morphology was also examined. The N-End formulations continue to show multiple peaks until 80 wt% prepolymer where the peaks are difficult to resolve but a shoulder is still present, indicating that the HDDA/ prepolymer end domain is becoming less prominent as the concentration of prepolymer increases. The R-End formulations also show two domains for the 70 wt% formulations; however, the more prominent peak now occurs at roughly -25°C and a second peak occurs at 55°C. The continued lowering of the temperature at which the second peak occurs is likely due to more small, soft butyl acrylate chains being distributed through the photopolymer network. At the 80 wt% concentration, the R-End formulation no longer displays multiple peaks and now shows a single peak at -25°C. On the other hand, the N-Random formulations show similar behavior at all concentrations and show a single, broad transition at prepolymer concentrations. The $\tan(\delta)$ peak continues to occur at -25°C and becomes more prominent with increased prepolymer concentration as is reasonable given the higher concentration of butyl acrylate segments. Further, the N-Random samples broke repeatedly at higher temperatures indicating that the large heterogeneities appear to weaken the films. Interestingly, the R-Random formulations show the least change as the concentration of prepolymer increases. As the prepolymer concentration increases the $\tan(\delta)$ peak shifts from roughly 60°C in the 60 wt% formulation to 45°C in the 80 wt% formulation. The shift to lower temperature is as would be expected with more of the low T_g butyl acrylate in the network while the much

higher T_g also indicates that the networks being formed may have the small sections of HDDA heterogeneities within an overall more homogenous network. It is important to note the difference between the R-End and R-Random prepolymers. Though both prepolymers allow the resulting networks to undergo rearrangements during photopolymerization, only the R-End samples show multiple domains. Further, as more RAFT prepolymer is incorporated, the R-End materials no longer show multiple $\tan(\delta)$ peaks suggesting that the rearrangements may promote greater homogeneity in addition to relaxation of inside the final network.

As systems with end-functionalized prepolymers synthesized by both methods display multiple $\tan(\delta)$ maxima, it is logical that these materials will have different thermomechanical properties than those formulated with randomly functionalized prepolymers. Figure 6.4A shows the stress strain behavior in tensile mode for the nitroxide synthesized prepolymer formulations and Figure 6.4B shows the same behavior for RAFT synthesized materials. For the nitroxide synthesized materials, a significant difference is evident, especially at lower prepolymer concentrations with the end-functionalized materials showing higher moduli and elongation at break. At 60wt% prepolymer, the N-End material displays approximately double the modulus and twice the elongation at break of the N-Random control. At 70 wt% the N-End formulations still show roughly twice the modulus of their randomly functionalized controls, although both materials now fail at slightly above 10% elongation. Above 70 wt% prepolymer both end and random functionality materials appear to have very similar modulus and elongation at break, suggesting that the high concentration of butyl acrylate from the prepolymers as

the small molecule cross-linker is now the driving factor in network morphology and thermomechanical properties.

The RAFT synthesized prepolymer formulations, due to the inherent network relaxation during polymerization and potential for network homogenization via distribution of rubbery domains, show much different stress strain behavior as seen in Figure 6.4B.

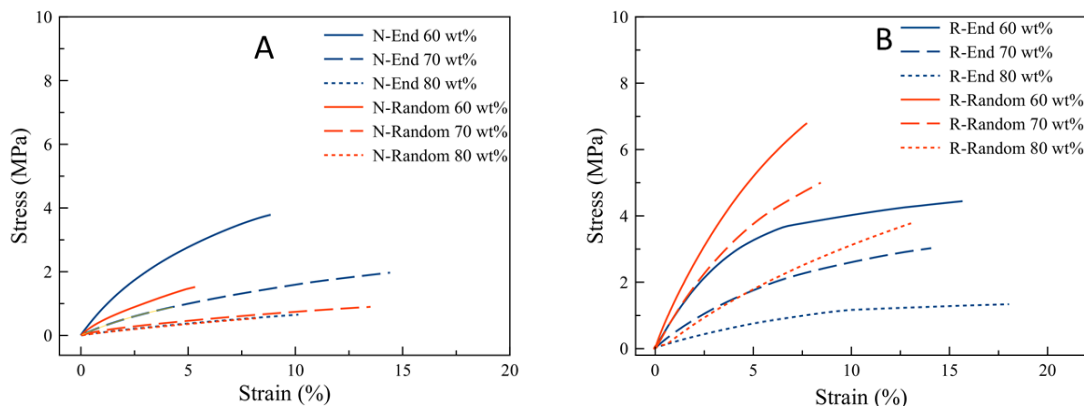


Figure 6.4. Stress strain behavior at 25°C for end and randomly functionalized prepolymer formulations synthesized by NMP (A) or RAFT (B). All samples were photopolymerized at 10 mW/cm² with 0.5 wt% DMPA for 10 minutes.

Interestingly, many of the trends previously observed appear to be dramatically different when the network is allowed to relax with an active RAFT agent now part of the prepolymer. At 60 wt% prepolymer the randomly functionalized material appears to have the largest modulus of any formulation investigated in this study, almost three times that observed in the N-Random 60 wt% prepolymer formulation. The R-End 60 wt% resin has a similar modulus to that observed in the N-End resin, but the RAFT based resin also shows double the elongation at break. The reason for this improvement in tensile elongation is believed to be a combination of network relaxation coupled with greater and

more equal distribution of soft butyl acrylate segments throughout the network via RAFT rearrangements. Indeed, if the network relaxations alone were responsible for the increased elongations we would expect both the R-End and R-Random formulations to behave more alike. Instead, as the concentration of prepolymer increases to the 70wt% and 80wt% formulations, we observe that R-Random formulations maintain a relatively high modulus compared to the R-End systems. It appears from the stress-strain behavior that the presence of residual RAFT materials allows for a significant strengthening of the final cured films. While N-End formulations appear to have higher moduli and similar if not greater elongation at break than their N-Random materials, both NMP materials perform poorer than their RAFT counter parts. It appears that the enhanced elongation present in the R-End formulation suggests that there is some degree of separation between the highly reactive prepolymer chain ends and the unreactive middle block. When these domains are better distributed via the RAFT rearrangement the final network loses some resistance to strain but produces a more thermoplastic like material with enhanced elongation at break. Meanwhile, the lack of a distinct soft segment allows the R-Random materials to likely have a more amorphous network, thus achieving a higher modulus as the entire film is crosslinked. Simultaneously, the trithiocarbonate on the R-Random materials produces an amorphous network likely without the shrinkage stress that would limit the application of these materials highlighting the importance of synthetic procedure on polymer morphology.

As the network relaxations appear to greatly influence the thermomechanical properties and possible domain sizes it is probable that these materials will respond much differently to a rapid onset of stress. Figure 6.5 shows the strain response of NMP (Figure

6.5A) and RAFT (Figure 6.5B) prepolymer formulations as a function of time at 25°C to a 1 MPa stress. At low concentrations of the N-End prepolymer, very little deformation is observed during the initial 10 minute strain period.

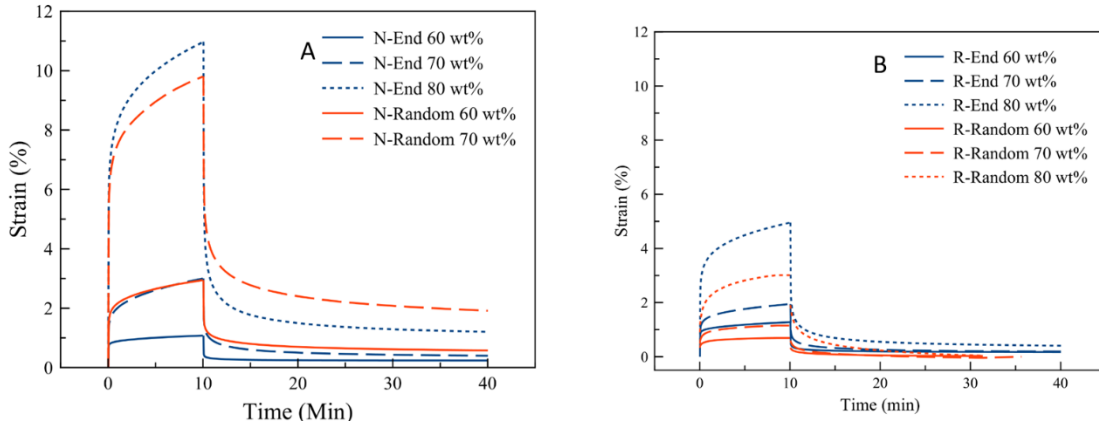


Figure 6.5. Strain as a function of time for end and randomly functionalized prepolymer formulations synthesized by NMP (A) or RAFT (B). 1 MPa of stress was applied for 10 minutes. Strain recovery was observed for 30 minutes after the initial strain was removed. All samples were photopolymerized at 10 mW/cm² with 0.5 wt% DMPA for 10 minutes.

The N-Random 60 wt% prepolymer resin comparatively has twice the deformation of the end-functionalized materials though they both recover almost all of the stress. However, as the concentration of nitroxide synthesized prepolymer increases, the differences become much more prominent. At 70 wt% prepolymer, the N-Random materials show roughly five times the deformation of the end functional comparison during the strain period. Further, the N-Random sample retain over 2% permanent deformation while the N-End formulation show less than 0.5% permanent deformation. At higher concentrations of NMP synthesized prepolymer, the randomly functionalized sample repeatedly breaks at the onset of 1 MPa of stress while the end functional materials, likely due to their continuous hard domains of HDDA and reactive chain ends show only 1% deformation after 30 minutes of recovery and being displaced over ten

times more. The strain response of the RAFT synthesized samples observed in Figure 6.5B highlights the effects of network relaxation and prepolymer architecture. Lower concentrations of both R-End and R-Random prepolymers show very little deformation during the initial stress period. R-End samples do show higher deformations during the 10 minute stress period. However, all of the samples recover to less than 1% permanent deformation once stress is removed. Yet, at the 80 wt% prepolymer the R-End sample experiences almost twice the deformation during the stress period and recovers slightly less than half that of the R-Random counterpart. Interestingly, since the RAFT synthetic method allows the networks to relax, the deformation at high prepolymer concentrations is much lower than what is seen in the NMP synthesized samples. We believe that this is due to the different network structures induced by the different prepolymer architectures. In the presence of a continuous hard domain, as is likely present in the N-End samples, the onset of stress can be mitigated to some extent, but the lack of a continuous domain causes the N-Random samples to break. The greater homogeneity of the RAFT modified networks appears to allow lower overall deformation. As in the R-End samples, where soft butyl acrylate segments are dispersed more even through the network, it is plausible that these smaller domains limit deformation compared to the larger domains likely in the N-End formulations. Indeed, at the 80 wt% formulation the R-End samples experience half the deformation of the N-End samples due to greater network homogeneity. Meanwhile, for the R-Random samples, the highly crosslinked, highly homogenous nature of these materials, which appear to lack any detectable domains, prevents deformation from 1 MPa of stress. The different responses to rapid stress onset

emphasize that prepolymer architecture and network relaxation combine to change network morphology and thermo-mechanical properties.

Given the large changes observed in basic network characteristics, because of network rearrangement via the RAFT synthetic pathway, it is reasonable to believe that these same rearrangements will reduce shrinkage stress in these systems. Figure 6.6 shows the normalized shrinkage stress for 60 wt% prepolymer samples. Here we observe that the N-Random materials display the highest degree of shrinkage stress. The N-End materials appear to provide an almost 20% reduction in shrinkage stress. We believe this reduction is due to the soft butyl acrylate segments and the reactive chain ends occupying space within to resulting photocured network and hence limiting the free volume change and induction of shrinkage stress. The R-Random sample meanwhile shows less than half the shrinkage stress of the N-Random sample, hence exhibiting the importance of the network rearrangements permitted via the RAFT adduct. The nearly 60% reduction in shrinkage stress is most likely entirely due to the ability for the curing photopolymer network to undergo rearrangements that will dramatically reduce and limit the shrinkage stress observed in these systems. Lastly, the R-End system appears to experience the lowest degree of shrinkage stress due to easily rearranged soft domains which continue to limit the free volume change and promote relaxation due to their proximity to the RAFT adduct. The combined factors of prepolymer architecture and network flexibility allow for a decrease by almost an order of magnitude for the resulting photocurable systems. The ability to decrease the shrinkage stress during the photopolymerization event via both synthetic method and prepolymer architecture underline the utility of this research as a method of modifying photocurable materials.

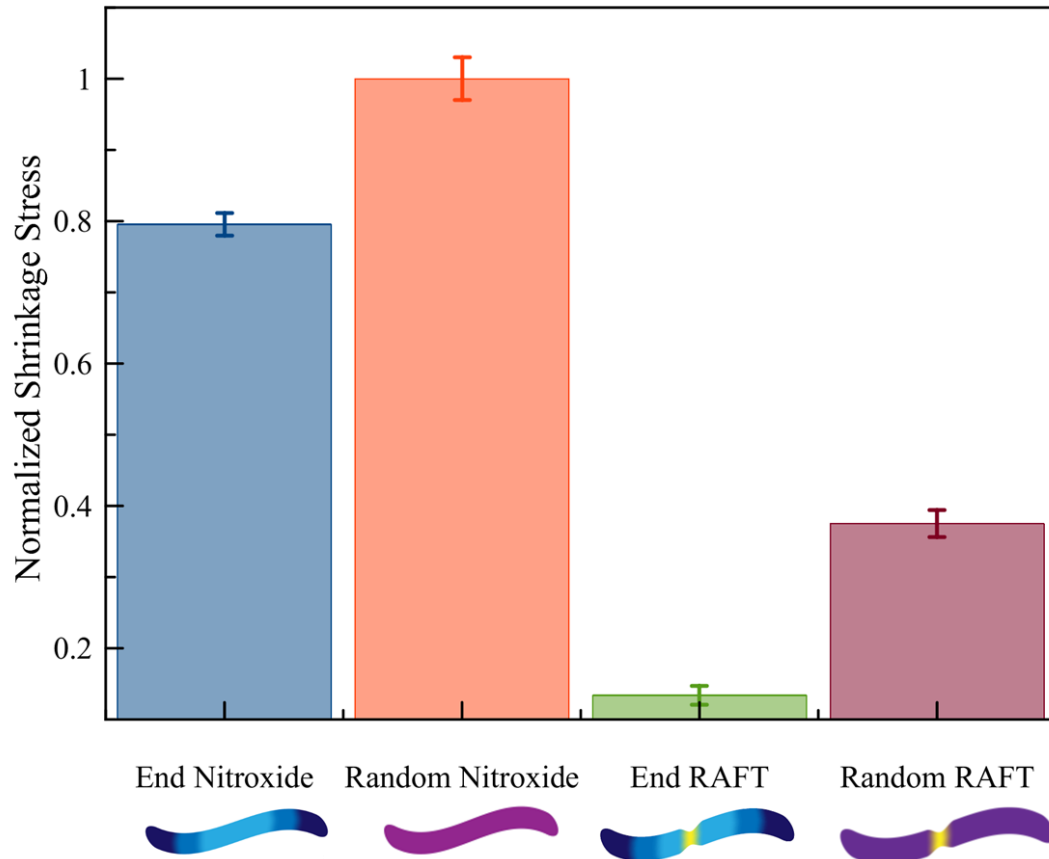


Figure 6.6. Shrinkage Stress normalized to the N-Random sample. All samples were photopolymerized at 10 mW/cm² with 0.5 wt% DMPA and 40 wt% HDDA for 10 minutes.

Conclusions

Herein we report the control of reactive prepolymer architecture to modify the resulting photocured polymer networks and thermomechanical properties. Both NMP and RAFT controlled radical polymerization techniques were used to synthesize both random and end function prepolymer molecules for use in photocurable formulations using HDDA as a reactive diluent. Materials synthesized via NMP show enhanced polymerization rates and overall reactive group conversion as compared to their RAFT synthesized counterparts. End-functionalized RAFT synthesized materials achieve higher overall conversions than the R-Random formulations, likely due to the increased mobility

with the trithiocarbonates next to soft and unreactive butyl acrylate. On the other hand, R-random samples also show more homogenous morphology with potentially higher crosslink densities than the nitroxide N-Random counter parts. Thermomechanical analysis revealed multiple $\tan(\delta)$ peaks suggesting multiple domains present in both NMP and RAFT end-functionalized prepolymer formulations and broad glass transitions for the randomly functionalized counterparts. Due to the network rearrangements promoted via RAFT agents in the prepolymer structure, the R-End formulation shows broader glass transitions as the concentration of butyl acrylate is dispersed to a greater degree in the network, compared to the N-End formulations. The R-Random series also demonstrate a broad glass transition temperature 25°C higher than that observed for the other materials, likely due to a highly crosslinked amorphous network. Additionally, the likely higher crosslinked, more homogenous RAFT prepolymer networks showed higher moduli and lower permanent deformation compared to other prepolymer formulations, especially the N-Random formulation. Shrinkage stress is also affected by reactive group placement, but even more so by the residual RAFT moieties from the prepolymer synthesis due to their ability to promote network rearrangements. The RAFT agents still incorporated in the prepolymer molecules significantly lower the overall shrinkage stress compared to their NMP synthesized counterparts. Overall, this work highlights the importance of reactive group placement and the choice of prepolymer synthetic route on photopolymerization kinetics, thermomechanical properties and shrinkage stress.

References and Notes

- (1) Gorsche, C.; Seidler, K.; Knaack, P.; Dorfinger, P.; Koch, T.; Stampfl, J.; Moszner, N.; Liska, R. *Polym. Chem.* **2016**, 6 (16), 2553–2562.
- (2) Sykam, K.; Donempudi, S. *Polymer* **2015**, 62, 60–69.
- (3) Pineda Contreras, P.; Agarwal, S. *Polym. Chem.* **2016**, 7 (18), 3100–3106.
- (4) Anseth, K. S.; Wang, C. M.; Bowman, C. N. *Polymer* **1994**, 35 (15), 3243–3250.
- (5) Chen, C.; Liu, J.; Sun, F.; Stansbury, J. W. *J. Polym. Sci. Part A Polym. Chem.* **2014**, 52 (19), 2830–2840.
- (6) Szczepanski, C. R.; Pfeifer, C. S.; Stansbury, J. W. *Polymer*. **2012**, 53 (21), 4694–4701.
- (7) Anseth, K. S.; Bowman, C. N.; Peppas, N. A. *Polym. Bull.* **1993**, 233 (3), 229–233.
- (8) Anseth, K. S.; Walker, T. A.; Bowman, C. N. In *Multidimensional Spectroscopy of Polymers*; 1995; Vol. 1, pp 166–182.
- (9) DePierro, M. a.; Carpenter, K. G.; Guymon, C. A. *Chem. Mater.* **2006**, 18 (23), 5609–5617.
- (10) Lin, Y.; Stansbury, J. W. *Polymer (Guildf)*. **2003**, 44 (17), 4781–4789.
- (11) Clapper, J. D.; Pearce, M. E.; Guymon, C. A.; Salem, A. K. **2008**, 1188–1194.
- (12) Clapper, J. D.; Guymon, C. A. *Macromolecules* **2007**, 40 (22), 7951–7959.
- (13) Clapper, J. D.; Skeie, J. M.; Mullins, R. F.; Guymon, C. A. *Polymer* **2007**, 48 (22), 6554–6564.

- (14) Kim, S. K.; Baguenard, C.; Guymon, C. A. *Macromol. Symp.* **2013**, 329 (1), 173–192.
- (15) Alzahrani, A. a.; Nair, D. P.; Smits, D. J.; Saed, M.; Yakacki, C. M.; Bowman, C. N. *Chem. Mater.* **2014**, 26 (18), 5303–5309.
- (16) Podgórski, M.; Becka, E.; Chatani, S.; Claudino, M.; Bowman, C. N. *Polym. Chem.* **2015**, 6 (12), 2234–2240.
- (17) Baranek, A.; Song, H. B.; McBride, M.; Finnegan, P.; Bowman, C. N. *Macromolecules* **2016**, 49 (8) 3250-3259.
- (18) Hoyle, C. E.; Bowman, C. N. *Angew. Chem. Int. Ed. Engl.* **2010**, 49 (9), 1540–1573.
- (19) Cilurzo, F.; Gennari, C. G. M.; Minghetti, P. *Expert Opin. Drug Deliv.* **2012**, 9 (1), 33–45.
- (20) Murtezi, E.; Yagci, Y. *Macromol. Rapid Commun.* **2014**, 1–6.
- (21) McBride, M. K.; Gong, T.; Nair, D. P.; Bowman, C. N. *Polymer* **2014**, 54 (12) 430-442.
- (22) Hawker, C. J.; Bosman, a W.; Harth, E. *Chem. Rev.* **2001**, 101 (12), 3661–3688.
- (23) Yoshida, E. *Colloid Polym. Sci.* **2011**, 289 (14), 1625–1630.
- (24) Keddie, D. J.; Moad, G.; Rizzardo, E.; Thang, S. H. *Macromolecules* **2012**, 45 (13), 5321–5342.

- (25) Mori, H.; Tsukamoto, M.; Da, P. E. G. *Polymer* **2011**, 52 (3), 635–645.
- (26) Rizzardo, E. and D. H. S. *Aust. J. Chem.* **2012**, 65 (3), 945–969.
- (27) Edeleva, M. V.; Parkhomenko, D. a.; Morozov, D. a.; Dobrynin, S. a.; Trofimov, D. G.; Kanagatov, B.; Kirilyuk, I. a.; Bagryanskaya, E. G. *J. Polym. Sci. Part A Polym. Chem.* **2014**, 52 (7), 929–943.
- (28) Zhang, G.; Zhang, Q.; Wang, Q.; Zhan, X.; Chen, F. *J. Appl. Polym. Sci.* **2015**, 42936.
- (29) Smith, A. E.; Xu, X.; McCormick, C. L. *Prog. Polym. Sci.* **2010**, 35 (1), 45–93.
- (30) Holmberg, A. L.; Karavolias, M. G.; Epps, T. H. *Polym. Chem.* **2015**, 6 (3), 5728–5739.
- (31) Fenoli, C. R.; Wydra, J. W.; Bowman, C. N. *Macromolecules* **2014**, 47 (3), 907–915.
- (32) Cook, W. D.; Schiller, T. L.; Chen, F.; Moorho, C.; Thang, S. H.; Bowman, C. N.; Scott, T. F. *Macromolecules* **2012**, 45 (2), 9734–9741.
- (33) Meng, Y.; Fenoli, C. R.; Aguirre-Soto, A.; Bowman, C. N.; Anthamatten, M. *Adv. Mater.* **2014**, 26 (37), 6497–6502.
- (34) Szczepanski, C. R.; Stansbury, J. W. *Eur. Polym. J.* **2015**, 67, 314–325.
- (35) Jon P. Scholte, Soon Ki Kim, Christopher L. Lester, and C. A. G. *J. Polym. Sci. Part a-Polymer Chem.* **2016**. (In Press)
- (36) Forney, B. S.; Guymon, C. A. *Macromolecules* **2010**, 43 (20), 8502–8510.

- (37) Callister, W. D.; Rethwisch, D. G. *Material Science and Engineering*, 9th ed.; Wiley: New York, 2013.

CHAPTER 7

EFFECTS OF MONOMER COMPOSITION AND ENVIRONMENTAL IMPACT ON CATIONIC PHOTOPOLYMERIZATION

Introduction

Photopolymerization is a type of reaction that uses light to cause monomer species to join and form larger molecules.^{1,2} Most academic knowledge pertaining to photopolymerization has focused on free radical induced methods. However, ring-opening cationic photopolymerization has been of significant recent research.^{3,4} One reason for interest in cationic photopolymerization was the development of ‘Crivello’ onium salts, which form superacids to initiate the cationic photopolymerization reaction.⁵ These salts have overlapping absorbances with common photopolymerization irradiation sources, allowing for easier implementation and research on the resulting cationic initiation and photopolymerization mechanism.⁶

Interestingly, as opposed to the traditional and relatively straightforward radical photopolymerization mechanism, many of the monomers that could undergo a cationic ring-opening reaction also show competing side reactions.^{7,8} While the advent of onium salts provided the opportunity to study ring-opening photopolymerization, the actual polymerization mechanism has been poorly understood. Many of the initial linear epoxide monomers exhibit low vapor pressures and boiling points, resulting in rapid evaporation of the monomer during the photopolymerization.⁹ On the other hand, glycidyl ether monomers and bulkier cycloaliphatic epoxides have been examined.¹⁰ The ether monomers produce lower T_g networks and have slower kinetics. One explanation for the slow photopolymerization kinetics was the formation of crown ether like

complexes around the protonating center.¹¹ These complexes trap the propagating centers and limit the conversion of the reaction during photopolymerization, requiring a thermal cure to ensure high conversion and reliable thermomechanical properties. While the necessity of a thermal “bump” was not ideal, the glycidyl ether monomers provided an initial route toward tuning photocurable cationic resins.^{12,13}

In order to overcome these limitations, and allow for greater control of the final resin properties, monomers outside of the customary epoxide moieties have received increased interest. Vinyl ether monomers are known to undergo the cationic photopolymerization reaction, but they are much more expensive compared to other similarly reactive monomers, thus, limiting their widespread use and study, both industrially and academically.^{14,15} Oxetane monomers on the other hand are much cheaper and environmentally friendly to synthesize.¹⁶ These monomers can also be used to easily manipulate oligomer structure and thus alter the resulting thermomechanical properties. However, neat oxetane monomers have similar issues to glycidyl ether monomers with prolonged inhibition times and low conversions during photopolymerization.^{17,18} Until recently, these limitations have left oxetanes without a significant role in photopolymerization.

Terpene oxide monomers can readily form tertiary oxonium ions that act as the propagating/initiating center for cationic photopolymerizations.¹⁶ Their ability to quickly form the propagating center may accelerate the overall photopolymerization reaction for all monomers involved. Due to their bulk compared to other reactive monomers, it is also possible that the terpene monomers would affect the thermomechanical properties that are evaluated in this chapter.¹⁹ These terpene monomers require a copolymer as the

homo-polymerization cannot be achieved. Combined, these reasons provide a strong ground work for the investigation of the copolymerization of terpene oxides with various other cationic monomer groups to examine for copolymerization synergy.^{17,20-22}

The following research aims to evaluate the factors that impact the rate of photopolymerization and the overall monomer conversion via photo-differential scanning calorimetry. The role of monomer composition on the overall reaction kinetics was also evaluated to determine the optimal composition of epoxide to oxetane that results in the greatest overall rate of photopolymerization using a simplex lattice 3 component experiment to create a response surface for maximum rate of polymerization. Epoxidized terpenes were also examined as a viable alternative monomer for cationic systems. The effects of terpene oxides on epoxide and oxetane photopolymerization kinetics was examined via FTIR. The effects of the incorporation of the terpene oxides on network structures was also evaluated via dynamic mechanical analysis. We hypothesize that the screening knowledge obtained in early studies will allow for greater tuning of cationic photopolymerization kinetics and as well as the implementation of epoxidized terpenes as a new additive to cationic formulations.

Experimental

Materials

Neopentyl diglycidyl ether (NPGDGE, Sigma Aldrich), 3,4-Epoxycyclohexylmethyl 3,4-epoxycyclohexanecarboxylate (EEC, Sigma Aldrich), bis[(2,2-dihydromethyl) butyl] ether (DOX, Toagosei), Limonene Mono- and Dioxide, (BASF, LMO and LDO respectively) and PC-2506 (Polyset), a diaryliodonium hexafluoroantimonate photoinitiator, were used as received.

Methods

Photopolymerization behavior of prepolymer/monomer mixtures was examined utilizing a Perkin Elmer Diamond differential scanning calorimeter modified with a medium pressure mercury arc lamp (photo-DSC). Photopolymerization profiles were compared using the evolved polymerization heat per unit mass of photocurable resin during the polymerization. Photopolymerization profiles were compared using the evolved polymerization heat per unit mass of photocurable resin during the polymerization to determine the normalized polymerization rate according to equation 1.²³

$$\frac{R_p}{[M_0]} = \frac{Q * MW}{m * n * \Delta H_p} \quad (1)$$

Where R_p is the extensive rate of polymerization, $[M_0]$ is monomer concentration, Q is heat flow, MW is the monomer molecular weight, m is sample mass, n is number of reactive groups per molecule, and ΔH_p is the enthalpy of polymerization 107, 114, 118 kJ/mol for oxetane, epoxides, and cycloaliphatic epoxides relatively.^{16,24} Rates of photopolymerization were measured at an irradiation intensity of 10mW/cm². Real time infrared spectroscopy was performed using a Thermo Nicolet nexus 670. One mg of sample was placed on a sodium chloride plate covered with 15 μ m spacer beads and sandwiched with an additional sodium chloride plate. The laminate nature of this testing geometry prevents oxygen and water from diffusing into the system. Analysis was performed at ambient temperature and atmosphere. Oxetane and epoxide conversions were determined by monitoring the decrease of the absorbance bands at 980 cm⁻¹ and 790 cm⁻¹ respectively.²²

Dynamic mechanic analysis (DMA, Q800 DMA TA Instruments) was conducted to investigate the effect of polymer architecture on ultimate mechanical and visco-elastic properties of cured polymers. To fabricate rectangular 6 x 25 mm and 0.15 mm thick films, two thick glass plates, covered by amorphous polyvinylidene fluoride films (PVDF, Teflon® AF, Dupont) for easy release, were used. Adhesive tape spacers (150 µm thick) were attached on each edge of the bottom plate to control the film thickness. Approximately 3g of liquid sample mixture were placed on the bottom glass plate and dried for 30 minutes. The liquid samples were then tightly pressed using the upper glass plate and secured using binder clips. Filled molds were irradiated for 10 minutes using a high pressure mercury lamp (250-500 nm) at an irradiation intensity of 10 mW/cm². To measure the modulus and glass transition temperature of the samples, the temperature of films was increased from -70°C to 150°C at a heating rate of 3°C/min. DMA tensile mode was utilized under constant strain at a frequency of 5 Hz.

Results and Discussion

Even with the significant increase in interest in photocurable cationic systems, little work has been focused on quantitatively designating the differences between cationically photopolymerizable reactive groups. While research has characterized the polymerization of groups independently, copolymerization of these monomers has not been examined to any significant degree, especially regarding spectroscopic evidence regarding reactivity and physical properties originating from copolymerization. To that end, this study aims to determine basic copolymerization kinetics for common cationic photopolymer moieties. This study also examines epoxidized terpenes as monomeric

alternatives and accelerators to cationic photopolymerization and their effects on thermomechanical properties.

Several of photocurable cationic monomers form stable intermediates or crown ether complexes with the cationic active centers, limiting the rates and conversion during photopolymerization. Further, the rates of polymerization and monomer conversion for the cationic photopolymerization process are acutely affected by both the presence of atmospheric water and post-photopolymerization heating of the monomer. In an effort to evaluate the effect of the aforementioned variables and to provide a predictive model for both rates of polymerization and monomer conversion, a four factor two response half factorial screening experiment was performed using the experimental design shown in Table 7.1.

Table 7.1 Conditions for DOE screening of photopolymerization conditions for cationic photopolymerization

Run	Monomer Moiety	Post Photopolymerization Thermal Cure Time (hours)	Atmospheric Conditions	Post Photopolymerization Thermal Cure Temperature (°C)
1	cycloaliphatic epoxy	3	ambient	100
2	cycloaliphatic epoxy	0.5	ambient	60
3	cycloaliphatic epoxy	3	nitrogen	60
4	cycloaliphatic epoxy	0.5	nitrogen	100
5	glycidyl ether	3	ambient	100
6	glycidyl ether	0.5	ambient	60
7	glycidyl ether	3	nitrogen	60
8	glycidyl ether	0.5	nitrogen	100

Both glycidyl ether and cycloaliphatic epoxy moieties were studied as cationically photopolymerizable groups. The environmental conditions were either under ambient lab conditions or nitrogen while in the photo-DSC instrument. After two minutes of photopolymerization, samples were heated to one of the given temperatures and post-cured for times listed in Table 7.1. Table 7.2 gives the conversion response values of each run described in Table 7.1. Characteristic DSC traces for runs 1-8 can be observed in Figure 7.1.

Table 7.2. Responses from screening experiments

Run	Normalized Rate of Photopolymerization	X (%)
1	0.0337	59.2
2	0.0586	51.5
3	0.0243	40
4	0.043363	44.3
5	0.00603	61.3
6	0.0026	50.6
7	0.00237	53.3
8	0.005207	47.5

The half factorial screening experiment showed a higher rate of polymerization for the glycidyl ether monomers once the formulation was heated after the photopolymerization as observed in Figure 7.1. In all runs using glycidyl ether monomers, a secondary polymerization was evidenced, contributing to the overall functional group conversion. Based on the % conversion and normalized rates of polymerization for runs 1-8, models were designed utilizing the pareto charts to depict the half average values observed in Figure 7.2.

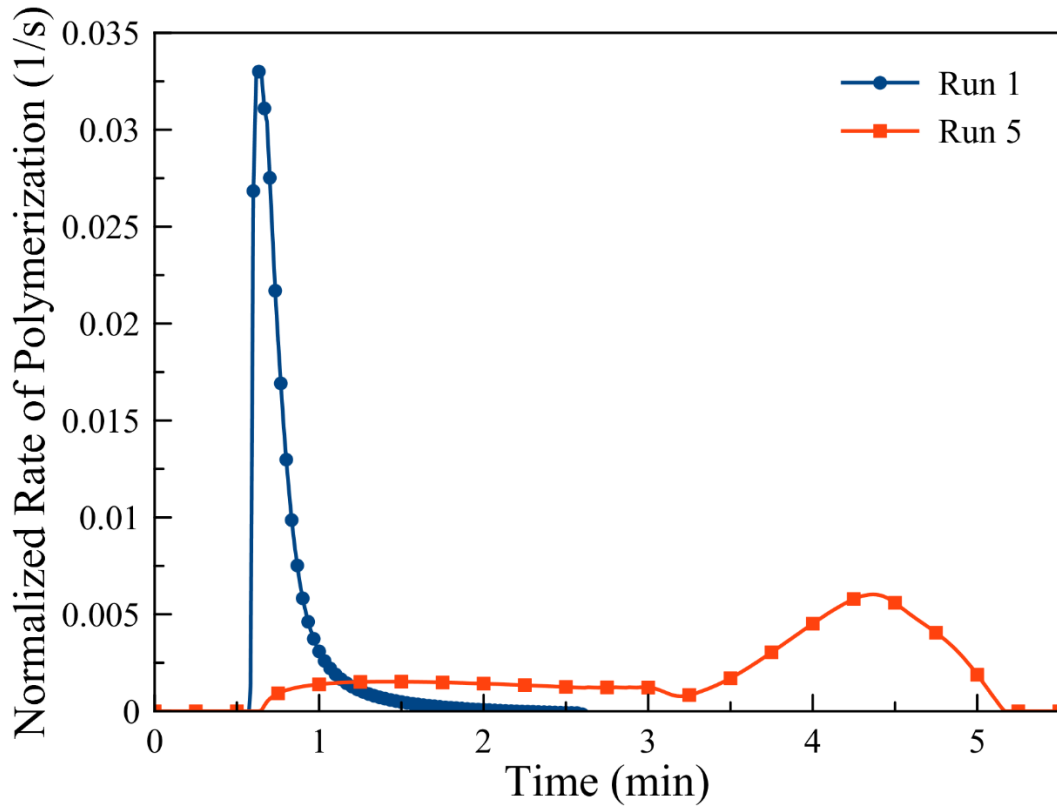


Figure 7.1. Normalized Rate of Polymerization for Run 1 vs Run 5 as described in Table 1. All samples were photopolymerized at 10 mW/cm² with 2 wt% PC-2506 for 2.5 minutes.

As shown in Figure 7.2a, the most influential values in predicting the overall monomer conversion are the atmospheric conditions, the monomer structure, and post photopolymerization thermal cure time. After building the model, it appears that the interaction of the atmospheric conditions and the post photopolymerization cure time is also influential. This is most likely due to greater solubility of atmospheric gasses at elevated temperatures into the formulation. Based on this simple experimental design, a general predictive equation to describe the overall monomer conversion is,

$$X = 50.96 + 2.21A - 1.74B - 5.44C + 2.11BC \quad (2)$$

where A is the type of monomer chosen, B is the post photopolymerization cure time, C

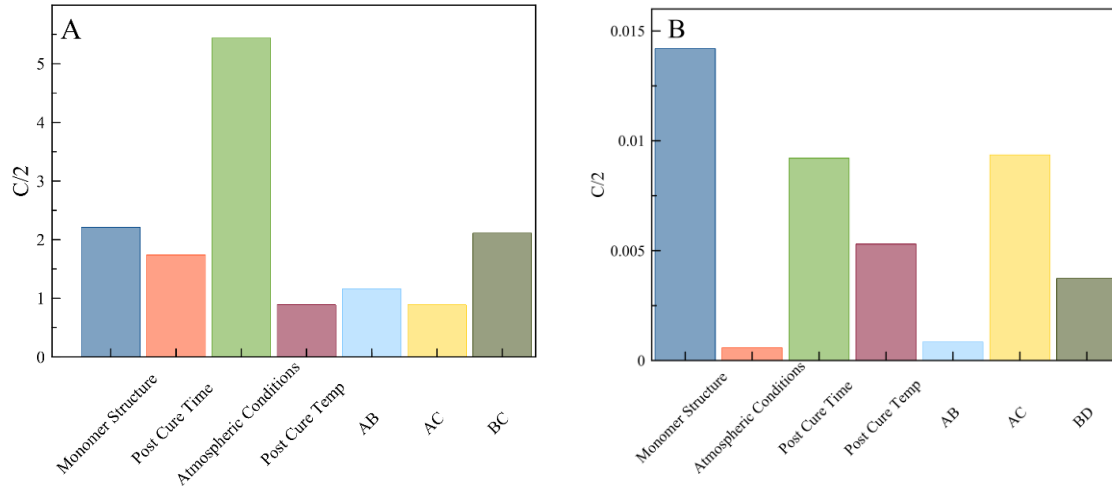


Figure 7.2. Pareto charts for models predicting percent monomer conversion (A) and maximum normalized rate of polymerization (B).

is the atmospheric condition in which the photopolymerization occurred, and BC is the interaction variable of post photopolymerization cure time and the atmospheric conditions in which the polymerization occurred. Based on this equation it appears that the atmospheric conditions during the photopolymerization are the most influential variable examined. Indeed, in runs that were purged with nitrogen the final conversion of all materials was almost 10% lower than observed for other materials. Perhaps more interesting is that while both monomers can regularly achieve between 55-60% conversion, the glycidyl ether system required the thermal curing post-photopolymerization much more than the cycloaliphatic epoxides. These values also show that the actual temperature at which the samples were heated post-photopolymerization is the only variable examined that does not play a significant role in the final monomer conversion. It is possible that this phenomenon is due to using a diaryl iodonium photoacid generator. Diaryl iodonium photoacid generators have been described in literature as decomposing into their super-acid forms at lower temperatures

than their triaryl sulfonium counterparts. Thus, it is possible that both temperatures selected were above the decomposition temperature for PC 2506, allowing the photoacid generator to decompose in all samples post photopolymerization.

In addition to predicting the overall monomer conversion, the normalized rate of polymerization was also recorded as a response factor. The most influential variables can be seen in Figure 7.2B from the highest half-effect values. Based on the response half-effect values from runs 1-8, it appears that the most influential factors are again monomer structure and atmospheric photopolymerization conditions. Additionally, a combination of monomer structure and atmospheric conditions seem to also influence the rate of polymerization. Based on this information the following predictive model can be obtained

$$R_{pn} = 0.0182 - 0.0142A + 0.00921C + 0.00936AC \quad (3)$$

From the equation it can be observed that selecting a cycloaliphatic epoxy monomer will yield higher rates of reaction. The higher observed rates of polymerization for these samples is likely due to the formation of stable crown ether complexes formed by the glycidyl ether monomers. Crivello *et al.* showed that this type of epoxy monomer forms such complexes, which limit the conversion and rate of polymerization.¹² It then follows that heating the gelled network potentially destabilizes the crown ether complex allowing the ring opening polymerization to occur as observed by the secondary polymerization event observed in run 5. These results suggest that atmospheric conditions and reactive groups must be considered for all cationically photocurable formulations.

In addition to both glycidyl ethers and cycloaliphatic epoxide moieties, oxetanes, or four-membered heterocyclic rings, can also undergo cationic photopolymerization. Oxetane monomers have received much more attention in recent years as they can dramatically increase the rate of polymerization in other cationic system. Figure 7.3 shows normalized rates of polymerization for glycidyl ether, cycloaliphatic, and oxetane monomers. As observed in Figure 7.3, glycidyl ether monomers show a low, slow polymerization reaction upon illumination. Comparatively, the cycloaliphatic epoxide monomers show a much higher normalized rate of reaction as well as a prolonged reaction during the illumination period. On the other hand, the oxetane monomers exhibit an exceptionally large rate of polymerization with though with a large delay before $R_{p,max}$. Both epoxide monomers monitored in Figure 7.3 achieve their $R_{p,max}$ within the first quicker than the oxetane monomer. However, the oxetane polymerization does not achieve its maximum rate of polymerization until almost a full minute of illumination.

These normalized rates of polymerization suggest that a combination of epoxide and oxetane monomers may synergistically enhance the overall rates of polymerization in terms of conversion and time to $R_{p,max}$. In order to quantify if the copolymerization of these cationic monomers may affect the rates of polymerization, simplex lattice 3 component experiment was performed, according to the runs observed in Table 7.3. Figure 7.4 shows the normalized rates of polymerization with the surface response in a ternary diagram where red indicates a higher $R_{p,max}$ and blue represents lower $R_{p,max}$ values. Based on the response surface, it appears that epoxide monomers on their own or while mixed produce the lowest overall rate of polymerization. With a 2:1 molar ratio of

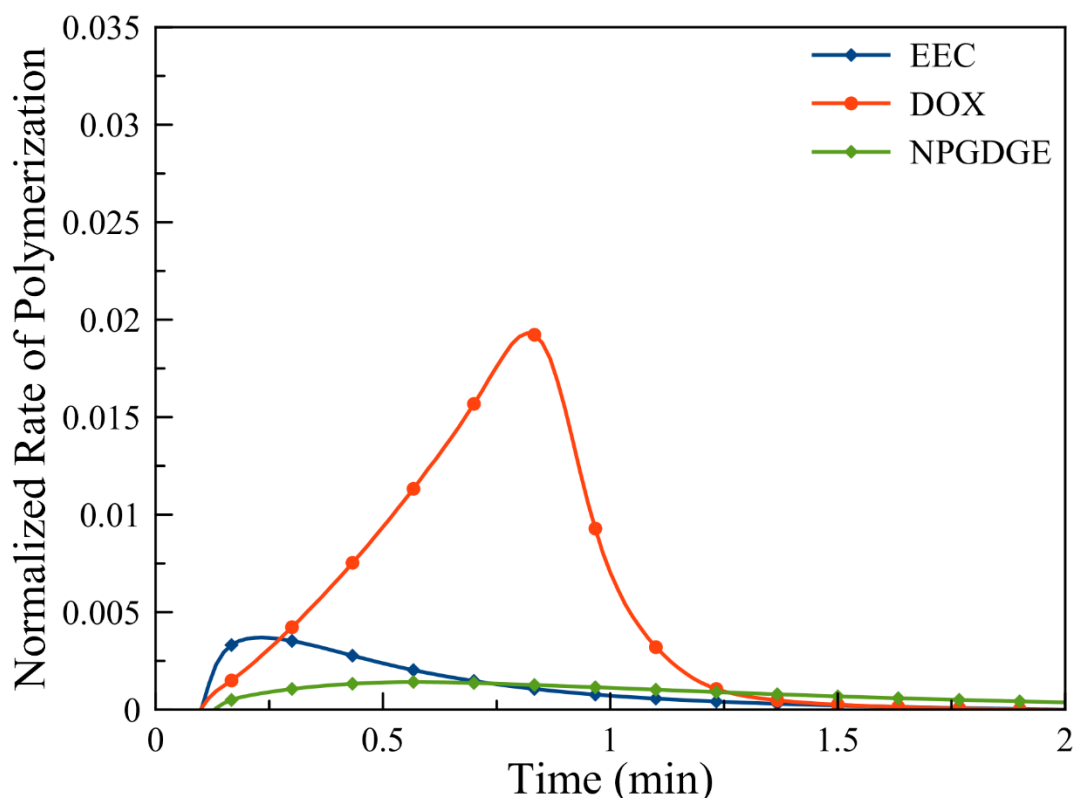


Figure 7.3. Rate of photopolymerization for NPGDGE, EEC, and DOX monomers when homopolymerized. All samples were photopolymerized at room temperature and 10 mW/cm^2 , using 2 wt% PC-2506 for 10 minutes.

epoxide to oxetane monomers is introduced, the rates of polymerization almost double. Interestingly, both a 2:1 glycidyl ether to oxetane molar composition and a 1:1:1 glycidyl ether to oxetane to cycloaliphatic epoxy mixture produce a slightly lower normalized rate of photopolymerization. This difference in rate of polymerization is likely due to the glycidyl ethers having a greater number of side reactions involving their formation of crown ether complex as compared to the cycloaliphatic epoxide monomer. As the composition shifts to a 1:2 epoxide to oxetane molar concentrations, the normalized rates of photopolymerization continue to increase. Again, likely due to the possible side reactions involved in the cationic photopolymerizations of the glycidyl ethers, their 1:2

molar compositions with oxetane monomers shows a lower $R_{p,max}$ value than the analogous system using the cycloaliphatic epoxide monomer.

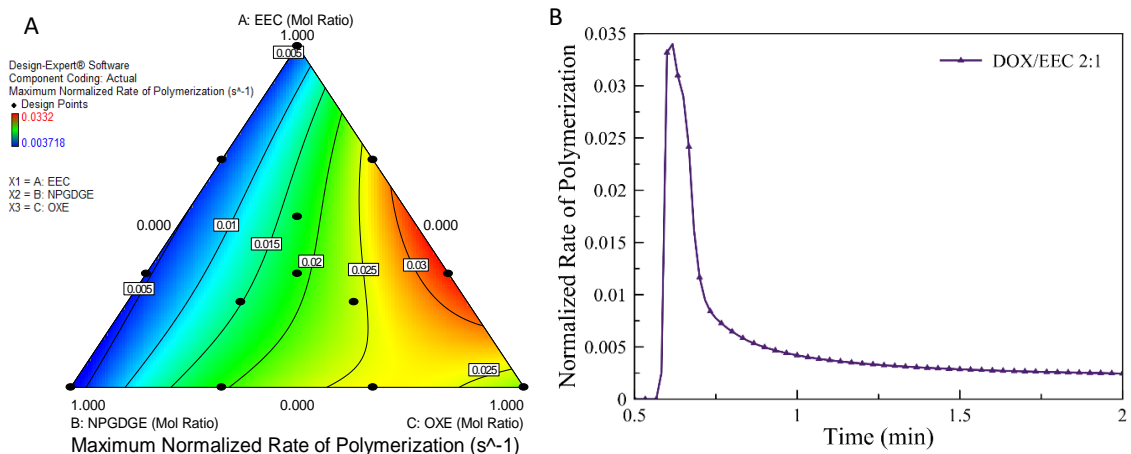


Figure 7.4. Normalized rates of polymerization as measured via photo-DSC. All samples were photopolymerized at room temperature and 10 mW/cm², using 2 wt% PC-2506 as a photoacid generator initiator.

Indeed, the 1:2 EEC to DOX molar formulation shows a significant increase in the rate of photopolymerization and the highest rate observed on the response surface, as observed in Figure 7.4B. The middle check points were added to further examine how a ternary formulation of both epoxide monomers and the oxetane monomer responded and matched the model. All predicted values when tested were between 13 and 20% higher than the actual R_p observed for the formulation. The lower $R_{p,max}$ values provide evidence to the complexities of cationic photopolymerization as well as the difficulties involved in accurate formulation modeling. Deviations are most likely due to the glycidyl ether crown ether side reactions consuming active centers early in the photopolymerization. In agreement with our initial hypothesis, the combination of epoxide and oxetane functionalities increased the rate of photopolymerization, but the delay characteristic of

oxetane photopolymerization is removed, highlighting the potential advantages of cationic copolymerization.

While these monomers are commonly used in photopolymerization, if alternatives could be used that achieve similar results without the drawbacks associated with most current monomer formulations, significant improvements and expansion in cationic photopolymerizations could be observed. One exciting avenue for such materials are epoxidized terpene oxides. An advantage of the epoxidized terpenes over standard cationic monomers is their ability to rapidly form tertiary oxonium ions. While attempts have been made to homopolymerize terpene epoxides, the tertiary oxonium can rapidly decay and form ketones as indicated recently reported by Crivello *et al.*¹² In order to examine the effects of epoxidized terpenes on the photopolymerization kinetics, RT-FTIR was used to monitor differences in monomer conversion rates. Figure 7.5 shows the conversion profiles for NPGDGE (Figure 7.5A), EEC (Figure 5B), and DOX (Figure 7.5C). As can be observed in Figures 7.5A and B, there is very little to no change in to the kinetic profiles of the epoxide monomers when a terpene oxide monomer is incorporated. On the other hand, the oxetane monomer experiences a significant acceleration. Without the incorporation of a terpene epoxide as an accelerant, the neat DOX system experiences an approximate four minute induction period. Interestingly, when a mono-epoxidized terpene is added to the system, it appears to increase the rate polymerization slightly more than the diepoxidized terpene. The mono-epoxidized terpene monomer may be more mobile as a preliminary reactive center compared to the limonene dioxide. Additionally, the second epoxy group may not form as stable of a

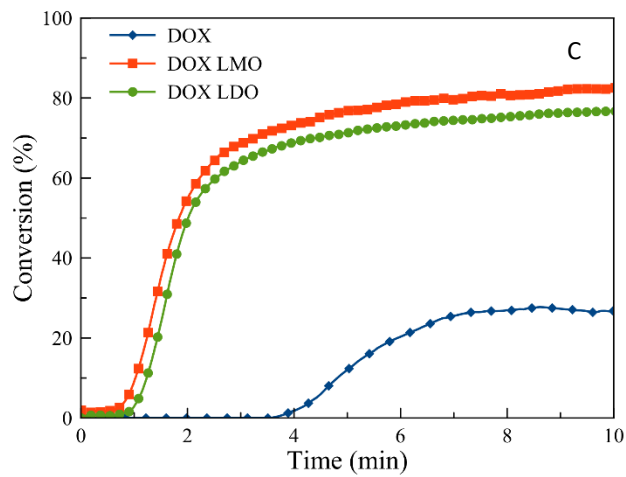
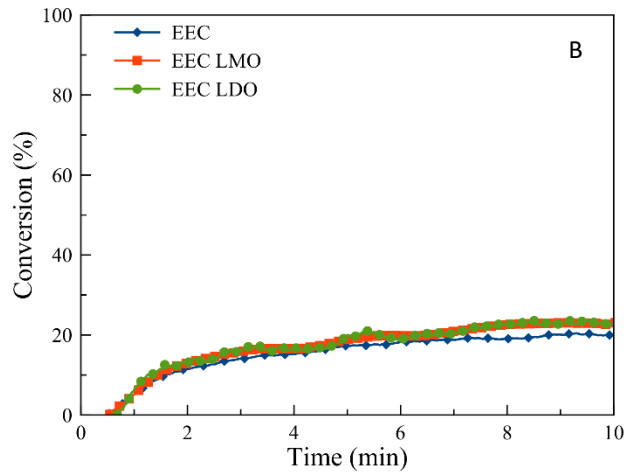
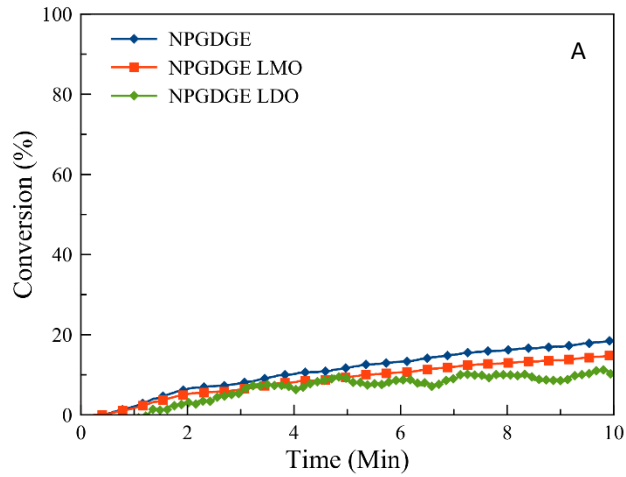


Figure 7.5. Conversion profiles for all formulations using common epoxide or oxetane monomers both neat and containing 5 mol% mono- and diepoxidized terpene accelerants. All samples were photopolymerized under at 30°C and 10 mW/cm² with 2 wt% PC-2506 for 10 min.

tertiary oxonium ion which would also account for the small differences in rate of polymerization. Lastly, the actual conversion for these materials which incorporate the limonene mono- or dioxides achieve almost double the oxetane conversion as compared to the neat DOX systems.

With the acceleration of the oxetane photopolymerization and higher conversion, it is also likely that the presence of limonene oxides would affect the thermomechanical properties of the photocured networks. Thermomechanical properties were examined utilizing dynamic mechanical analysis (DMA) to observe both the storage modulus and the effect of comonomers on the glass transition temperature, as seen by $\tan(\delta)$. Figures 7.6A, B, and C show the storage moduli for the glycidyl ether, cycloaliphatic, and oxetane formulations, respectively. While the presence of the limonene comonomers do not appear to affect the kinetics of the glycidyl ether or cycloaliphatic photopolymerization kinetics, they do appear to have an effect on the thermomechanical properties. The glycidyl ether monomers display the sharpest transition. The neat NPGDGE system has sharp glassy to rubbery plateau transition occurring at roughly 50°C. The incorporation of the limonene monoxide appears to lower the temperature of the transition while the polymer still undergoes a very sharp transition. Interestingly the incorporation of the dioxide copolymer actually increases the temperature of the transition. This increase in transition temperature is not likely due to changes in the relative crosslink density observed in the neat system (i.e. all monomers present are multifunctional), but the structure of the limonene dioxide may decrease the network

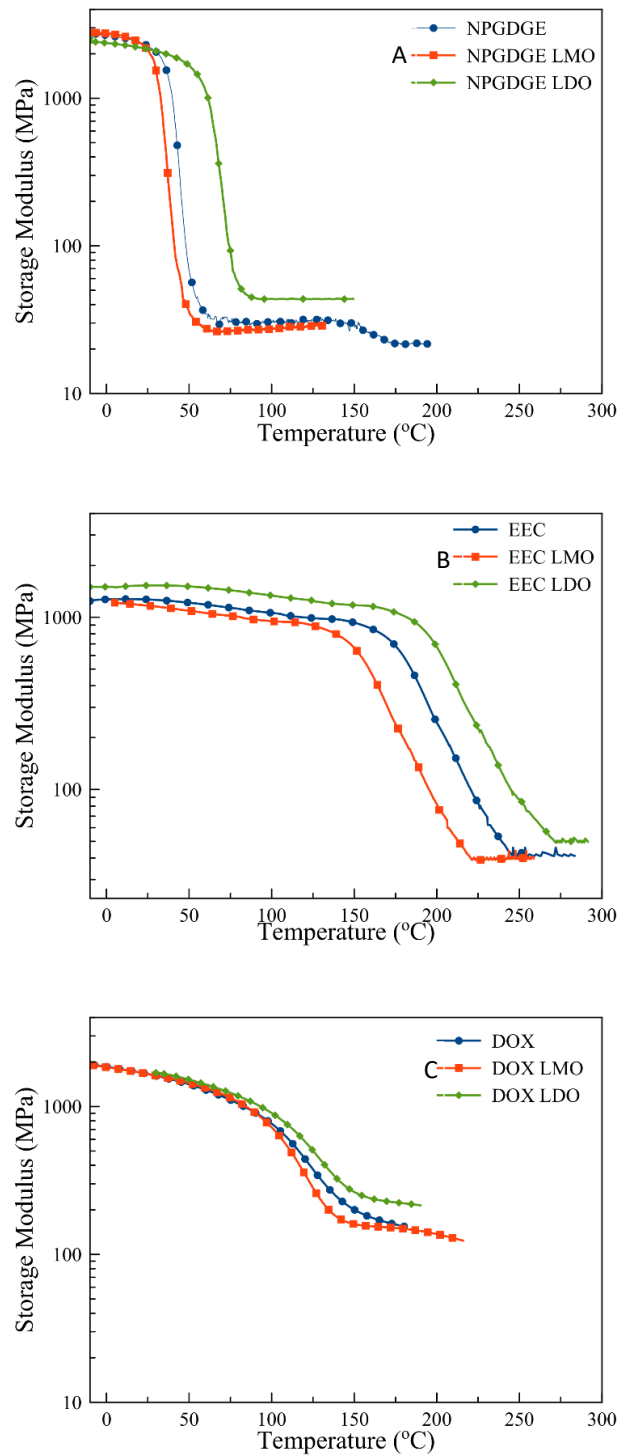


Figure 7.6. Storage modulus as a function of temperature of glycidyl ether (A), cycloaliphatic epoxy (B), and oxetane monomer systems (C) copolymerized with 5 mol% limonene mono- and dioxide. All samples were photopolymerized at 10 mW/cm² with 2 wt% PC-2506 for 10 min.

flexibility. The results for the EEC systems in Figure 7.6B seem to corroborate this idea. As both epoxide monomers exhibit fairly low conversion during the photopolymerization, it is possible that the LMO and LDO are either plasticizing the network or causing additional crosslinking, respectively. These plasticizing and crosslink differences most likely cause the approximate 25°C shift for the glassy plateau transition for the two systems. LMO seems to effect EEC thermomechanical properties to a much greater extent than the glycidyl ether monomer. The more dramatic shift is likely due to EEC independently having a high T_g and forming a highly crosslinked network. The bulky LDO monomer also seems to raise the T_g of the EEC due to a change in the flexibility of the chains within the crosslinked network. A similar trend is observed in Figure 7.6C in which the neat system has a slightly higher transition than the formulation using LMO. Similarly, to the glycidyl ether systems, it appears that the DOX copolymerized with LDO as an accelerant to overcome the inhibition period induces a higher storage modulus and a slightly prolonged glassy plateau compared to the neat and LMO systems. These changes in behavior are potentially due to the photopolymerization reaction having a much greater conversion than observed for the epoxide monomer systems and as such may not allow the rearrangements to occur via any dark cure. These results suggest that while epoxidized terpenes may not affect the rates of epoxide photopolymerization, they can be used as additives to change the thermomechanical properties of the final films.

If the storage modulus of the resulting photocured films is affected to such a degree by the terpene additives, it is also possible that the glass transitions of these materials would be altered. One method of observing the glass transition of a material is

to plot the loss factor, $\tan(\delta)$, of the film as measured by dynamic mechanical analysis versus temperature. Maxima in the plot were taken to represent the temperature at which the material undergoes a glassy to rubbery transition, i.e. the T_g . Figure 7.7 shows the $\tan(\delta)$ plots as a function of time for the oxetane and epoxide formulations. As is expected from Figure 7.6A, the glycidyl ether monomers show a very sharp peak for all samples occurring between approximately 40°C and 80°C. The inclusion of LMO appears to slightly lower the glass transition of the material as the monofunctional monomer likely disrupts an otherwise, apparently highly regular network. By limiting the degree of crosslinking, the apparent peak became slightly narrower and occurs at 40°C, as compared to the neat NPGDGE system which had a T_g at approximately 50 °C. Meanwhile, the inclusion of the comparatively bulkier LDO monomer appears to elevate the glass transition of the resulting thin film. The shift in T_g is again likely to the subtle changes in the network crosslinking and incorporation of LDO, decreasing network flexibility at lower temperatures where the primarily aliphatic ether crosslinks would be expected to be mobile.

Figure 7.7B shows the same behavior for the photopolymer networks formed via the cycloaliphatic epoxide moiety. The neat system shows a broad T_g occurring at roughly 225°C. The inclusion of a plasticizing agent present in the LMO alters the crosslink density and lowers the T_g of the resulting systems by almost 50°C. LDO on the other hand raises the T_g by limiting the mobility of the network. Interestingly, the LDO shifts the T_g to a much lower degree than that observed in the glycidyl ether system, producing in conjunction with EEC only a 15°C increase. The cycloaliphatic epoxide monomers showed a much broader peak, almost 100°C in some cases, in relation to the much

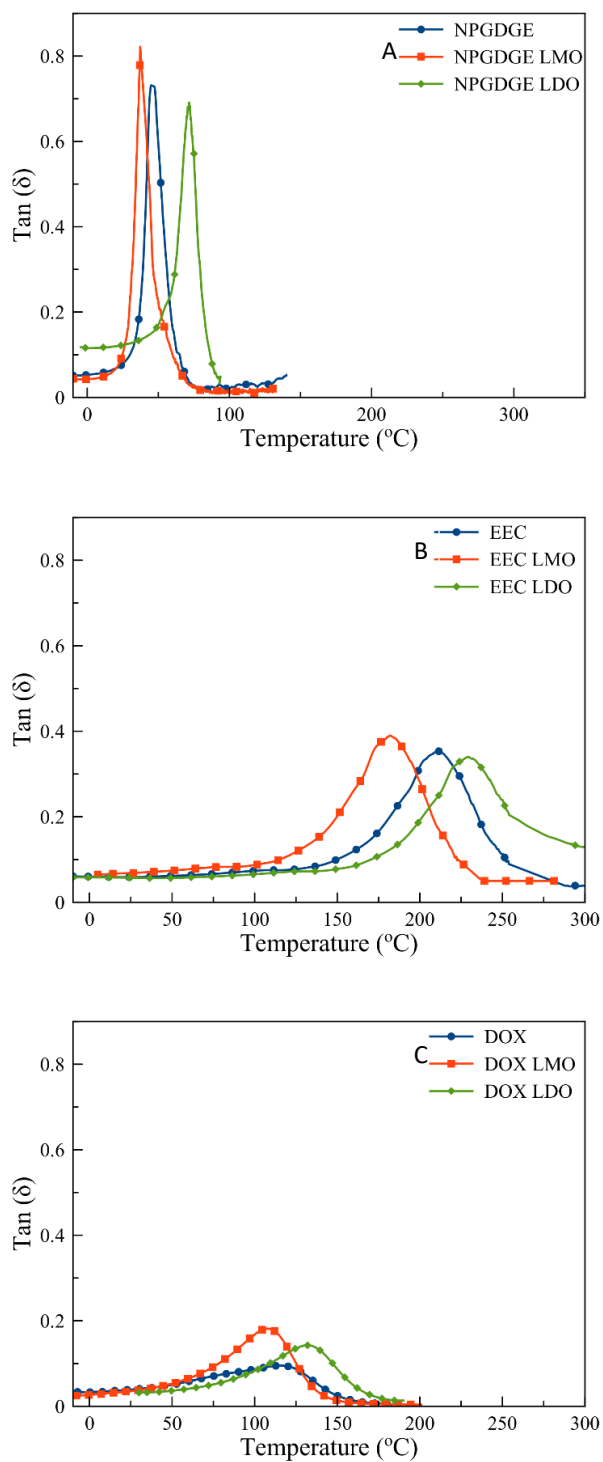


Figure 7.7. $\tan(\delta)$ as a function of temperature of glycidyl ether (A), cycloaliphatic (B), and oxetane monomer systems copolymerized with 5 mol% limonene mono- and dioxide. All samples were photopolymerized using 2 wt% PC-2506 under standard room temperature conditions at 10 mW/cm² for 15 min.

narrower glycidyl ether peaks, suggesting that these networks are much less regular than those formed by the glycidyl ether monomers.

The oxetane monomers, shown in Figure 7.7C, meanwhile produce very broad peaks analogous to the EEC systems. The neat DOX photopolymerization shows a peak at roughly 120°C, though it is by far the smallest and broadest peak of any formulation tested. The incorporation of the epoxidized terpenes have a similar effect to that observed for the epoxide systems; however, the networks continue to produce very small $Tan(\delta)$ peaks. LMO shifts the peak roughly 25°C degrees lower than the neat system while LDO, again, raises the T_g to a lesser extent than when incorporated into the NPGDGE formulation. The difference in T_g is most likely due to the lower network mobility and flexibility of the oxetane systems, as compared to the glycidyl ether monomers. It is possible that the limonene monoxide is rapidly tautomerizing to produce a plasticizing component while the limonene dioxide, via multiple reaction sites, is more easily incorporated into the polymer network.¹⁶ This explains why the LMO appears to lower the T_g of the network while LDO raises the T_g . Together with the kinetic information in Figure 7.5, it becomes apparent that epoxidized terpenes may form a unique method of altering cationic photocurable polymer resins.

Conclusion

Herein we report two models that predict the role of processing and formulation variables integral to the use of cationic photopolymerization. In particular, the role of atmospheric condition and monomer moiety are the best predictors of photopolymerization rate. The temperature of a thermal post cure appears to be not as important so long as the temperature was above 60°C though the duration of the cure did

have some small effect on the overall monomer conversion. Copolymerization of epoxide and oxetane monomers may overcome the specific limitations of each material individually with a copolymer formulation increasing the maximum rate of polymerization. Glycidyl ethers increase the overall rate of photopolymerization; however, likely due to side reactions inherent to monomer structure, they produced a smaller effect compared to the cycloaliphatic epoxies. Additionally, both mono- and diepoxidized terpenes show potential as accelerants in cationic photopolymerization. The terpene oxides exhibit suitable behavior for the rapid initiation of oxetane monomers in order to achieve much higher photopolymerization rates and conversions compared to the neat oxetane monomer formulation, possibly by avoiding stable intermediates formed via the oxetane monomers and easily forming propagating centers. While the epoxidized terpenes do not show any kinetic effect on the epoxide monomers, these monomers modify the storage modulus and T_g of all systems examined in this study. In summary, this work provides a fundamental study of cationic copolymerization kinetics and examines a new type of comonomer that may be of special interest for modifying cationic photopolymer networks.

References and Notes

- (1) Zhang, J.; Dumur, F.; Xiao, P.; Graff, B.; Gigmes, D.; Pierre Fouassier, J.; Lalevée, J. *J. Polym. Sci. Part A Polym. Chem.* **2015**, *54*, (15) 4302–4311.
- (2) Forney, B. S.; Guymon, C. A. *Macromolecules* **2010**, *43* (20), 8502–8510.
- (3) Erdur, S.; Yilmaz, G.; Colak, D. G.; Cianga, I.; Yagci, Y. **2014** *47* (21), 7296–7302.
- (4) Bermeshev, M. V.; Bulgakov, B. a.; Genaev, A. M.; Kostina, J. V.; Bondarenko, G. N.; Finkelshtein, E. S. *Macromolecules* **2014**, *47* (16), 5470–5483.
- (5) Crivello, J. V. *J. Polym. Sci. Part A: Polym. Chem.* **1999**, *37*, (42) 4241–4254.
- (6) Crivello, J. V. *Adv. Polym. Sci.* **1984** *62* (1) 3–44.
- (7) Crivello, J. V. *J. Polym. Sci. Part A Polym. Chem.* **2006**, *44*, (1) 3036–3052.
- (8) Bulut, U.; Crivello, J. V. *J. Polym. Sci. Part A Polym. Chem.* **2005**, *43* (15), 3205–3220.
- (9) Nalli, T. W.; Stanek, L. G.; Molenaar, R. H.; Weidell, K. L.; Meyer, J. P.; Johnson, B. R.; Steckler, T. T.; Wackerly, J. W.; Studler, M. J.; Vickerman, K. L.; Klankowski, S. a. *J. Org. Chem.* **2013**, *78* (8), 3561–3569.
- (10) Lalevée, J.; Tehfe, M.-A.; Morlet-Savary, F.; Graff, B.; Allonas, X.; Fouassier, J. *P. Prog. Org. Coatings* **2011**, *70* (1), 23–31.
- (11) Crivello, J. V.; Aldersley, M. F. *J. Polym. Sci. Part A Polym. Chem.* **2013**, *51* (4), 801–814.

- (12) Crivello, J. V. *J. Polym. Sci. Part A Polym. Chem.* **2006**, *44*, (13) 6435–6448.
- (13) Crivello, J. V. *J. Polym. Sci. Part A Polym. Chem.* **2011**, *49* (1), 2147–2154.
- (14) Song, J.; Xu, J.; Tang, D. *Polymer* **2015**, *55* (13) 3451–3455.
- (15) Mowers, W. A.; Crivello, J. V. *J. Polym. Sci. Part A Polym. Chem.* **1999**, *37* (13) 4007–4019.
- (16) Crivello, J. V. *J. Polym. Sci. Part A Polym. Chem.* **2014**, *52* (13) 2934–2946
- (17) Verstegen, E. J. K.; Kloosterboer, J. G.; Lub, J. *J. Appl. Polym. Sci.* **2005**, *98* (4), 1697–1707.
- (18) Crivello, J. V.; Falk, B.; Zonca, M. R. *J. Polym. Sci. Part A Polym. Chem.* **2003**, *41* (12), 1630–1646.
- (19) Sainz, M. F.; Souto, J. A.; Regentova, D.; Johansson, M. K. G.; Timhagen, S. T.; Irvine, D. J.; Buijsen, P.; Koning, C. E.; Stockman, R. A.; Howdle, S. M. *Polym. Chem.* **2016** *14* (12) 2305–2317.
- (20) Crivello, J. V. *J. Polym. Sci. Part A Polym. Chem.* **2015**, *53* (4), 594–601.
- (21) Torron, S.; Johansson, M. *J. Polym. Sci. Part A Polym. Chem.* **2015**, *53*, 2258–2266.
- (22) Sangermano, M.; Malucelli, G.; Bongiovanni, R.; Priola, A. *Eur. Polym. J.* **2004**, *40* (2), 353–358.
- (23) Forney, B. S.; Guymon, C.A. *Macromolecules* **2013**, *45* (11) 234–246.
- (24) Crivello, J. V. *J. Polym. Sci. Part A Polym. Chem.* **2014**, *53* (12) 586–593.

CHAPTER 8

CONCLUSIONS AND RECOMMENDATIONS

One of the limitations of photopolymer systems is the lack of control over network structure and morphology. Traditional photocurable formulations employ a variety of monomers, yet few which truly act to govern network formation. Step growth polymerizations involving various “click” chemistries have been examined both academically and industrially, though for various reasons, they have yet to see broader applications to significantly replace the more common acrylate and epoxide formulations. Controlled radical polymerization provides one avenue to generate macromolecules with specific structures and reactive group placement necessary to identify the next generation of photopolymer materials to address specific limitations such as shrinkage stress and enhanced toughness. In this work, architected prepolymers were studied to provide fundamental understanding of the role of prepolymer structure on network formation and properties.

On the basis that the placement of reactive groups may serve as a method for directing and controlling network heterogeneities, butyl acrylate homopolymers were synthesized via nitroxide mediated polymerization (NMP) with epoxy groups located at both ends or randomly distributed along the prepolymer backbone. The butyl acrylate prepolymers with epoxide groups at the ends slightly alter the kinetics, in turn yielding reproducible rates of polymerization, as compared to prepolymers with randomly distributed epoxide groups. Moreover, the networks produced by the end functionalized prepolymer formulations yield significantly different thermomechanical properties. The placement of the epoxy moieties at the ends of butyl acrylate chains allow the non-

reactive center segments to be embedded throughout an otherwise continuous network of the reactive diluent and reactive ends, while the randomly functionalized prepolymers produce amorphous networks with little control over local nanoscale domains or structures. The differences in nanoscale network structures is most prominent in the glass transitions of the resulting thin films where the non-reactive butyl acrylate segments provide one transition within the network, while the crosslinking reactive diluent provide a higher T_g . On the other hand, the thin films produced via the photopolymerization of the randomly functionalized butyl acrylate prepolymers show a single broad transition. The tensile behavior of the thin films also exemplifies that prepolymer structure can govern mechanical properties. Plots of stress-strain behavior reveal how the continuous hard domain, produced by the highly cross-linked regions, may yield one deformation modulus, while the rubbery butyl acrylate center segments provide a second deformation mechanism. Furthermore, the continuous hard domain present in the end functional prepolymer formulations prevent creep to a significantly greater extent than the randomly functionalized films.

NMP was also employed to synthesize a series of architected prepolymers with cycloaliphatic epoxide moieties located in the center of their structure or randomly distributed along the prepolymer backbone. Nitroso-compounds were identified to enable the controlled polymerization of methacrylate monomers as traditional nitroxide radicals are incapable of controlling the methacrylate polymerization. Interestingly, the long aliphatic tails at the ends of the center functional prepolymers appear to cause segregation of the reactive diluent prior to the photopolymerization as suggested by the irregular kinetics displayed by some formulations. Both photo-DSC and real time FTIR data

exhibit apparent local reactivity differences based on prepolymer architecture. The ability for the center functionalized prepolymers to govern network heterogeneities was also shown to be affected by photopolymerization rate. When limonene dioxide is present as an accelerant for the reactive dioxetane diluent, the T_g of all formulations increases likely due to heterogeneity formation from the reactive diluent. The stress-strain behavior of the films, in tensile mode, appears to support this as modulus increases with the inclusion of a terpene oxide accelerant. The nanoscale morphology of the films also appears significantly different between the materials. Films that incorporated the random prepolymers show very little in and out of phase behavior in AFM images. Also, when no accelerant is present, center functionalized prepolymers result in significant in and out of phase behavior with larger domains forming. Further, based on these nanoscale heterogeneities, films produce more hydrophobic surfaces via the long aliphatic tails at the surface of the films when center functionalized films were utilized.

Building on the ability of architected prepolymers to govern heterogeneities in photocured epoxy systems, prepolymers with the acrylate moieties were synthesized with multiple controlled radical methods. In addition to NMP, reversible addition fragmentation chain transfer (RAFT) was also used to enable photoplasticity within the network. In acrylate systems the NMP prepolymers behave similarly the epoxy systems, with end functionalized prepolymers generating different nanoscale morphologies due to the unreactive butyl acrylate and highly cross-linked domains. The RAFT systems meanwhile show markedly different properties due to their ability for network rearrangement. The end functional materials synthesized via RAFT exhibit multiple $\tan(\delta)$ peaks at high reactive diluent concentrations; however, as the prepolymer content

increases, and the rubbery butyl acrylate disperses to a greater extent throughout the network, these peaks combine indicating more homogeneity. Random prepolymers made via RAFT polymerization show much higher T_g 's. This higher glass transition is likely due to the networks having extremely high crosslink densities within an amorphous network, which prevent flexibility in the network at lower temperatures observed for all other formulations. The ability for the network to rearrange also strengthens the network overall, producing more mechanically robust films with higher moduli and even lower creep than their NMP counterparts. Including the end architected prepolymers may also reduce shrinkage stress, with the combination of end architecture and RAFT polymerization lowering the shrinkage stress by an order of magnitude.

Preliminary work with epoxide monomers reveal that several factors influence the rates of cationic photopolymerization. Environmental conditions and monomer structure are the most influential factors of those examined when predicting both rate of photopolymerization and monomer conversion. Furthermore, copolymer blends of epoxide and oxetane monomers significantly increases the rate of photopolymerization. Building upon the copolymer studies, epoxidized terpene monomers were studied as a potential additive for cationic resins. These materials have the most significant impact on the photopolymerization of oxetane monomers. The addition of a small amount of terpene oxides eliminates the well-documented inhibition time of oxetane monomers, but did not affect the photopolymerization rate of the glycidyl ether or cycloaliphatic epoxide monomers. Monofunctional terpene oxides decrease the glass transition of the network, most likely through a plasticization process in which the highly crosslinked systems more easily reptate. On the other hand, difunctional terpene oxide additive increase the T_g of all

systems most likely due to its comparatively large molecular structure restricting movements within the network.

Building upon the use of thermally labile nitroxide radicals to control acrylate and methacrylate polymerizations, one avenue for ongoing research may be the use of photoinitiated nitroxide radicals. These novel NMP photoinitiators could serve as a means to modify network structures purely based off of the selection and design of the initiator. By controlling the photopolymerization reaction, more uniform networks may form. Greater network uniformity in acrylate systems, as observed in off stoichiometric thiol-acrylate systems, may lead to more robust thermomechanical properties.¹ Furthermore, by altering the nano-gelation through the relative radical reactivity, it may be possible to also limit the degree of shrinkage in these systems. NMP photoinitiators would also give rise to stage curable radical formulations. The ability to partially react a formulation would allow for complex mechanical structures to be built independently or for patterned surfaces to be produced, which could yield low gloss surfaces or increased hydrophobicity via surface roughening. The ability to reinitiate the photopolymerization reaction would also allow any radical formulation to be easily grafted to or from systems for further modification, such as amphiphobic fluoro monomers or anti-fouling zwitterionic coatings. Additionally, by using the reactivity of the nitroxide radical, it may be possible to generate phase-separated systems by tuning the reactivity ratios of the monomers. As nitroxides traditionally do not properly control methacrylate monomers, it is possible for methacrylate/acrylate networks to form separately. This new type of photoinitiator may provide a relatively simple method to significantly diversify the thermomechanical properties of common photocurable resins.

Continuing research into cationic photopolymerization may take several forms. Fundamental understanding of the reactivity ratios between various monomers, such as glycidyl ethers, cycloaliphatic epoxides, and oxetanes in this work may allow for phase separation in cationic systems. Other monomers that undergo cationic photopolymerization, like styrene and vinyl esters, would provide further abilities to generate phase separation via the manipulation of reaction kinetics and reactivity ratios. As these vinyl monomers do not undergo a ring opening reaction, it is possible that the differences in reaction kinetics may be sufficient to cause different networks to form. The inclusion of terpene oxide additives, to either accelerate oxetane monomer polymerization or to modify network structures and tune the T_g of the resulting film, provide an additional avenue for cationic resin formulation. Beyond fundamental examinations of cationic monomer formulations, radical promoted cationic photopolymerization (RPCP) is another area with significant potential, and may yield large benefits both industrially and academically. The Liska group recently published studies that utilize RPCP to initiate frontal polymerizations with glycidyl ether monomers.² These cationic frontal polymerizations have been shown to overcome the limits of light penetration and are capable of quickly curing complex geometries. However, the reactions undergo significant discolorations and exceptionally high exotherms. Modifications to the resin composition or selection of photoacid generator may limit the discoloration. Further, immobilization of the RPCP additives onto cellulose or other nanofillers, such as silica nanoparticles, may act to further offset the heat during the frontal polymerization and increase its industrial applicability. Frontal cationic photopolymerizations nonetheless provide an interesting opportunity toward overcoming

some of the classical shortcomings of photopolymerization, namely light penetration and geometry selection.

While block copolymers served as an inspiration for this research, it may be possible through architected prepolymers to generate thermosets that are essentially crosslinked block copolymers. In a similar fashion, it may be possible to generate a poly-(methyl methacrylate co-butyl acrylate) if the butyl acrylate prepolymers were photopolymerized with methyl methacrylate. This may allow for photocurable poly-(methyl methacrylate) with enhanced impact and creep resistance. As observed with the end-functionalized prepolymers in both the acrylate and epoxide systems, one T_g appears to be strongly influenced by the T_g of the nonreactive backbone monomer. It may be possible via reactive diluent selection and Fox's T_g to produce films with easily targeted secondary glass transition temperatures. In addition to thermoset block copolymers, prepolymers with reactive groups present only at one side would provide a diblock analogue to further characterize how architected prepolymers influence network heterogeneity formation. Diblock copolymers are often used to modify the rheology and morphology of a triblock copolymer. The architected prepolymers with the reactive groups placed only at one end may act to similarly provide greater soft segment entanglements that may modify the viscosity and elongation at break of these systems. Together, block copolymer thermosets and diblock analogues provide a strong next step for future research regarding architected prepolymers in photopolymer systems.

While RAFT polymerization was found to greatly influence how the prepolymers behaved in the photoreactive species, only one RAFT agent was utilized to synthesize the monomers. Dibenzyl trithiocarbonate (DBTTC) is uncommon amongst RAFT agents as it

builds in multiple directions simultaneously. Future studies examining prepolymer structure and synthetic route would be advised to examine other common RAFT agents that build linearly. In this fashion, other trithiocarbonates could be evaluated for their ability to limit shrinkage stress as well as promote network rearrangements, and the effects of prepolymer architecture could be examined. It is plausible that if the RAFT agents are too close to the crosslinking domains the shrinkage stress reduction may be limited. From these studies it would be possible to completely decouple the prepolymer architecture and synthesis process as causes for the observed decrease in shrinkage stress. Dithiobenzoates may also be a secondary class of RAFT agent for prepolymer synthesis. In contrast to trithiocarbonates, dithiobenzoates have much higher transfer constants and the reduction in conversion and photopolymerization kinetics may be alleviated to some extent. Photoplasticity in these systems should also be evaluated. The dynamic RAFT adducts allow for the network to rearrange and have been shown to allow for increased permeability of the crosslinked networks. The role and influence of prepolymer architecture and RAFT agent placement through the synthetic route on photoplasticity may lead to networks with unique adhesion and permeability properties. These studies would serve to advance the fundamental science involved in the use of RAFT agent additives in photopolymerization reactions.

In summary, this work has established prepolymer architecture as a method for modifying network heterogeneities to better understand and modify macroscopic thermomechanical properties. By simply altering the placement of reactive groups, such as epoxides and acrylates, this work demonstrated that the polymer network morphology can be modified in achieving significant enhancements to polymer toughness, creep

resistance and shrinkage stress reduction. Continued research into the use of architected prepolymers may lead to even greater knowledge regarding network heterogeneity formations as well as methods to alleviate common photopolymerization issues, like shrinkage stress and brittleness. These enhancements provide the basis for a new generation of photocurable materials to advance the fundamental and practical applications of photopolymerization.

References and Notes

- (1) Kim, S. K.; Baguenard, C.; Guymon, C. A. *Macromol. Symp.* **2013**, 173–192.
- (2) Bomze, D.; Knaack, P.; Liska, R. *Polym. Chem.* **2015**, 8161–8167.